Polynomial Chaos Based Uncertainty Quantification for Stochastic Electromagnetic Scattering Problems

Zdravko Zubac

Promotoren: prof. dr. ir. D. Vande Ginste, prof. dr. ir. D. De Zutter
Proefschrift ingediend tot het behalen van de graad van
Doctor in de ingenieurswetenschappen: elektrotechniek

Vakgroep Informatietechnologie
Voorzitter: prof. dr. ir. D. De Zutter
Faculteit Ingenieurswetenschappen en Architectuur
Academiejaar 2015 - 2016

UNIVERSITEIT GENT

ISBN 978-90-8578-911-6
NUR 959
Wettelijk depot: D/2016/10.500/43

Polynomial Chaos Based Uncertainty Quantification for Stochastic Electromagnetic Scattering Problems

Zdravko Zubac

Dissertation submitted to obtain the academic degree of
Doctor of Electrical Engineering

Publicly defended at Ghent University on August 16th, 2016

Supervisors:

prof. dr. ir. D. Vande Ginste
prof. dr. ir. D. De Zutter
Electromagnetics group
Department of Information Technology
Faculty of Engineering and Architecture
Ghent University
St.-Pietersnieuwstraat 41
B-9000 Ghent, Belgium
`http://emweb.ugent.be`

Members of the examining board:

prof. dr. ir. R. Van de Walle (chairman)	Ghent University, Belgium
prof. dr. ir. G. Crevecoeur (secretary)	Ghent University, Belgium
prof. dr. ir. D. Vande Ginste (supervisor)	Ghent University, Belgium
prof. dr. ir. D. De Zutter (supervisor)	Ghent University, Belgium
prof. dr. L. Daniel	Massachusetts Institute of Technology, USA
prof. dr. ir. M.C. van Beurden	Eindhoven University of Technology, Netherlands
prof. dr. ir. D. Botteldooren	Ghent University, Belgium

"Every human generation has its own illusions with regard to civilization; some believe they are taking part in its upsurge, others that they are witnesses of its extinction. In fact, it always both flames and smolders and is extinguished, according to the place and the angle of view."

IVO ANDRIĆ

Acknowledgments

Four years have passed, and here we are, at the end of one of the exceptional stories of my life. Of course, a lot of my life stories were more or less exceptional in one way or another; some in a bad way, like passing my childhood in war, and a lot of them in an exceptionally good way: like studying in Belgrade, the city that never sleeps, or meeting good and smart people and even becoming their friend. In overall, the time spent in Ghent was filled with hope and motivation like every important step in my career and I am happy that this eventually led to writing this thesis and thus summarizing the research I have done.

This kind of moment, when you finish one job and you are at the beginning of something new and unknown, like choosing a next career step, is a good opportunity to take a look at the past times and give an overall hindsight. I came to Ghent four years ago, filled with hope and enthusiasm, to come up with something new, and purely scientific, to get excellent research results, and to obtain a *summa cum laude* degree. During these four years, there were lot of ups and downs, I was losing hope, and I was getting hope again, I was happy with my results, and I was nervous when results were not good and when it seemed that my research starts looking like science for dummies :). It was hard to resist this desperate feeling when a lot of excellent Belgian beer was around me, and I could forget all my hopes and disappointments by enjoying a few trappist beers. But excellent people were around me and with me. They gave me strength, and by helping me to overcome my problems, they embedded themselves into this thesis. For this reason the first words of this thesis, are thankful words for the exceptional people I met.

First of all, I would like to thank my first promoter, professor Dries Vande Ginste, for all the support he provided during these four years. The conversations with him helped me to acquire a scientific way of thinking. His trust in my skills was the wind in the sails in many difficult moments and his encouraging words helped me to find motivation and to be satisfied with my results. Special thanks for sending me to Massachusetts Institute of Technology (MIT) which was a great step in my career. And, of course, his corrections of my papers helped me to learn how to use “a” articles.
I would also like to thank my second promoter professor Daniël De Zutter, who promptly replied to my application and gave me the opportunity to work in this excellent group on a computational topic. The suggestions and theoretical knowledge that he shared with me helped me to truly understand some physical concepts I thought I was aware of long time before I came to Ghent. His papers and the discussions we had are responsible for the ongoing traveling through the joy of electromagnetic modeling.
After I combined electromagnetic and stochastic methods and investigated very large problems that were not solvable on one computer anymore, MPI-man appeared. Work-

ing with professor Jan Fostier was an excellent experience. Many thanks for giving me the Nero code. Moreover, I would like to express special gratitude for the wonderful conversations and for helping me to obtain a deep insight into parallel computing.
The research at MIT was an extremely good experience where I learned a lot and met some wonderful people in the Computational Prototyping Group, whom I want to thank for the wonderful time spent there: Lily, Bichoy, Zheng, Richard, Luca and Arezoo. I am also thankful to professor Jacob White for the scientific conversations we had. My deepest gratitude is reserved for my MIT promoter, professor Luca Daniel for giving me an opportunity to become a part of his group and for spreading my views, and learning me how to think out of the box and to be concerned about the real applications for my research. His course helped me to understand well-known concepts in a new way and to get real joy from developing numerical methods.
At this point I would also like to thank all my professors and colleagues from the School of Electrical Engineering at the University of Belgrade, especially the people of the Microwave Engineering Group. My personal gratitude goes to professor Dragan Olćan, my master's thesis promoter, who supported me considerably when I was planning my future career.
I would like to thank all the members of my examination board, which also included Prof. Martijn van Beurden, Prof. Guillaume Crevecoeur, Prof. Dick Botteldooren, and a chairman, Prof. Rik Van de Walle, for their suggestions, comments and questions, which helped me to improve the quality of this thesis.

Not only professors were the ones who helped me to extend my knowledge and reach beyond, at first sight, an impossible limit. Smart colleagues that I shared the office with were also a pushing force for me which helped me to understand hard theoretical problems and to easily solve many small technical problems. One of them is Giorgos Karagounis, who will, as one other colleague prophesied, be at the one of highest leading positions in our world. Discussion with him about EM-relating or programming problems was constant learning to me. His views about politics, economy, social topics make me to believe that he is the most educated person I have ever met; true and bright erudite.
Spending time to do youthful things together with Giorgos and Marco, like drinking, traveling, playing social games, gave me an energy to work on my thesis. I was so lucky to meet these two guys, who are now my closest friends. Sure, Marco was always complaining and he was making tremendous effort to be funny (OMG, that is annoying), but you must like that guy. He says what he thinks, he enjoys friendships and he always organizes good social events with the wonderful food he makes. Thank you, Marco, for all those secrets of Italian kitchen you revealed, like putting paprika in the bolognese sauce and making pizza with ketchup. He was always interested in PCE related discussion and I am happy that we were working on a similar topic. I hope we will continue this friendship until death do us part :).
Gert-Jan is the colleague with whom I spent a lot of time speaking about real engineering problems. Whenever something from circuit theory and EMC was not clear to me, Gert-Jan was there to explain, and he was always prepared to help me to solve my problems. He is the kind of man I respect, silent and untalkative, but when he speaks,

the beauty is in listening.
I am also thankful to other present and former colleagues from Electromagnetic Group: Pieter-Jan (thanks for all technical support at the beginning), Marina, Celina, Maryna, Mykola, Bart, Freek, Yves, Dieter, Peter, Luigi, Sam A., Sam L., Thijs, Olivier, Martijn, Steven, Michiel, Simon, Irven, Niels, Arne and Paolo (thanks for discussions we had). Special thanks go to our former secretary, Isabelle, for all her support and help with administrative matters.

The friends from Serbia were the other driving force in Ghent. It was easy to adapt to new conditions, once you have people from your country with you. I would like to thank to a lot of Serbian people I met here: Vanja, Ivana, Vedran, Danilo, Tijana, Miloš, Marko, Stevan, Maja, Miloš, Sanja, Ana, Sandra, Milena, Ksenija, Dimitrije and Mario. The Serbian guys that I spent most time with were Aleksandar and Atila. I will miss lunches in De Brug, but I won't miss Atila's favourite topics. Many thanks to Mima for waiting at the train station on the first day I came to Ghent and the time we had together on -T floor at Technicum. I am also thankful to Ljubomir for giving me good advice and making nice jokes which always cheered me up.
My special gratitude go to my flatmates: Marko, Nenad and Djordje. I spent wonderful time with them and they were nice people to live with. I must say that I started getting the intellectual acuity and correctness from Nenad and the philosophical spirit from Djordje, in this last year, when my PhD studies were about to finish. Our flatmate gatherings, watching games and speaking about Serbian politics and the humorous remarks we made, are the moments I will never forget.
One person that had a large influence on me, is my ex-flatmate and close friend, Jelena. I am so happy that she accepted me as her closest friend and I enjoyed the time we spent together. She also introduced me to her family, mother Radojka and brother Ivan, who accepted me as their own close relative. Every weekend in Antwerp I recharged my batteries and got the strength to solve problems on Monday. I am also thankful to her, for introducing me to Milan (Otac) and his wonderful family. Both of them helped me to start getting back something I lost in the past: *faith*.

My friends and family living in Serbia and Herzegovina were also supportive during these four years. I am thankful to my friends in Trebinje: Nemanja, Bojana, Vuk, Bojan, Nikola, Ilija, Vladan, Željko and Vladimir for the wonderful time spent on holidays and for the constant belief in my abilities. I am also thankful to my friends from the student dormitory: Miljan, Vladan ("Hvala Vlade, brate") and Darko ("Hvala za sve prosti paore").
My closest friends were also the ones who motivated me. Therefore, I am thankful to: Ilija (for his visit during my first year and time we spent in chatting), Nino (for the wonderful time we had in Norway), Nikola and Milenko. I would also like to express special gratitude to Milan (Inženjer Babić), for his irrational faith in me ("Daleko sam ja od stručnjaka kakvim me smatraš"). I hope he will always be one of the best experts in his domain. My "zamalo kum" Ivan was also a person who motivated me and was almost my idol as the best engineer of my generation 2006/10 at the University of Belgrade. The time I spent with him and his lovely wife Vesna was always filled with

joy, laugh and happiness.
During the holidays, when I went back to Belgrade, two flatmates were always finding place for me in their apartment. One of them is Bojan (Shkenny Maestro), my ex roommate, with whom I spent a lot of good moments in Belgrade, Brčko (many thanks to his family) and on Skype. Another one is Branko, my student (Učenik), a bright and intelligent young man, who will become the owner of some good company one day and make *Profa* happy and rich. If someone is responsible for not being 100 % dedicated to my thesis, that is Danilo, with whom I had conversations almost every day. However, the time we spent on chatting, increased my efficiency and therefore he also helped me to deliver good output, even though I was sometimes distracted from work ("Hvala Meks").

Last but not least, I would like to express my deepest gratitude to my parents, Branko and Ana, for raising me to be the kind of person I am and for all their support, sacrifice during the hard times and all the love they gave to me. I am also thankful to my brother Slavko for his unconditional support and understanding. Every success of me is theirs as well. I am also thankful to the good people of Serbia and Republika Srpska who suffered in the near past, but still they were able to give birth to many open-minded people filled with love like the ones I mentioned above. All my work is dedicated to these heroes and my fatherland, and I hope my work and professional achievements will bring benefit to them. I am grateful to God, whose hand leads me and whose mercy is always upon me.

Ghent, June 2016
Zdravko Zubac

Contents

Samenvatting

Veldsimulatoren gebaseerd op de vergelijkingen van Maxwell kunnen worden ingezet bij de modellering van complexe elektromagnetische structuren zoals antennes, verstrooiers, transmissielijnen, gedrukte schakelingen, fotonische systemen, enz. De simulatoren beschouwen de geometrische beschrijving van de structuren, alsook de elektrische eigenschappen van de gebruikte materialen en het type excitatie van het probleem. Na het oplossen van integraal- en/of differentiaalvergelijkingen leveren ze dan typisch veld- en stroomdistributies, evenals andere interessante grootheden, zoals bijvoorbeeld parasitaire impedanties en antennewinst. Het gebruik van deze simulatoren heeft geleid tot het beter modelleren van circuits en systemen tijdens hun ontwerp. Nauwkeurigheid en efficiëntie van deze simulatoren is dus cruciaal voor vele applicaties waarbij signalen worden overgebracht via elektromagnetische golven, zoals bijvoorbeeld bij navigatiesystemen gebaseerd op het *Global Positioning System* (GPS), mobiele telefonie, Wi-Fi, en ook defensiesystemen. Dientengevolge is er een voortdurende vraag naar uitbreiding van deze veldsimulatoren voor het modelleren van nieuwe technologieën en naar verder onderzoek inzake hun nauwkeurigheid en efficiëntie.

De stand van de technologie is vandaag zo ver gevorderd dat de huidige veldsimulatoren niet meer toereikend zijn qua nauwkeurigheid. Dit komt omdat fabricageprocessen verschillende soorten variabiliteit introduceren en deze kunnen niet op een deterministische manier worden beschreven. Onze elektromagnetische modellen moeten stochastisch zijn en de veldsimulatoren moeten stochastische effecten kunnen capteren. Vanuit het standpunt van de implementatie van dergelijke simulatoren betekent dit dat nieuwe uitbreidingen dienen te worden toegevoegd aan de bestaande implementaties en/of dat (delen van) de software volledig dienen te worden herschreven.

In dit proefschrift ligt de voornaamste focus op stochastische methodes die een volledige wijziging van bestaande deterministische simulatoren vergen. De deterministische simulator waarop we ons hier baseren, vertrekt van randintegraalvergelijkingen (*Boundary Integral Equation* – BIE) die worden opgelost via de momentenmethode (*Method of Moments* – MoM). De berekening van een matrix-vector product (MVP) wordt versneld door gebruik te maken van de snelle multipoolmethode (*Multilevel Fast Multipole Method* – MLFMM). Deze aanpak kan worden ingezet om de verstrooiing aan twee-dimensionale (2D) perfect elektrisch geleidende (*perfect electrically conducting* – PEC) en diëlektrische objecten die worden belicht door een transversaal magnetische (TM) golf te analyseren. Het is in het verleden reeds aangetoond dat MLFMM een heel efficiënte methode is die toelaat de verstrooiing aan elektrische grote objecten te modelleren. Onderzoek werd gevoerd naar diverse aspecten van de implementatie: parallellisatie, combinatie met *Singular Value Decomposition* (SVD), toepassing op verschillende soorten elektromagnetische problemen, enz. Daarom

gebruiken we hier de goedgekende MLFMM als startpunt voor de ontwikkeling van nieuwe, efficiënte stochastische simulatoren.

In het inleidend hoofdstuk wordt, aan de hand van enkele typische voorbeelden, de variabiliteit van klassieke structuren geschetst en wordt de noodzaak aan stochastische elektromagnetische analyse toegelicht. Eveneens wordt er meer aandacht geschonken aan de beschrijving van stochastische methodes dan aan MLFMM, maar er worden wel veel referenties gegeven die MLFMM exhaustief behandelen. Stochastische methodes kunnen worden ondergebracht in twee categorieën: methodes gebaseerd op het nemen van monsters (*sampling-based*) en niet-*sampling-based* methodes. In het bijzonder wordt er dieper ingegaan op methodes die gebaseerd zijn op de ontwikkeling van de relevante grootheden in polynomen, de zogeheten *Polynomial Chaos Expansion* (PCE) methodes. Deze kunnen worden onderverdeeld in intrusieve methodes, die een complete wijziging van bestaande deterministische simulatoren vereisen, en niet-intrusieve methodes. Tevens wordt er in dit hoofdstuk aandacht geschonken aan multidimensionale numerieke integratie, aangezien dit een belangrijk onderdeel vormt van PCE methodes.

Het tweede hoofdstuk beschrijft de Stochastische Galerkin Methode (SGM) en zijn toepassing op de standaard MoM voor de analyse van verstrooiing van elektromagnetische golven aan PEC objecten die worden gekenmerkt door twee verschillende en representatieve types variabiliteit: (i) oppervlakteruwheid, beschreven door een verzameling van gecorreleerde random variabelen en (ii) variaties van de posities van de objecten, beschreven door een verzameling onafhankelijke random variabelen. Hiertoe wordt de belangrijkste te bepalen grootheid, namelijk de stroomdichtheid op het oppervlak van het object, uitgedrukt als een som van enerzijds gekende orthonormale polynomen met onbekende coëfficiënten in het domein van de random variabelen en anderzijds pulsbasisfuncties in het spatiale domein waarin de verstrooier zich bevindt. Aangezien de objecten groter zijn dan de golflengte, treden er golfeffecten op. Galerkinprojectie levert de onbekende coëfficiënten, en zodoende de gezochte oppervlaktestroomdichtheid.

De SGM-MoM uit het tweede hoofdstuk werd niet eerder getest in de context van elektromagnetische verstrooiing. Maar de echte nieuwe bijdragen van dit werk worden beschreven vanaf het derde hoofdstuk. In Hoofdstuk 3 wordt immers de SGM gecombineerd met de MLFMM. Het belangrijkste probleem hierbij is het bewaren van de nauwkeurigheid en de efficiëntie. Het grote aantal stochastische onbekenden en de twee Galerkinprojecties in de MLFMM zorgen ervoor dat het ontwerpen van een geschikte SGM-MLFMM heel uitdagend is. De verstrooiingsproblemen die beschouwd worden in dit hoofdstuk omvatten random variaties van de posities van de verstrooiiers. Zodoende kan de stochastische geometrie beschreven worden aan de hand van een verzameling van onafhankelijke random variabelen. De nieuwe, voorgestelde SGM-MLFMM leidt tot een ijle polynomiale beschrijving van de typische MLFMM intermediaire grootheden (namelijk de aggregatie- en desaggregatiematrices), wat heel voordelig is voor wat betreft de computationele efficiëntie. Daarenboven wordt in Hoofdstuk 4 een preconditioneringsalgoritme voor de SGM-MLFMM voorgesteld

dat de oplossing van de stochastische verstrooiingsproblemen verder versnelt. De Galerkinprojecties introduceren wel afrondingsfouten die, samen met de traditionele MLFMM nauwkeurigheid, de globale precisie van de methode beïnvloeden.

Het aantal variabelen van beide types, stochastisch en spatiaal, kan zo groot worden dat een simulatie op één enkele computer niet meer mogelijk is. Daarom wordt parallellisatie van het SGM-MLFMM algoritme bestudeerd in Hoofdstuk 5. De parallellisatie wordt hier uitgevoerd in het spatiale domein, wat betekent dat de onbekenden verdeeld worden over verscheidene computationele nodes door gebruik te maken van het traditionele, deterministische, geparallelliseerde MLFMM algoritme. Dit algoritme is gebaseerd op hiërarchische partitionering, wat inhoudt dat de brongroepen en hun stralingspatronen in de laagste lagen van de MLFMM worden toegewezen aan één computer, terwijl de stralingspatronen in hogere lagen worden gedistribueerd. De standaard MLFMM operaties die worden uitgevoerd op deze stralingspatronen (aggregatie, interpolatie, translatie, anterpolatie en desaggregatie) zijn echter compleet opnieuw geïmplementeerd om te kunnen worden gebruikt binnen het kader van het SGM algoritme. De nieuwe en efficiënte geparallelliseerde methode is toegepast op optische systemen.

Oppervlakteruwheid is een belangrijk type variabiliteit dat een aanzienlijke invloed heeft op de verstrooide velden. In tegenstelling tot positionele variabiliteit dient de oppervlakteruwheid te worden beschreven aan de hand van een verzameling *gecorreleerde* random variabelen, wat nefast is voor de efficiëntie en nauwkeurigheid van de methode. Het belangrijkste knelpunt is de multidimensionale integratie. In Hoofdstuk 6 wordt dit opgevangen door een Cholesky decompositie in te voeren, zodoende opnieuw ijle polynomiale beschrijvingen te verkrijgen. Onderhavig werk toont aan dat de voorgestelde SGM beter presteert dan de standaard niet-intrusieve methodes.

Het zevende hoofdstuk beschrijft onzekerheidskwantificatie (*Uncertainty Quantification* – UQ) methodes die gebaseerd zijn op tensordecompositie. Aangezien PCE-gebaseerde methodes in feite *big data* problemen zijn, kunnen deze data worden behandeld als tensors. Door de redundantie in de data te benutten, worden de tensoren herschreven als benaderingen van lage rang. Dergelijke methodes zijn puur *sampling-based*, maar kunnen worden toegepast op zowel intrusieve als niet-intrusieve wijze. In Hoofdstuk 7 wordt de basis gelegd voor verder onderzoek in dit domein. Er wordt immers aangetoond dat deze tensormethodes kunnen worden gecombineerd met de zogeheten Statistische Moment Behoudende Model Orde Reductie (SMOR) techniek en met MLFMM.

Ten slotte worden in het laatste hoofdstuk de voornaamste conclusies, resulterend uit het onderzoek gepresenteerd in dit proefschrift, geformuleerd. De in onderhavig werk voorgestelde algoritmes zijn toepasbaar op 2D verstrooiingsproblemen. Hun uitbreiding, aanpassing en verdere ontwikkeling voor 3D applicaties is een uitdagend onderzoeksonderwerp. Verscheidene mogelijkheden tot verder onderzoek naar UQ methodes voor elektromagnetische problemen worden daarom voorgesteld.

Summary

Full-wave Maxwell equation solvers have proven their ability to model complex electromagnetic structures such as antennas, scatterers, transmission lines, printed circuit boards, photonics systems, etc. These solvers start from the geometrical description of the structure, the electrical properties of the materials and the type of excitation and, after solving integral or differential equations, they produce field and current distributions, as well as values for other parameters of interest, e.g. parasitic impedances, antenna gain, etc. Using these solvers has improved the modeling of many circuits and devices in the design stage, so their accuracy and efficiency is crucial for many applications where signals are transmitted via electromagnetic waves, including the Global Positioning System (GPS), mobile phone, Wi-Fi and defense systems. Therefore, there is a constant demand for making these full-wave solvers applicable to new technologies and for ongoing research in improving their efficiency and accuracy.

Nowadays, technology is going beyond the current ability of the Maxwell solvers for accurate modeling. Manufacturing processes introduce several kinds of variability that cannot be deterministically described. This means that our electromagnetic models need to be stochastic and the Maxwell solvers should be capable of capturing these stochastic effects. From an implementation viewpoint, this means that new features need to be added to the current solvers and/or that (some parts of the solvers) need to be completely rewritten.

In this thesis, the main focus is on the type of stochastic methods which require complete modification of the existing deterministic solver. The deterministic solver used here is based on solving Boundary Integral Equations (BIE) by means of the Method of Moments (MoM). Calculation of a matrix-vector product (MVP), evolving from the BIE-MoM, is sped up by leveraging the Multilevel Fast Multipole Method (MLFMM). The application range for the solver is scattering from two dimensional (2D) perfect electrically conducting (PEC) and dielectric objects under transverse magnetic (TM) incidence. In the past, MLFMM was shown to be the most efficient tool for the modeling of extremely large scattering problems and research was conducted on different aspects of its implementation: parallelization, combination with a singular value decomposition (SVD), application to different kinds of electromagnetic problems, etc. Therefore, we have used well-studied MLFMM as a starting point for developing efficient stochastic solvers.

The general introduction explains why stochastic electromagnetic analysis is needed by presenting some examples of variability on different structures. Also in the introductory chapter, more attention is devoted to stochastic methods than to the core of MLFMM modeling, but extensive references are provided for the latter one. Stochastic methods

are classified in sampling based and non-sampling based methods, and among them, methods based on polynomial chaos expansion (PCE) are considered in detail. Two main classes of PCE based methods can be distinguished: intrusive methods, which require a complete modification of existing deterministic solvers, and non-intrusive methods. Moreover, algorithms for multidimensional numerical integration, which are found to be at the core of PCE based methods, are explained.

The second chapter describes the formalism of an intrusive Stochastic Galerkin Method (SGM) and its application to the standard MoM for scattering analysis of PEC scatterers with two different and representative types of variability: (i) surface roughness described with a set of corellated random variables and (ii) variations in position described by a set of independent variables. The primary quantity of interest (QoI) which is, for scattering problems, the unknown current distribution, is expressed as a sum of known orthonormal polynomials with unknown coefficients over the space on which random variables are defined and pulse base functions over the spatial domain on which the scatterer is defined. The structure is larger than the operating wavelength and hence, full-wave effects are present. Galerkin projection leads to finding these unknown coefficients.

Although the SGM-MoM of Chapter 2 was not described in the context of scattering problems before, the novel contributions of the thesis start with the third chapter. In this chapter a combination of SGM and MLFMM is described. The main problem is to maintain accuracy and efficiency. The large number of stochastic unknowns and the two Galerkin projections in the MLFMM, make it challenging to derive the desired SGM-MLFMM method. The considered scattering problems deal with random position variations described by independent sets of random variables. This is shown to result in a sparse polynomial approximation of intermediate quantities (namely aggregation and disaggregation matrices), which has a very beneficial effect on the computational efficiency. In Chapter 4, a preconditioner for the SGM-MLFMM algorithm is derived and implemented, as such further expediting the solution of stochastic scattering problems. The Galerkin projections introduce truncation errors and, together with the standard MLFMM accuracy limits, influence the overall accuracy of the new method.

The number of both type of variables, stochastic and spatial, can become so large that simulation on one computer is not possible. Therefore, the parallelization of the novel method is considered in the fifth chapter. The parallelization is performed in the spatial domain, which means that unknowns are distributed to different computational nodes by using the standard deterministic algorithm for the parallel MLFMM . This algorithm is based on hierarchical partitioning, which means that on lower levels of the MLFMM the group of sources and their radiation patterns are assigned to the same computer, and for higher levels the radiation patterns are distributed. The standard MLFMM operations on radiation patterns (aggregation, interpolation, translation, anterpolation and disaggregation) are completely rewritten according to the SGM algorithm. This new and efficient parallelized method is applied to optical systems.

Surface roughness is an important type of variability with a substantial influence on the scattered fields. In contrast to position uncertainty, roughness statistics are described by *correlated* random variables which has a large effect on the efficiency and accuracy of the method. The main bottleneck is the required multidimensional integration. In Chapter 6, this is treated by introducing Cholesky decomposition which tends to produce sparse polynomial approximations. Our work shows that the SGM method outperforms standard non-intrusive methods.

The seventh chapter introduces state-of-the-art uncertainty quantification (UQ) tools based on tensor decomposition. Since PCE-based methods become big data problems, these data are treated as a tensor and by exploiting data redundancy, a tensor can be efficiently represented by a low-rank approximation. These methods are purely sampling-based, but they can be applied intrusively as well as non-intrusively. This chapter paves the way for future research in this domain, as it is shown that these tensor methods may be combined with Statistical Moments preserving Model Order Reduction (SMOR) and MLFMM.

Finally, the last chapter formulates main conclusions drawn from the research and results presented in this thesis. The algorithms that are developed throughout this thesis are applicable to 2D scattering problems, but their improvement, modification and development for 3D problems is a further research challenge. Several paths for continuation in the domain of UQ of electromagnetic problems are proposed. This thesis clearly illustrates the effect of uncertainties on the electromagnetic characteristics of scatterers. The same effects are captured with a traditional Monte Carlo (MC) method, SGM-MoM, SGM-MLFMM and their non-intrusive counterparts. The difference is in the simulation time needed for extraction of stochastic parameter of interest. This thesis proposes efficient MLFMM-based algorithms for 2D problems, but also indicates that the right method for UQ is dependent on many factors. The efficiency of UQ methods is of a great importance, so knowledge the inherent properties of them is a first step in choosing right one. The novel method expands the application range where intrusive SGM method can be efficiently applied.

List of Abbreviations

1D	One dimension / one-dimensional
2D	Two dimensions / Two-dimensional
3D	Three dimensions / Three-dimensional
ANOVA	Analysis of Variance
BIE	Boundary Integral Equation
CDF	Cumulative Distribution Function
CEM	Computational Electromagnetics
CFIE	Combined Field Integral Equation
CMOS	Complementary Metal Oxide Semiconductor
CPU	Central Processing Unit
EFIE	Electric Field Integral Equation
EMC	Electromagnetic Compatibility
EMI	Electromagnetic Interference
FD	Finite Difference
FDTD	Finite Difference Time Domain
FEM	Finite Element Method
FMM	Fast Multipole Method
gPC	generalized Polynomial Chaos
IPW	Incoming Plane Waves
KL	Karhunen-Loève
KLT	Karhunen-Loève Transformation
LoP	Level of Partitioning
MC	Monte Carlo
MLFMM	Multilevel Fast Multipole Method

MoM	Method of Moments
MPI	Message Passing Interface
MVP	Matrix Vector Product
OPW	Outgoing Plane Waves
p.u.l.	per unit length
PCE	Polynomial Chaos Expansion
PDF	Probability Density Function
PEC	Perfect Electric Conductor / Perfectly Electrically Conducting
PIM	Parallel Iterative Methods
RCS	Radar Cross Section
RDF	Random-Dopant Fluctuations
RHS	Right-Hand Side
RV	Random Variable
SCM	Stochastic Collocation Method
SFC	Space Filling Curve
SGM	Stochastic Galerkin Method
SMOR	Statistical Moment Preserving Model Order Reduction
ST	Stochastic Testing
TFQMR	Transpose-Free Quasi-Minimal Residual Method
TM	Transverse Magnetic
TT	Tensor-Train
UQ	Uncertainty Quantification
VSC	Flemish Supercomputer Center

List of Publications

Articles in International Journals

- Z. Zubac, D. De Zutter, and D. Vande Ginste, "Scattering from two-dimensional objects of varying shape combining the Method of Moments with the Stochastic Galerkin Method", *IEEE Transactions on Antennas and Propagation*, vol. 62, no. 9, pp. 4852–4856, Sep. 2014.
- Z. Zubac, D. De Zutter, and D. Vande Ginste, "Scattering from two-dimensional objects of varying shape combining the Multilevel Fast Multipole Method (MLFMM) with the Stochastic Galerkin Method (SGM)", *IEEE Antennas and Wireless Propagation Letters*, vol. 13, pp. 1275–1278, Jul. 2014.
- Z. Zubac, J. Fostier, D. De Zutter, and D. Vande Ginste, "Efficient uncertainty quantification of large two-dimensional optical systems with a parallelized Stochastic Galerkin Method", *Opt. Express*, vol. 23, no. 24, pp. 30 833–30 850, Nov. 2015.
- Z. Zubac, L. Daniel, D. De Zutter, and D. Vande Ginste, "A Cholesky-based SGM-MLFMM for stochastic full-wave problems described by correlated random variables", letter submitted to *IEEE Antennas and Wireless Propagation Letters*.

Articles in Conference Proceedings

- Z. Zubac, D. Olćan, A. Djordjević, D. Zorić, and B. Kolundžija, "On real-time method-of-moments analysis using graphics processing unit", in *Proceedings of the 2012 IEEE International Symposium on Antennas and Propagation*, Jul. 2012.
- Z. Zubac, J. Fostier, D. De Zutter, and D. Vande Ginste, "Preconditioner for a scattering solver based on the intrusive stochastic galerkin method accelerated with MLFMM", in *Computational Electromagnetics International Workshop*, Izmir, Turkey, 2015, pp. 14–15.
- Z. Zubac, J. Fostier, D. De Zutter, and D. Vande Ginste, "A parallel, distributed-memory MLFMA for the stochastic galerkin method", conference contribution submitted to *FEM 2016*.

Polynomial Chaos Based Uncertainty Quantification for Stochastic Electromagnetic Scattering Problems

1 Introduction

1.1 Motivation

In order to meet the specifications in terms of available bandwidth and speed, electronic circuits operate at high frequencies. Therefore, modeling of these circuits and structures requires dealing with all high-frequency phenomena, which can only be achieved by a full-wave approach, i.e. by accurately solve Maxwell's equations for the problem under consideration. Moreover, owing to technology scaling and miniaturization of components, process variations have a significant impact on the circuit performance [1]. These variations are the result of manufacturing and include geometrical variations and electrical properties variations [2]. Geometrical variations include shape variations due to the lithographic process and line edge roughness or width variations because of etching. Electrical properties variations may be induced by, e.g. random-dopant fluctuations (RDF) in CMOS technology [3]. Also, in the context of textile patch antennas, substrate compression causes the variation of the electrical permittivity [4]. Several types of geometrical variations are presented in Figs. 1.1, 1.2 and 1.3.
Variations may also be induced by the designer in order to optimize the design. These variations can be topological, when a completely different arrangement of the components constituting the circuit is put forward, and non-topological, when the dimensions of the components and the distances between them are varied [8]. The first type of variations doesn't share any similarity with some "initial" structure and topology is completely changed, so the topology is suitable for the standard deterministic simulation using the existing tools. The second type of variations, however, are of the same type as the process variations in the sense that it concerns (small) variations with respect to a nominal design.
Process variations are often not known in a deterministic way. Similarly, design variations of the second type can be treated as stochastic processes. The same holds for variations of the behavior due to aging of electronic devices or due to changing

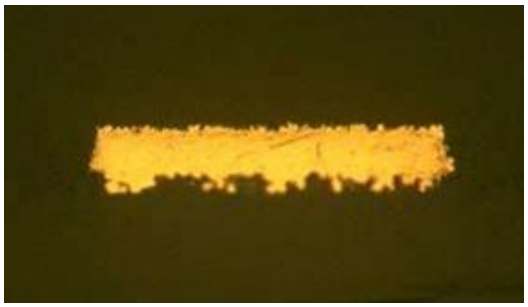

Figure 1.1: Surface roughness of an inner-layer copper trace. Reprint from [5].

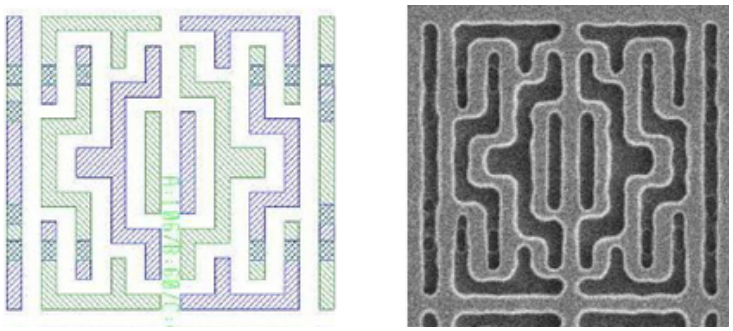

Figure 1.2: Example of a 45 nm M1 first metal-interconnect layer affected by line edge roughness. Left: nominal design; Right: image of the realized pattern on the wafer. Reprint from [6].

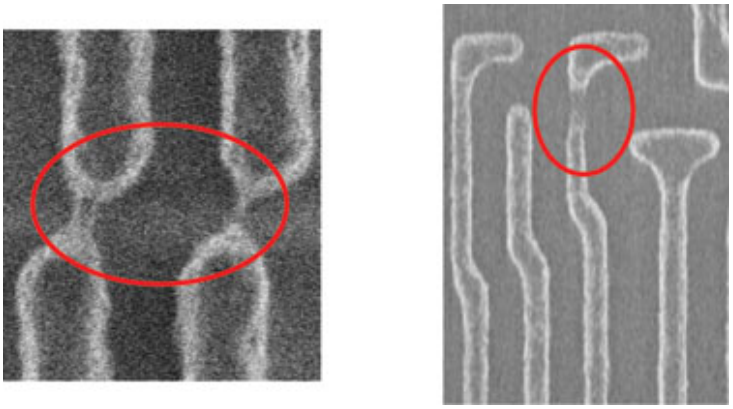

Figure 1.3: Undesired electrical shorts (left) and open (right) caused by lithography process variations. Reprint from [7].

environmental conditions, such as temperature, humidity and power supply fluctuations. Consequently, the development of stochastic modeling tools has received great attention during the recent years. The variations incorporated in novel mathematical models, and that are not known when the model is derived, are called uncertainties. To aid the design, the goal is now to model the novel electronic devices, including these uncertainties. In particular, the influence on the device's behavior needs to be quantified. This kind of modeling is called Uncertainty Quantification (UQ). Traditionally, UQ is carried out by means of the well-known Monte Carlo (MC) method, which is unfortunately found to be computationally expensive [9]. Recently, novel variation-aware methods based on Polynomial Chaos Expansion (PCE), have been developed for interconnect and lumped circuit analysis [10]–[13]. To asses high-frequency phenomena, PCE-based methods are developed in combination with Computational ElectroMagnetics (CEM) methods such as the Finite Element Methods (FEM) [14], the Finite Difference Time Domain (FDTD) method [15] and the Method of Moments (MoM) [16], [17].
A certain class of electromagnetic problems are conveniently described by means of Integral Equations (IE) that are solved via the MoM (see Section 1.2.2). This is the case for antenna structures, scatterers and the full-wave analysis of interconnects. Morover, the Multilevel Fast Multipole Method (MLFMM) (Section 1.2.3) can be used to expedite the solution of the linear system that evolves from the MoM [18].
In this work, the goal is to develop novel MLFMM-based variation-aware methods for UQ of full-wave electromagnetic problems. In particular, the focus is on variations of two-dimensional (2D) electromagnetic scatterers and optical systems.

1.2 Electromagnetic modeling

1.2.1 Scattering problem

A set of mathematical equations describing the connection between the electric and magnetic fields as well as between current densities and charges (as a sources of those fields) was put forward by James Clerk Maxwell [19]. These equations are written in integral or differential form, but cannot be directly interpreted by a computer. Converting these equations into appropriate computational models, which can be evaluated by the computer, is the focus of CEM.
For radiation and scattering problems, CEM methods are often based on Boundary Integral Equations (BIE), described in terms of the electric ($\boldsymbol{J}_s$) and magnetic ($\boldsymbol{M}_s$) current densities at the interfaces between media [20]. This current densities are then the only unknowns of the problem. Once they have been determined, the electromagnetic fields in every point in space can be computed.
A typical scattering problem, where an incident field impinges upon an object, as such inducing current densities at the interface as well as a scattered field, is schematically presented in Fig. 1.4. Throughout this thesis we will restrict ourselves to 2D scatterers, i.e. scatterers that are infinitely long cylinders with arbitrary cross-section. Moreover, we investigate Transverse Magnetic (TM) scattering, which means that the magnetic field has a component that is transversal with respect to the axis of invariance. As

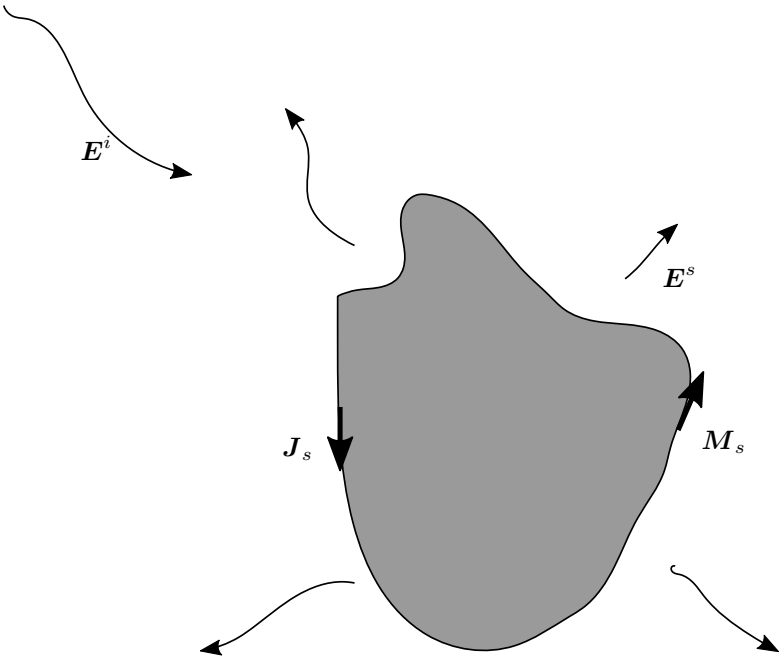

Figure 1.4: An incident electromagnetic wave $\boldsymbol{E}^i$ impinges upon an arbitrary shaped object and produces current densities at the interface as well as a scattered field $\boldsymbol{E}^s$.

indicated before, solving the scattering problems requires two steps [21]:

- Solving the pertinent integral equation(s) to find unknown current densities $\boldsymbol{J}_s$ and/or $\boldsymbol{M}_s$,
- Integrating the current densities to determine the scattered fields.

For simplicity, let us assume here that the scatterer is made of a Perfectly Electrically Conducting (PEC) material and, thus, only $\boldsymbol{J}_s$ exists on the surface of the object. (In Chapter 5, dielectric objects will be considered too.) The scattered electrical field, which only has a z-component is given by [20]:

$$E_z^s(\boldsymbol{\rho}) = -j\omega\mu \int_S G(\boldsymbol{\rho}, \boldsymbol{\rho}') J_z(\boldsymbol{\rho}') d\boldsymbol{\rho}', \tag{1.1}$$

where $J_z(\boldsymbol{\rho}')$ is the unknown current density on the scatterer (which also only has a z-component), μ is permeability of the background medium, S is the surface of the scatterer, and $G(\boldsymbol{\rho}, \boldsymbol{\rho}')$ is the 2D Green's function

$$G(\boldsymbol{\rho}, \boldsymbol{\rho}') = \frac{j}{4} H_0^{(2)}(k|\boldsymbol{\rho} - \boldsymbol{\rho}'|), \tag{1.2}$$

where $H_0^{(2)}(\cdot)$ is the zeroth-order Hankel function of the second kind, and $k = \omega/c$ is the wavenumber, with ω the angular frequency of the incident wave and c the speed of light in the background medium. To create the BIE, we impose the boundary condition for the tangential electrical field at the surface of the PEC object:

$$E_z^i = -E_z^s. \tag{1.3}$$

Inserting (1.1) into (1.3), and evaluation for observation points $\boldsymbol{\rho}$, yields the sought-for BIE, which is here an Electric Field Integral Equation (EFIE)

$$\lim_{\boldsymbol{\rho}\to S} E_z^i(\boldsymbol{\rho}) = -j\omega\mu \lim_{\boldsymbol{\rho}\to S} \int_S G(\boldsymbol{\rho}, \boldsymbol{\rho}') J_z(\boldsymbol{\rho}') d\boldsymbol{\rho}' \tag{1.4}$$

1.2.2 Method of Moments

The EFIE can be cast as

$$\mathcal{L}(J_z) = E_z^i, \tag{1.5}$$

where $\mathcal{L}$ represents the linear integral operator. To solve integral equation (1.5) by means of the MoM [22], the scatterer is discretized, i.e., divided in segments. Then, the current density J_z is expanded as a sum of pulse basis functions $b_j(\rho)$ with unknown coefficients I_j ($j = 1, ..., N$):

$$J_z(\boldsymbol{\rho}') = \sum_{j=1}^{N} I_j b_j(\boldsymbol{\rho}'). \tag{1.6}$$

The discretized integral equation is then written as:

$$\sum_{j=1}^{N} I_j \mathcal{L}(b_j) = E_z^i. \tag{1.7}$$

After projecting of both sides of (1.7) on the same set of basis functions, called Galerkin projection, a linear system of N equations and N unknowns I_j is obtained:

$$Z_{ij} I_j = V_i, \;\; i = 1, ..., N, \tag{1.8}$$

with

$$Z_{ij} = < \mathcal{L}(b_j), b_i >, \tag{1.9}$$

$$V_i = < E_z^i, b_i >, \tag{1.10}$$

where the projection was performed by using the inner product $< \cdot, \cdot >$ of the corresponding Hilbert space. The linear system can also be written in matrix form:

$$\overline{\boldsymbol{Z}}\boldsymbol{I} = \boldsymbol{V}. \tag{1.11}$$

Usually, for scattering problems the EFIE-MoM system matrix $\overline{\boldsymbol{Z}}$ is dense. To solve system (1.11) using an iterative method, the computational complexity scales as $RO(N^2)$, which is complexity of one matrix-vector product (MVP) multiplied by the number of iterations R that are required to reach the predefined accuracy. Clearly, this procedure becomes expensive for large scatterers that need to be discretized into a large number of segments N.

1.2.3 Multilevel Fast Multipole Method

One way to deal with the poor scaling properties of the traditional MoM is to exploit the structure of the matrix $\overline{\boldsymbol{Z}}$. Each element of this matrix, as seen from (1.9), describes the interaction between two segments of the scatterer. Instead of considering these N^2 "connections" individually, the scatterer can be subdivided into groups of sources. Interaction between elements in different groups is then performed in three steps. Firstly, during the aggregation step, the aggregated radiated field from many sources b_j residing in a source group g_s is calculated. Secondly, during the translation step, this field is transferred to another observation group g_o. In the last step, called disaggregation step, the incoming field in the observation group g_o is projected onto every observer b_i in that group. In this way, each matrix element can be factorized as [23]:

$$Z_{ij} = D_{i,g_o} T_{g_o,g_s} A_{g_s,j} \tag{1.12}$$

Equation (1.12) is the core of the one-level Fast Multipole Method (FMM), first introduced by Rokhlin [24]. This decomposition is valid only for source and observation groups that are sufficiently separated in space. Otherwise, the electromagnetic interaction needs to be calculated in the classical MoM way. For implementation details, the reader is refered to [18], where it is also shown that the complexity of one MVP can be reduced to $O(N^{1.5})$ [18].
For even better efficiency, one-level FMM is extended to the Multilevel Fast Multipole Method (MLFMM) by hierarchically organizing the groups of sources into a tree-like structure [21]. The computational cost of one MVP calculated in this way can be reduced to $O(N)$[18].

1.3 Uncertainty quantification and stochastic electromagnetic modeling

The term uncertainty quantification (UQ) refers to techniques that quantitatively characterize uncertainties in computational models. An example is the scattering problem of Section 1.2.1, but with a random geometry. The randomness may stem from a non-deterministically known position of the scatterer and/or from variations on the shape of its surface S. Consequently, since $\boldsymbol{\rho}$ and $\boldsymbol{\rho}'$ in the EFIE (1.4) are no longer deterministic, this leads to variability of the current density J_z and of the scattered field.

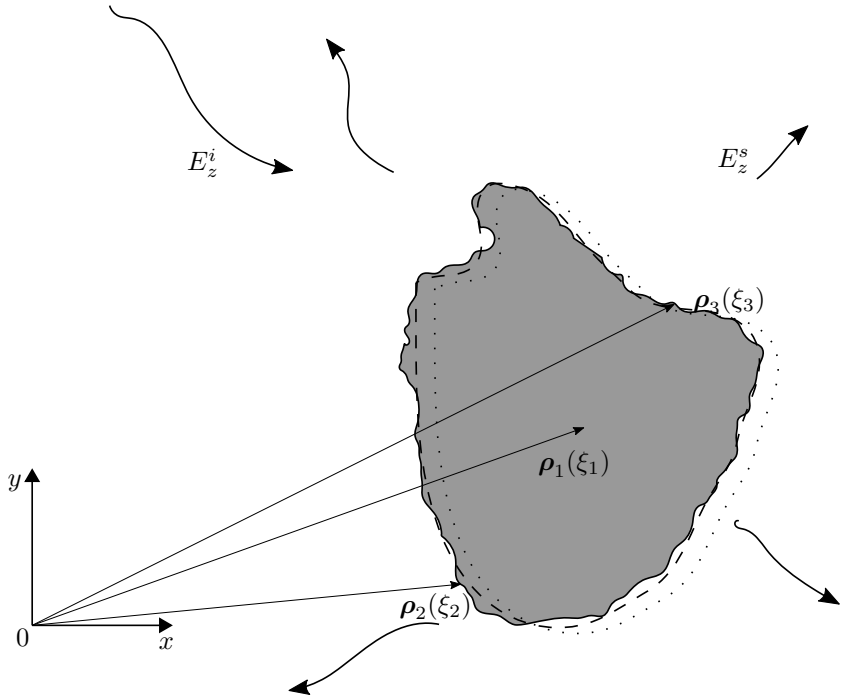

Figure 1.5: An incident electromagnetic wave E_z^i impinges upon an arbitrarily shaped object prone to variability. The randomness is induced by the unknown and random position (dashed) of the nominal structure (dotted) denoted by $\boldsymbol{\rho}_1(\xi_1)$, where ξ_1 is a random variable. Another source of randomness is the roughness of the scatterer which is described by the vectors of unknown points on the surface, e.g. $\boldsymbol{\rho}_2(\xi_2)$ and $\boldsymbol{\rho}_3(\xi_3)$, with ξ_2 and ξ_3 being random variables.

1.3.1 Problem statement

Let assume that the scatterer presented in Fig. 1.4 is prone to variability. Its position is described by random variables (RVs) and/or it possesses a randomly varying rough surface which is also described by a set of RVs as depicted in Fig. 1.5. All these RVs are collected in a vector $\boldsymbol{\xi}$ defined with probability density function (PDF) $W(\boldsymbol{\xi})$ defined over the probabilistic space Ω. Assume, for now, that variables in $\boldsymbol{\xi}$ are mutually independent and that the size of this vector is M. (The case with correlated RVs is treated in Chapter 6.) Given the geometrical variability, all quantities in (1.11) are dependent on $\boldsymbol{\xi}$:

$$\overline{\boldsymbol{Z}}(\boldsymbol{\xi})\boldsymbol{I}(\boldsymbol{\xi}) = \boldsymbol{V}(\boldsymbol{\xi}). \tag{1.13}$$

The system in (1.13) is no longer deterministic, but stochastic. In particular, we can consider the stochastic scattering problem as a system with a given input variability $\boldsymbol{\xi}$ and unknown output variability $\boldsymbol{I}(\boldsymbol{\xi})$. The goal is to find how the input variability propagates through the system.

1.3.2 Monte Carlo method

A standard and traditional technique for UQ is the Monte Carlo (MC) method [9]. This method considers many random realizations of the geometry, i.e. of the surface S. Each such realization is described by a specific value $\boldsymbol{\xi}_g$ of the random vector $\boldsymbol{\xi}$ and, as such, a deterministic MoM system is created:

$$\overline{\boldsymbol{Z}}(\boldsymbol{\xi}_g)\boldsymbol{I}(\boldsymbol{\xi}_g) = \boldsymbol{V}(\boldsymbol{\xi}_g), \tag{1.14}$$

and solved with a standard deterministic solver. From a set of such solutions, one can readily calculate all statistical information, such as mean, variance, PDF, etc. The mean of the random process $\boldsymbol{I}(\boldsymbol{\xi})$ is computed as:

$$\mathtt{E}[\boldsymbol{I}(\boldsymbol{\xi})] = \frac{\sum_{g=1}^{N_s} \boldsymbol{I}(\boldsymbol{\xi}_g)}{N_s}, \tag{1.15}$$

where N_s represents the number of MC realizations. The operator $\mathtt{E}[\cdot]$ denotes the mathematical averaging or mean. The variance is calculated as:

$$\mathtt{Var}[\boldsymbol{I}(\boldsymbol{\xi})] = \frac{\sum_{g=1}^{N_s} |\boldsymbol{I}(\boldsymbol{\xi}_g) - \mathtt{E}[\boldsymbol{I}(\boldsymbol{\xi})]|^2}{N_s - 1}. \tag{1.16}$$

MC is robust and easy to implement. Unfortunately, it converges relatively slowly with a rate of $O(1/\sqrt{N_s})$. Consequently, a large number of repetitive executions of the deterministic solver is required, which can rapidly become intractable in the case of full-wave scattering problems.

1.3.3 Generalized Polynomial Chaos

Contrary to the MC method, which is a sampling-based method as the many realizations $\boldsymbol{\xi}_g$ are sampled according to PDF $W(\boldsymbol{\xi})$, there are also methods that fall into the category of non-sampling-based methods. One of them is the perturbation method, where the output variability is expanded as a Taylor series around the mean value [8]. The problem with this method is that it can only handle small variations and it cannot take the variability over the whole random space into account.
A more elegant way to quantify the output variability is by means of polynomial representations. The generalized Polynomial Chaos (gPC) approach was developed by Ghanem and inspired by the theory of Wiener [25]. The idea is to represent a stochastic process as a linear combination of orthogonal (in our case orthonormal) basis functions, namely polynomials. The polynomial basis is chosen according to the Wiener-Askey scheme [26]. In this scheme, different polynomials are orthogonal with respect to different weighting functions. In the case of gPC, these weighting functions are the pertinent PDFs. If output variation is smooth enough that can be represented with polynomials, then optimal convergence is achieved, if, for example, Hermite polynomials, are chosen for Gaussian distributions, Legendre polynomials for uniform distribution, Laguerre polynomials for Beta distributions, etc.

In the case of scattering problems, stochastic process $\boldsymbol{I}(\boldsymbol{\xi})$ is subjected to Polynomial Chaos Expansion (PCE) [27]:

$$\boldsymbol{I}(\boldsymbol{\xi}) \approx \sum_{k=0}^{K} \boldsymbol{I}_k \phi_k(\boldsymbol{\xi}), \tag{1.17}$$

where $\boldsymbol{I}_k$ is an (as yet unknowns) PCE coefficient and $\phi_k(\boldsymbol{\xi})$ represents a multivariate polynomial ($k = 0, ..., K$). These multivariate polynomials are created as products of univariate polynomials, as follows:

$$\phi_k(\boldsymbol{\xi}) = \prod_{i=1}^{M} \phi_i^{i_k}(\xi_i), \tag{1.18}$$

where $\phi_i^{i_k}$ is the i-th univariate polynomial, chosen according to the Wiener-Askey scheme, dependent on the single RV ξ_i. This polynomial is of order i_k. The total polynomial order of the multivariate polynomial $\phi_k(\boldsymbol{\xi})$ is given by:

$$P = \sum_{i=1}^{M} i_k. \tag{1.19}$$

For a predefined maximum polynomial order P, called *total degree*, the number of polynomials that can be created and used in (1.17) is given by:

$$K + 1 = \frac{(M + P)!}{M!P!} \approx \frac{M^P}{P!}. \tag{1.20}$$

It is clearly visible that the number of polynomials $K + 1$ grows rapidly with the number of RVs M and this introduces the so-called curse of dimensionality to the gPC approach. Once the PCE coefficients $\boldsymbol{I}_k$ are known, one can easily find the mean and the variance [28]:

$$\mathtt{E}[\boldsymbol{I}(\boldsymbol{\xi})] = \boldsymbol{I}_0, \tag{1.21}$$

$$\mathtt{Var}[\boldsymbol{I}(\boldsymbol{\xi})] = \sum_{k=1}^{K} |\boldsymbol{I}_k|^2. \tag{1.22}$$

The advantage of gPC compared to MC is its much better convergence.

1.3.3.1 Numerical integration

The PCE coefficient can be calculated via projection:

$$\boldsymbol{I}_k =< \boldsymbol{I}(\boldsymbol{\xi}), \phi_k(\boldsymbol{\xi}) >= \int_{\boldsymbol{\xi}} \boldsymbol{I}(\boldsymbol{\xi}) \phi_k(\boldsymbol{\xi}) W(\xi) d\boldsymbol{\xi}. \tag{1.23}$$

This involves a multidimensional integration over M dimensions. Standard integration schemes in one dimension are often based on Gauss quadrature rules [29]. The

integral is then approximated by a weighted sum of function values. For example, the 1D integration of a function $f(x)$ with weighting function $w(x)$ within the domain $x \in]-B, B[$ is evaluated as:

$$\int_{-B}^{B} f(x)\, w(x)\, dx = \sum_{i=1}^{n} w_i\, f(x_i), \tag{1.24}$$

and w_i and x_i are the weights and nodes resp., chosen according to the weighting function. The limits of integration are, e.g. $B = 1$ for uniform distribution and $B = \infty$ for Gaussian distribution. The number of weights and nodes n determines the accuracy. In the M-dimensional case, if over each dimension, the integration is performed using n quadrature points, then the total number of points is n^N. This approach is called the full tensor-product integration. Even when a small number of points is used in each dimension, e.g. $n = 2$, the total number of points for, e.g., $M = 30$ is already $2^{30} > 10^9$, which is prohibitively high.
Sparse grids are methods proposed to avoid this huge number of integration points. They are based on Smolyak's algorithm, which chooses a subset of points from tensor products [30]. The problem with this method is that the integration weights can become negative. For functions that are not smooth enough, this can lead to physically impossible results [31].
Note that, to calculate the coefficient corresponding to the polynomial with order P, the integration rule needs to be exact to, at least, order $2P$. Even though the number of points is reduced by using sparse grids, the curse of dimensionality remains, as the total number of Smolyak integration points needed to integrate polynomials up to polynomial order $2P + 1$ is still [32]:

$$N_{Smolyak} \approx \frac{2^P}{P!} M^P. \tag{1.25}$$

For high dimensional problems, due to this curse of dimensionality, sometimes MC remains the only acceptable choice for UQ.
Besides Smolyak's rule, Stroud's rules can be used. This rule produce the smallest number of integration points for a given dimension [32]. Unfortunately, these integration rules are only suitable for PCE with a polynomial order that does not exceed 1.

1.3.3.2 Intrusive and non-intrusive methods

Whithin the framework of gPC, there are two classes of methods for the UQ of the output variability: intrusive and non-intrusive methods [28]. Non-intrusive methods rely on (1.23), i.e. one finds projection coefficients of the output quantity $\boldsymbol{I}(\boldsymbol{\xi})$ by using an integration scheme. The advantage of this method is that it is easy to apply, much like MC, it can be considered as a sampling based method, in the sense that it requires reusing a traditional deterministic solver to asses several realizations of the random process, chosen according to the nodes of the integration scheme. Contrary to MC, these realization points are not random, but chosen smartly according to the

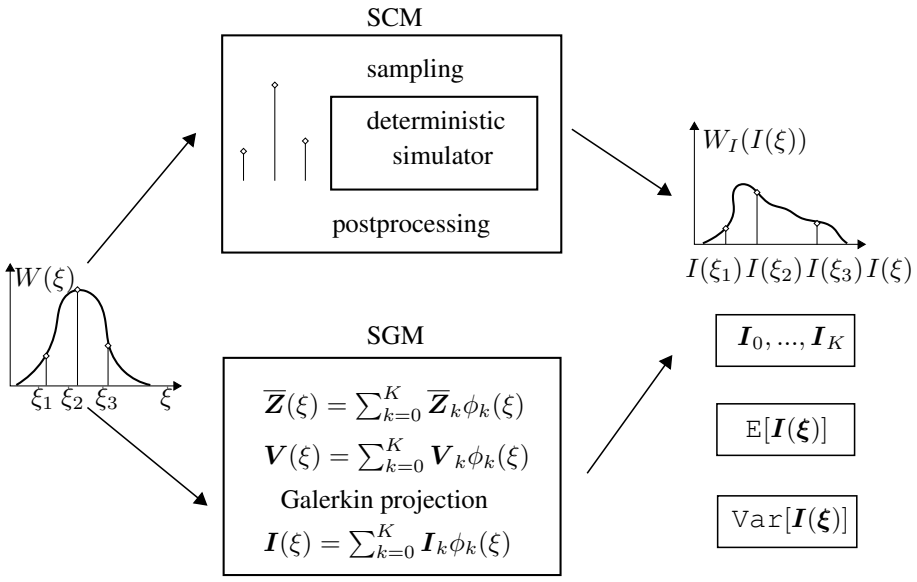

Figure 1.6: Schematic representation of the non-intrusive collocation (upper) and intrusive stochastic Galerkin (bottom) method. The output quantities of both methods are PDF, PCE coefficients, mean, variance.

PDF, such that good convergence of the result is preserved. This method is often called the Stochastic Collocation Method (SCM). Note that, in literature, a difference between collocation methods based on integration by using Smolyak points (pseudo spectral approach) and an approximation of polynomials with Lagrange interpolation is described [33].

In an intrusive approach, the computational model is changed. Schematically, the difference between intrusive and non-intrusive methods is presented in Fig. 1.6. A well established intrusive technique is the Stochastic Galerkin Method (SGM), described in the next chapters. In this method, all quantities ($\overline{\boldsymbol{Z}}(\boldsymbol{\xi})$, $\boldsymbol{V}(\boldsymbol{\xi})$ and $\boldsymbol{I}(\boldsymbol{\xi})$) in (1.13) are represented via PCE and the unknown coefficients $\boldsymbol{I}_k$ are found via Galerkin projection. Contrary to SCM, where many uncoupled deterministic systems are solved, in the SGM method, $K+1$ coupled deterministic equations need to be solved. The deterministic complexity of the SCM scales with $N_{Smolyak}$. For SGM, the discussion of the complexity is not so straightforward, as it largely depends on the specific problem and the (implementation of the) algorithm. Comparison of SCM and SGM for several scattering problems can be found in the next chapters and it will be shown that SGM scales with the number of polynomials $K+1$, and outperform SCM $K < N_{Smolyak}$.

For completeness it is mentioned that members of the UQ community also focus on non-intrusive methods that are combined with Analysis of Variance (ANOVA) [34], L_1 sparse approximation [35] and low rank tensor recovery [36]. Recently, the Stochastic Testing (ST) method was developed and this method can either be intrusive or non-intrusive depending its implementation [37].

1.4 Outline of the thesis

This thesis is divided into eight chapters, of which this introduction is the first one.
The second chapter deals with the intrusive SGM and its combination with the MoM. An efficiency and accuracy analysis is performed and the results are compared with the non-intrusive SCM and with MC. Combination of MoM and SGM was already investigated in the context of interconnect problems, but here we study full-wave scattering problems.
The next chapter introduces the novel method that leverages MLFMM, as the motivation of our work is to develop fast and efficient methods for scattering problems. The theoretical framework is developed and applied to geometrical structures described by *independent* random variables. A comparison with the SGM-MoM of Chapter 2 with focus on the computation of one matrix-vector product (MVP), reveals that MLFMM can hugely accelerate the SGM-MoM.
To speed up the iterative solution of the linear system evolving from the MLFMM-accelerated MoM, a preconditioner is specially developed for the novel SGM-MLFMM formalism. This part is covered in Chapter 4.
Still, for certain problems, the SGM-MLFMM needs to deal with many unknowns, which cannot be stored and handled by one computational node. Chapter 5 introduces the parallelization of the novel stochastic method. To show the necessity of the developed parallelization strategy, extremely large optical systems, prone to variability, are simulated. A thorough CPU timing and parallel scalability analysis is presented.
Combination of MLFMM and SGM for *correlated* random variables, e.g. needed to describe the rough surfaces, is presented in Chapter 6. Often, the standard Karhunen-Loève transformation is used to decorrelates the random variables, but we show that Cholesky decomposition is a better choice in case of scattering at rough surfaces. In particular, for low correlation lengths this lead to a considerable reduction of the setup and solution time.
Whereas Chapters 2-6 put more emphasis on intrusive methods, Chapter 7 describes a state-of-the art non-intrusive method, based on tensor-train (TT) decomposition. It is shown that the hybridization of this TT method with a Statistical Moment Preserving Model Order Reduction (SMOR) approach, may lead to efficient ways to tackle the UQ of scattering problems.
Finally, in Chapter 8, the main conclusions and an outline for future research are given.

References

[1] S. Natarajan, M. Breuer, and S. Gupta, "Process variations and their impact on circuit operation", in *1998 IEEE International Symposium on Defect and Fault Tolerance in VLSI Systems,*, Nov. 1998, pp. 73–81.

[2] D. S. Boning and S. Nassif, "Models of process variations in device and interconnect", in *Design of High Performance Microprocessor Circuits, chapter 6*, IEEE Press, 1999.

[3] C. Shin, X. Sun, and T.-J. K. Liu, "Study of random-dopant-fluctuation (RDF) effects for the trigate bulk mosfet", *IEEE Transactions on Electron Devices,*, vol. 56, no. 7, pp. 1538–1542, Jul. 2009.

[4] M. Rossi, S. Agneessens, H. Rogier, and D. V. Ginste, "Stochastic analysis of the impact of substrate compression on the performance of textile antennas", *IEEE Transactions on Antennas and Propagation*, IEEE Early Access, 2016, DOI 10. 1109 / TAP. 2016. 2543780.

[5] S. Hinaga, M. Koledintseva, P. Anmula, and J. Drewniak, "Effect of conductor surface roughness upon measured loss and extracted values of PCB laminate material dissipation factor", in *Proc. IPC 2009 APEX/EXPO Conference*, Las Vegas, Mar. 2009, pp. 14–15.

[6] V. Wiaux, "Double-patterning-compliant split and design", *SPIE Newsroom*, Feb. 2009. [Online]. Available: `http://spie.org/newsroom/technical-articles-archive/1430-double-patterning-compliant-split-and-design`.

[7] *The (design) house always wins—how dfm improves the odds of tapeout success*, `http://chipdesignmag.com/display.php?articleId=4616`.

[8] T. El-Moselhy, "Field solver technologies for variation-aware interconnect parasitic extraction", PhD thesis, Massachusetts Institute of Technology, 2010.

[9] G. C. Fishman, *Monte Carlo: Concepts, Algorithms, and Applications*. New York: Springer-Verlag, 1996.

[10] D. Vande Ginste, D. De Zutter, D. Deschrijver, T. Dhaene, P. Manfredi, and F. Canavero, "Stochastic modeling-based variability analysis of on-chip interconnects", *IEEE Transactions on Components, Packaging and Manufacturing Technology*, vol. 2, no. 7, pp. 1182–1192, Jul. 2012.

[11] P. Manfredi, D. Vande Ginste, D. De Zutter, and F. Canavero, "Uncertainty assessment of lossy and dispersive lines in spice-type environments", *IEEE Transactions on Components, Packaging and Manufacturing Technology,*, vol. 3, no. 7, pp. 1252–1258, Jul. 2013.

[12] A. Biondi, D. Vande Ginste, D. De Zutter, P. Manfredi, and F. Canavero, "Variability analysis of interconnects terminated by general nonlinear loads", *IEEE Transactions on Components, Packaging and Manufacturing Technology,*, vol. 3, no. 7, pp. 1244–1251, Jul. 2013.

[13] Q. Su and K. Strunz, "Stochastic circuit modelling with hermite polynomial chaos", *Electronics Letters*, vol. 41, no. 21, pp. 1163–1165, 2005.

[14] C. Chauvière, J. S. Hesthaven, and L. C. Wilcox, "Efficient computation of RCS from scatterers of uncertain shapes", *IEEE Transactions on Antennas and Propagation*, vol. 55, no. 5, pp. 1437–1448, May 2007.

[15] A. Austin and C. Sarris, "Efficient analysis of geometrical uncertainty in the FDTD method using polynomial chaos with application to microwave circuits", *IEEE Transaction on Microwave Theory and Techniques*, vol. 61, no. 12, pp. 4293–4301, Dec. 2013.

[16] T. El-Moselhy and L. Daniel, "Variation-aware stochastic extraction with large parameter dimensionality: Review and comparison of state of the art intrusive and non-intrusive technique", in *2011 12th International Symposium on Quality Electronic Design (ISQED 2011), 14-16 March 2011, Santa Clara, CA, USA*, 2011, pp. 508–517.

[17] T. El-Moselhy and L. Daniel, "Stochastic integral equation solver for efficient variation-aware interconnect extraction", in *2008 45th ACM/IEEE Design Automation Conference*, vol. 1 and 2, 2008, pp. 415–420.

[18] W. C. Chew, J. M. Jin, E. Michielssen, and J. Song, *Fast and Efficient Algorithms in Computational Electromagnetics*. Norwood, MA: Artech House, 2001.

[19] J. Maxwell, "On physical lines of force", *Philosophical Magazine*, vol. 90, pp. 11–23, 2010.

[20] C. A. Balanis, *Advanced Engineering Electromagnetics*. New York: Wiley, 1989.

[21] W. C. Gibson, *The Method of Moments in Electromagnetics*. CRC press, 2008.

[22] R. F. Harrington, *Field Computation by Moment Methods*. New York: IEEE Press, 1993.

[23] D. Vande Ginste, "Perfectly matched layer based fast multipole methods for planar microwave structures", PhD thesis, Ghent University, 2005.

[24] V. Rokhlin, "Rapid solution of integral equations of classical potential theory", *Journal of Computational Physics*, vol. 60, no. 2, pp. 187 –207, 1985.

[25] R. G. Ghanem and P. D. Spanos, *Stochastic Finite Elements. A Spectral Approach*. New York: Springer-Verlag, 1991.

[26] D. B. Xiu and G. E. Karniadakis, "The Wiener-Askey polynomial chaos for stochastic differential equations", *SIAM Journal on Scientific Computing*, vol. 24, no. 2, pp. 619–644, 2002.

[27] F. Heiss and V. Winschel, "Likelihood approximation by numerical integration on sparse grids", *Journal of Econometrics*, vol. 144, no. 1, pp. 62–80, May 2008.

[28] D. Xiu, "Fast numerical methods for stochastic computations: A review", *Communications in Computational Physics*, vol. 5, no. 2-4, pp. 242–272, Feb. 2009.

[29] J. H. W. Gene H. Golub, "Calculation of gauss quadrature rules", *Mathematics of Computation*, vol. 23, no. 106, 221–s10, 1969.

[30] S. Smolyak, "Quadrature and interpolation formulas for tensor products of certain classes of functions", *Doklady Akademii Nauk SSSR*, vol. 4, pp. 240–243, 1963.

[31] P. Tsuji, D. Xiu, and L. Ying, "Fast method for high-frequency acoustic scattering from random scatterers", *International Journal for Uncertainty Quantification*, vol. 1, no. 2, pp. 99–117, 2011.

[32] D. Xiu and J. S. Hesthaven, "High-order collocation methods for differential equations with random inputs", *SIAM Journal on Scientific Computing*, vol. 27, no. 3, pp. 1118–1139, 2005.

[33] D. Xiu, "Efficient collocational approach for parametric uncertainty analysis", *Communications in Computational Physics*, vol. 2, no. 2, pp. 293–309, Apr. 2007.

[34] Z. Zhang, X. Yang, I. V. Oseledets, G. E. Karniadakis, and L. Daniel, "Enabling high-dimensional hierarchical uncertainty quantification by ANOVA and tensor-train decomposition", *CoRR*, vol. abs/1407.3023, 2014.

[35] J. Hampton and A. Doostan, "Compressive sampling of polynomial chaos expansions: Convergence analysis and sampling strategies", *Journal of Computational Physics*, vol. 280, pp. 363–386, Jan. 2015.

[36] Z. Zhang, H. D. Nguyen, K. Turitsyn, and L. Daniel, "Probabilistic power flow computation via low-rank and sparse tensor recovery", *CoRR*, vol. abs/1508.02489, 2015.

[37] Z. Zhang, T. A. El-Moselhy, I. M. Elfadel, and L. Daniel, "Stochastic testing method for transistor-level uncertainty quantification based on generalized polynomial chaos", *Trans. Comp.-Aided Des. Integ. Cir. Sys.*, vol. 32, no. 10, pp. 1533–1545, Oct. 2013.

2

Scattering from two-dimensional objects of varying shape combining the method of moments with the stochastic Galerkin method

Zdravko Zubac, Daniël De Zutter and Dries Vande Ginste

Published in IEEE Transactions on Antennas and Propagation, vol. 62, no. 9, pp. 4852–4856, Sep. 2014.

★ ★ ★

In this chapter, the Electric Field Integral Equation for perfect electrically conducting scatterers is combined with the Stochastic Galerkin Method (SGM) to model the impact of stochastic variations of the shape of the scatterer on the radar cross-section and on the induced current distribution. The SGM is compared to the Stochastic Collocation Method (SCM) and it is shown that for a modest number of random variables the SGM is a good alternative to the SCM.

2.1 Introduction

Electromagnetic solvers are widely used in the analysis of scattering and remote sensing problems as well as in the analysis and design of antennas and high-speed systems, to model electromagnetic compatibility problems and in many other domains. The straightforward way to assess the influence of geometrical or material variations and uncertainties with these solvers is by implementing Monte Carlo (MC) simulations. The major drawback of MC is the slow convergence at a rate of $1/\sqrt{n}$, where n is the number of separate runs of the code. More sophisticated methods have been proposed based on the expansion of the quantities of interest into a (truncated) polynomial chaos expansion (PCE) using orthogonal polynomials depending on the particular distribution of the random variables [1]. These methods come in two flavors: the non-intrusive Stochastic Collocation Method (SCM) [2] and the intrusive Stochastic Galerkin Method (SGM) [3]. PCE-based methods are already used for variability analysis of (on-chip) interconnects [4][5][6]. Very recently, polynomial chaos was introduced in the Finite Difference Time Domain (FDTD) analysis of microwave circuits [7]. Furthermore, a thorough discussion of the use of a PCE-method, more particularly a multi-element SCM, for statistical EMC/EMI characterization, was presented in [8]. Calculation of the statistical properties of two-dimensional electromagnetic scattering from random rough surfaces combining the MC approach with a deterministic method of moments simulator is discussed in [9]. In view of the superiority of PCE-based methods over MC simulations, [10] presents the combination of the SCM with a time-domain Finite Element technique for scattering by two- and three-dimensional perfectly electrically conducting objects of varying shape.
In view of previous work, in particular [8], this chapter focusses on the use of the SGM as compared to the SCM to model stochastic scattering problems by means of integral equations and the Method of Moments (MoM). To the best knowledge of the authors, this communication is the first to discuss the SGM-MoM combination for scattering problems. We restrict ourselves to frequency domain scattering by two-dimensional PEC objects under TM-incidence to keep this communication sufficiently succinct. In order to see what the benefits and drawbacks of SGM are compared to SCM, of course we also provide the necessary numerical data to compare both approaches. Furthermore, we do not only present results for the radar cross-section, but also pay attention to the current distribution on the scatterer.
Section II first briefly introduces the electric field integral equation and its MoM discretization. Next, a discussion is provided on the polynomial chaos expansion in the MoM, with particular emphasis on the differences between SGM and SCM. In Section III, two pertinent examples are discussed in detail. In these examples we consider different distributions: uniform and uncorrelated in the first example and correlated with a Gaussian covariance matrix in the second example. Conclusions are formulated in Section IV.

2.2 The stochastic scattering problem

We consider two-dimensional frequency domain scattering by PEC objects, residing in free space, the geometry of which is not deterministic but varies stochastically. The z-axis is the axis of invariance. The incident wave is a TM-polarized plane wave with electric field $\boldsymbol{E}^i = E^i \mathbf{u}_z$. The $e^{j\omega t}$-dependence is suppressed. To determine the scattered field, we apply a surface integral equation technique. Although the electrical field integral equation (EFIE) can be used for both open and closed structures, the combined field integral equation (CFIE) is preferred for closed structures to avoid spurious resonances. For brevity, we assume that the reader is familiar with the EFIE. This integral equation can be solved by the MoM. N pulse basis functions $b_j, j = 1, 2, ..., N$, are introduced to expand the unknown surface current density J_z on the PEC scatterer as:

$$J_z(\boldsymbol{\rho}') = \sum_{j=1}^{N} I_j b_j(\boldsymbol{\rho}'), \tag{2.1}$$

with I_j the unknown expansion coefficients. Applying a Galerkin testing procedure then yields a $N \times N$ linear system in the unknown expansion coefficients I_j:

$$\sum_{j=1}^{N} Z_{ij} I_j = V_i, \quad i = 1, 2, ..., N \qquad \text{or} \qquad \overline{\boldsymbol{Z}}\boldsymbol{I} = \boldsymbol{V}. \tag{2.2}$$

We do not give the explicit expressions for $\overline{\boldsymbol{Z}}$ and $\boldsymbol{V}$ as the readers are undoubtedly familiar with them. Now suppose the scatterer is not defined deterministically but has a geometry which exhibits some inherent variability. This variability is described by a set of M random variables. We assume that these variables are independent random variables which are collected in the vector $\boldsymbol{\xi} = [\xi_1\ \xi_2\ ...\ \xi_M]$. The case of correlated variables can be treated as well by starting from a properly defined set of independent variables or, for Gaussian random variables, by adopting a Karhunen-Loève transformation (KLT) [11]. All quantities in (2.2) now depend on $\boldsymbol{\xi}$, i.e:

$$\overline{\boldsymbol{Z}}(\boldsymbol{\xi})\boldsymbol{I}(\boldsymbol{\xi}) = \boldsymbol{V}(\boldsymbol{\xi}). \tag{2.3}$$

The goal of solving (2.3) is to determine the full statistics of the induced currents, of the scattered fields, and in particular of the radar cross-section (RCS). To this end, all quantities of interest are represented in terms of a truncated polynomial chaos expansion

$$Z_{ij}(\boldsymbol{\xi}) = \sum_{k=0}^{K} Z_{ij,k}\phi_k(\boldsymbol{\xi}), \tag{2.4a}$$

$$V_i(\boldsymbol{\xi}) = \sum_{k=0}^{K} V_{i,k}\phi_k(\boldsymbol{\xi}), \qquad I_j(\boldsymbol{\xi}) = \sum_{k=0}^{K} I_{j,k}\phi_k(\boldsymbol{\xi}), \tag{2.4b}$$

where $Z_{ij,k}$, $V_{i,k}$ and $I_{j,k}$ are expansion coefficients and the $\phi_k(\boldsymbol{\xi})$ are multivariate polynomials that are orthonormal with respect to the probabilistic density functions relevant to the particular scattering problem that is treated. Hence, $< \phi_j(\boldsymbol{\xi}), \phi_k(\boldsymbol{\xi}) >= \delta_{jk}$,

with the inner product $< f(\boldsymbol{\xi}), g(\boldsymbol{\xi}) >$ defined as

$$< \quad f(\boldsymbol{\xi}), g(\boldsymbol{\xi}) \quad >= \int_{\xi_1} \cdots \int_{\xi_M} f(\boldsymbol{\xi}) g(\boldsymbol{\xi}) W(\boldsymbol{\xi}) d\xi_1 \cdots d\xi_M \tag{2.5}$$

and with $\delta_{jk} = 0$ for $j \neq k$ and $\delta_{jk} = 1$ for $j = k$. $W(\boldsymbol{\xi})$ is the probability density function associated with the random vector $\boldsymbol{\xi}$. As we work with independent stochastic variables, W is the product of the probability density functions $W_m, m = 1, 2, .., M$, of the individual random variables ξ_m. The polynomials $\phi_k(\boldsymbol{\xi})$ themselves are constructed as products of univariate polynomials only depending on a single random variable. For each multivariate polynomial, the *total degree*, i.e. the sum of the orders of the univariate polynomials, is at most P. This maximum order is a parameter that we can choose. The number M of random variables determines the number $K + 1$ of multivariate polynomials as follows:

$$K + 1 = \frac{(M + P)!}{M!P!}. \tag{2.6}$$

$Z_{ij,k}$ and $V_{i,k}$ in (2.4) are obtained through projection:

$$V_{i,k} =< V_i(\boldsymbol{\xi}), \phi_k(\boldsymbol{\xi}) >, \quad Z_{ij,k} =< Z_{ij}(\boldsymbol{\xi}), \phi_k(\boldsymbol{\xi}) > . \tag{2.7}$$

By substituting (2.4) into (2.2), we get

$$\sum_{k=0}^{K} V_{i,k} \phi_k(\boldsymbol{\xi}) = \sum_{j=1}^{N} \sum_{k=0}^{K} \sum_{l=0}^{K} Z_{ij,k} I_{j,l} \phi_k(\boldsymbol{\xi}) \phi_l(\boldsymbol{\xi}), \qquad \forall\, i. \tag{2.8}$$

Galerkin projection of both sides of (2.8) on ϕ_m finally leads to the following set of equations for the $I_{j,k}$ in (2.4b)

$$\tilde{\boldsymbol{V}} = \tilde{\overline{\boldsymbol{Z}}} \tilde{\boldsymbol{I}}, \tag{2.9}$$

where $\tilde{\overline{\boldsymbol{Z}}}$ is a deterministic matrix given by

$$\tilde{\overline{\boldsymbol{Z}}} = \sum_{k=0}^{K} \left(\begin{pmatrix} \gamma_{k00} & \gamma_{k10} & \cdots & \gamma_{kK0} \\ \gamma_{k01} & \gamma_{k11} & \cdots & \gamma_{kK1} \\ \vdots & \vdots & \ddots & \vdots \\ \gamma_{k0K} & \gamma_{k1K} & \cdots & \gamma_{kKK} \end{pmatrix} \otimes \overline{\boldsymbol{Z}}_k \right), \tag{2.10}$$

with $\gamma_{klm} =< \phi_k(\boldsymbol{\xi}) \phi_l(\boldsymbol{\xi}), \phi_m(\boldsymbol{\xi}) >$ and where $\otimes$ stands for the Kronecker product of matrices. The $N \times N$ matrix $\overline{\boldsymbol{Z}}_k$ is similar to $\overline{\boldsymbol{Z}}$ in (2.2), but with the Z_{ij} replaced by $Z_{ij,k}$; $\tilde{\boldsymbol{V}}^T = [V_{1,0}...V_{N,0}V_{1,1}...V_{N,1}...V_{1,K}...V_{N,K}]$ and similarly for $\tilde{\boldsymbol{I}}$. Eqn. (2.10) shows that the application of the SGM leads to a new system matrix the size of which is now much larger, i.e. $(K+1)N \times (K+1)N$ instead of $N \times N$. However, this new system is deterministic, as thanks to the Galerkin projection the dependence on $\boldsymbol{\xi}$ has vanished. Solving (2.9) yields $\tilde{\boldsymbol{I}}$. Inserting this solution into (1.4.b) then yields the full

statistics of the induced current. For example, the mean value of this current on the j-th segment ($j = 1, 2, ..., N$) is given by

$$\mathrm{E}[I_j(\boldsymbol{\xi})] = I_{j,0}, \tag{2.11}$$

where $\mathrm{E}[\cdot]$ denotes the expected value operator. The variance is computed as

$$\mathrm{E}[|I_j(\boldsymbol{\xi}) - \mathrm{E}[I_j(\boldsymbol{\xi})]|^2] = \sum_{k=1}^{K} |I_{j,k}|^2. \tag{2.12}$$

Besides the above stochastic moments, the probability density functions (PDF) and cumulative distribution functions (CDF) can also be readily computed from (2.4). Obviously, the SGM, presented above, is an intrusive method. The Stochastic Collocation Method (SCM) is non-intrusive. We refer the reader to [8] for details. In the SCM any quantity of interest $f(\boldsymbol{\xi})$ is expanded as:

$$f(\boldsymbol{\xi}) = \sum_{k=0}^{K} f_k \phi_k(\boldsymbol{\xi}), \tag{2.13a}$$

$$f_k = < f(\boldsymbol{\xi}), \phi_k(\boldsymbol{\xi}) > \approx \sum_{r=1}^{N_p} w_r f(\boldsymbol{\xi}_r) \phi_k(\boldsymbol{\xi}_r), \tag{2.13b}$$

where w_r and $\boldsymbol{\xi}_r$ are the weights and sampling points of the quadrature. Consequently, in the SCM, the desired statistical information is obtained by knowledge of the solution of (2.3) in N_p sampling points in the M-dimensional space of the random variables $\boldsymbol{\xi}$. The SCM can thus easily be built on top of a deterministic code by solving N_p deterministic problems (2.2).

2.3 Numerical examples

2.3.1 Scattering by a finite periodic array of PEC strips

As a first example, consider TM-scattering by a periodic but finite array of five PEC strips as depicted in Fig. 2.1. The x-coordinates of the position vectors of the centers of the strips remain fixed with constant spacing T. However, the widths of the strips w and their heights h w.r.t. a nominal plane are chosen to be independent uniformly distributed random variables, hence $M = 10$. The widths of the strips vary between $0.2T$ and $0.8T$, with $T = 3\lambda/4$, and the heights of the strips between $-\lambda/10$ and $\lambda/10$, where λ is the wavelength of the incident wave. In the MoM analysis, the discretization of each strip will be chosen fine enough and such that the number of divisions remains identical when considering varying widths.

As uniform distributions are considered, normalized Legendre polynomials are the appropriate functions to model the uncertainty. This implies that in (2.5), the multivariate polynomials $\phi_j(\boldsymbol{\xi})$ are constructed as products of univariate Legendre polynomials.

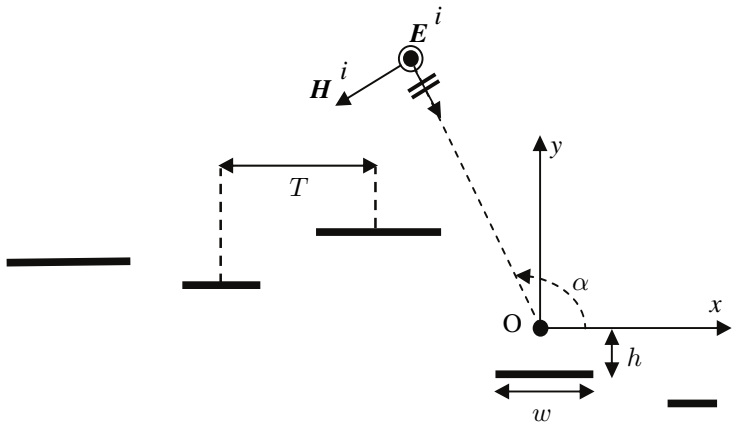

Figure 2.1: Periodic array of PEC strips. Widths w and heights h are random.

When calculating the matrix elements in (2.3) or (2.9), elements describing MoM interactions on the same strip only depend on a single random variable, i.e. the width, and all other matrix elements depend on four random variables, the two heights and the two widths. The right hand side data depend on two random variables. The incident wave is a TM-polarized plane wave impinging under an angle $\alpha = 3\pi/4$ with the positive x-axis.

The current on each of the five strips is modeled using 20 equal length subdivisions on which the current is taken to be constant, i.e. the total number of unknowns in the MoM is $N = 100$. For this example and the following ones, the quantities of interest (surface current, RCS, impedance matrix elements) are modeled using expansions of type (2.13a) with highest polynomial order, i.e. total degree, $P = 4$. Our experience shows that $P = 4$ suffices to accurately describe the wanted statistics. To assess the effect of this total degree, below, results for $P = 4$ will be compared to results for $P = 1$, $P = 2$ and $P = 3$. Due to the fact that calculating the expansion coefficients according to (2.13b) implies that, for $P = 4$, up to eight-order polynomials play a role, we opt for an integration scheme that assures correct integration up to and including order 9. When lowering the total degree P, we lower the accuracy of the integration scheme at the same time, as such using the most optimal approach.

Both in SGM and in SCM we have to calculate integrals of the form (2.13b) to obtain the expansion coefficients of the quantities of interest. In the present example, these integrals are integrals over a 10-dimensional parameter space. Naive application of Gauss-Legendre quadrature with 5 sampling points (to assure exact integration for polynomials up to order 9) leads to $N_p = 5^{10}$ sampling points in (2.13b). This huge number can however be avoided by applying Smolyak's rule. Smolyak's rule or Smolyak integration is a sparse grid technique to integrate high dimensional functions [12]. This particular sparse grid technique only requires $N_p = 8761$ sampling points for about the same accuracy, i.e. a reduction by more than a factor of 1000. For smaller values of P, even less Smolyak points are needed: $N_p = 21$ for $P = 1$, $N_p = 221$ for

$P = 2$ and $N_p = 1581$ for $P = 3$.
From (2.6), including multivariate polynomials up to total degree $P = 4$ in SGM, implies that $K+1 = 1001$. To find the $Z_{ij,k}$ in (2.8), Smolyak's rule requires $N_p \times N^2$ interaction integrals to be calculated followed by the solution of a *single* linear system (2.9) of dimension $(K+1)N \times (K+1)N$.
On the other hand, applying SCM again consists in calculating $N_p \times N^2$ MoM interaction integrals and the solution of not a single but of N_p linear systems of size $N \times N$. It is immediately clear that straightforward application of SGM leads to a numerical effort which vastly exceeds that of SCM. However, the purpose of the present example is to demonstrate that the above conclusion is not necessarily unavoidable when taking the particular nature of the considered problem into account. Indeed, remark that the Z_{ij} only depend on the width, when considering interactions on the *same* strip. For strip to strip interactions only four variables matter. Thus, in SGM, we do not need to consider the full ten-dimensional parameter space and this has a very considerable impact on the CPU-time as will become clear from the numerical results.
Before turning to these numerical results, let us also point out the following. Iteratively solving the large linear system (2.9) not only requires a lot of CPU-time but storing all matrix elements can lead to very high (or even impossibly high) memory requirements. To alleviate this problem, we only store the $Z_{ij,k}$ of matrix $\overline{\boldsymbol{Z}}_k$ in (2.10). It so turns out that quite a large number of the γ_{klm} also needed in (2.10) are zero. The non-zero ones can easily be stored and the Kronecker product is then calculated on-the-fly when iteratively solving (2.9).

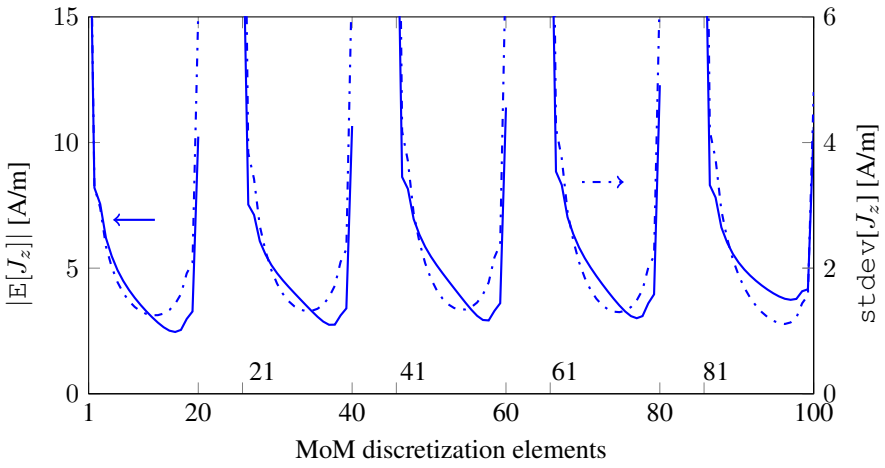

Figure 2.2: Magnitude of the mean value (full line) and standard deviation (dash-dotted line), of the current distribution for total degree $P = 4$ for the example of Fig. 2.1.

For $P = 4$, Fig. 2.2 shows the magnitude of the mean value $|\mathbb{E}(J_z)|$ (2.11) and the standard deviation (stdev) of the induced current, i.e. the square root of the variance defined in (2.12). Results for SGM, SCM and MC are indistinguishable on the scale of

the figure. For both SGM and SCM, CPU-time and memory requirements are given in Table 2.1 as a function of P, together with the mean value and variance of the absolute value of the center current on subdivision 10. For this particular example, the MC analysis was performed using 5×10^4 samples. The values obtained with SCM and

Table 2.1: Simulation data for the PEC strip array

method	P	memory	CPU-time	mean	variance
SGM	1	1.7 MB	3.8 s	3.5420	1.6726
SGM	2	10.3 MB	34.8 s	3.5527	1.7034
SGM	3	45.7 MB	290 s	3.5376	1.7177
SGM	4	172 MB	50 m	3.5369	1.7227
SCM	1	50 kB	5 s	3.5476	1.4366
SCM	2	403 kB	56 s	3.5319	1.6872
SCM	3	4.8 MB	394 s	3.5376	1.7258
SCM	4	71 MB	37 m	3.5370	1.7279
MC 5×10^4	-	-	3 h 30 m	3.5381	1.7242

SGM clearly converge to the same value, while the MC result has not yet converged to this value. In this example, SGM remains more CPU-time efficient than SCM up to $P = 3$. The radar cross-section (RCS) is given by

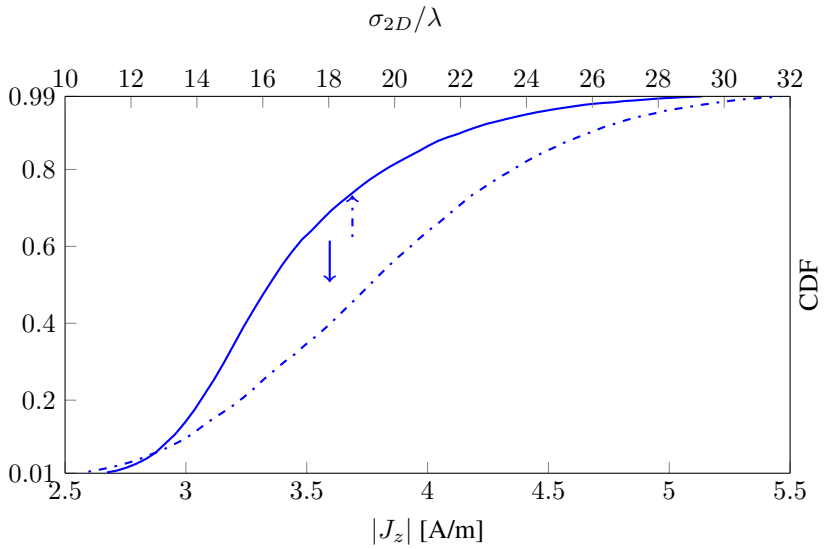

Figure 2.3: CDF for the amplitude of the current for the 10th MoM subdivision (full line) and for the RCS in the direction of specular reflection (dash-dotted line) for the example of Fig. 2.1.

$$\sigma_{2D} = \lim_{\rho \to \infty} 2\pi\rho \frac{|E_z^s|^2}{|E_z^i|^2}, \tag{2.14}$$

where ρ is the distance to the origin O in Fig. 2.1, E_z^i is the incident electric field and E_z^s is the scattered electric field which can be derived from the induced currents. Fig. 2.3 shows both the Cumulative Distribution Function (CDF) of the absolute value of the current induced on subdivision 10 and the CDF of the RCS in the specular reflection direction, i.e. in the direction making an angle of $\pi/4$ with the x-axis. Remark that both quantities vary considerably over the space of random variables. In order to correctly represent the relative behavior of the two CDFs, the minimum and maximum values on the horizontal axes for both current and RCS correspond to CDF-values of 0.01 and 0.99 respectively.

2.3.2 Non-smooth surface

As a second example consider the TM-scattering by a non-smooth finite PEC-strip of width w (see Fig. 2.4). The roughness of this strip is described by a stochastic Gaussian process. To this end the strip is divided in $M-1$ segments. The x-coordinates of the endpoints of each segment remain fixed and are equidistantly spaced, i.e. $\Delta x = w/(M-1)$. However, the corresponding y-coordinates are situated at a variable positive or negative height above a reference level, as also indicated on Fig. 2.4. We collect these y-coordinates in a height vector $\boldsymbol{h} = [y_1\ y_2\ ...\ y_M]^T$. The roughness is described by the following stochastic Gaussian process

$$P(\boldsymbol{h}) = \frac{1}{\sqrt[M]{2\pi}} e^{-\frac{1}{2}\boldsymbol{h}^T \overline{\boldsymbol{\Sigma}}^{-1} \boldsymbol{h}} \tag{2.15}$$

and a Gaussian correlation matrix the elements of which are

$$[\overline{\boldsymbol{\Sigma}}(x)]_{ij} = \sigma^2 e^{-\frac{|x_i - x_j|^2}{L_c^2}} \tag{2.16}$$

where L_c is the correlation length, σ the standard deviation and with x_j the x-coordinate of each end point. The dimension of the random space considered in this example is M. The correlated random variables are decorrelated by means of the KLT. First, the correlation matrix is diagonalized:

$$\overline{\boldsymbol{U}}^T \overline{\boldsymbol{\Sigma}}\, \overline{\boldsymbol{U}} = \overline{\boldsymbol{\Lambda}}. \tag{2.17}$$

Second, the random heights $\boldsymbol{h}$ are described in terms of a set of M independent *standard normal* random variables $\boldsymbol{\xi} = [\xi_1\ ...\ \xi_M]$ through

$$\boldsymbol{h} = \mathrm{E}[\boldsymbol{h}] + \overline{\boldsymbol{U}}\ \overline{\boldsymbol{\Lambda}}^{1/2}\ \boldsymbol{\xi} \tag{2.18}$$

where $\mathrm{E}[\boldsymbol{h}]$ is the mean value of random vector $\boldsymbol{h}$. In this case, the appropriate polynomials to model the uncertainty are orthonormalized Hermite polynomials. The incident wave is identical to the one used in the previous example except for the angle

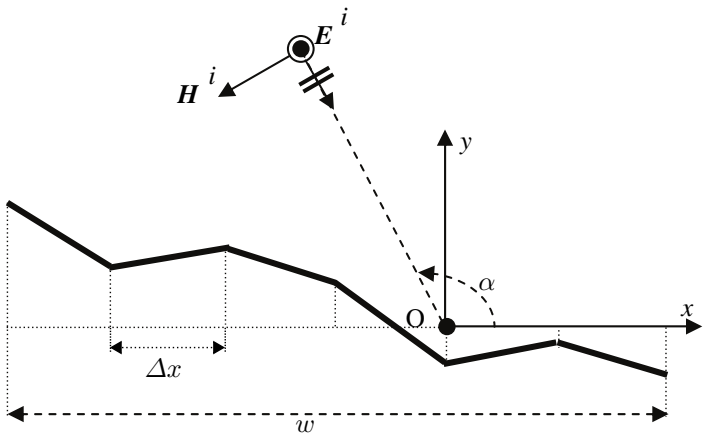

Figure 2.4: Non-smooth PEC surface described by a set of points with variable height w.r.t. a reference plane.

of incidence which is now $\alpha = 2\pi/3$.
The numerical results discussed below are for a strip with width $w = 2\lambda$. The roughness of this strip is modeled with $M = 10$ Gaussian correlated random height variables with standard deviation $\sigma = \lambda/30$ and correlation length $L_c = \lambda/3$ in (2.16). For $M = 10$, the strip is modeled by 9 straight segments and 20 elementary unknowns per segment are introduced for the MoM, i.e., $N = 180$. We again compare SCM and SGM results and complement them by a MC analysis based on 5×10^4 samples.
Fig. 2.5 displays the magnitude of the mean value and the standard deviation of the current on each of the 180 MoM subdivisions. All simulation results are collected in Table 2.2. The mean value and variance data are for the absolute value of the current near the center (MoM subdivision 90). Remark the excellent agreement between SGM and SCM, while, again, MC has not yet converged to yield correspondingly accurate results. For $P = 1$ and $P = 2$ the CPU-time needed, differs little, but the difference rapidly increases with P.

Similar to Fig. 2.3, Fig. 2.6 shows the CDF of the absolute value of the current induced on subdivision 90 and the CDF of the RCS in the specular reflection direction, i.e. in the direction making an angle of $\pi/3$ with the x-axis.

2.4 Conclusions

In this communication, we have shown how a frequency domain integral equation for scattering by two-dimensional PEC objects in free space can be combined with the intrusive Stochastic Galerkin Method. Attention is paid to the full statistics of the induced currents and the RCS due to stochastic changes in the geometry of the scatterer. The obtained results are compared to those of the non-intrusive stochastic collocation

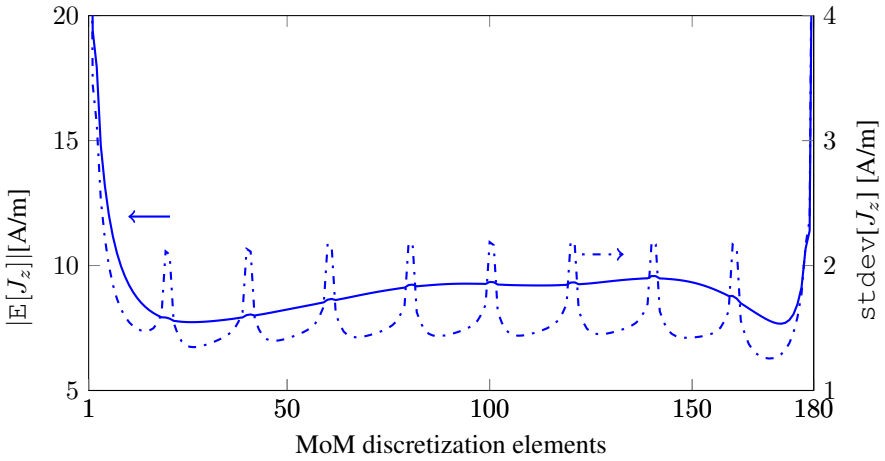

Figure 2.5: Magnitude of the mean value (full line) and standard deviation (dash-dotted line), of the current distribution for the maximum polynomial order 4 for the example of Fig. 2.4

Table 2.2: Simulation data for the non-smooth surface

method	P	memory	CPU-time	mean	variance
SGM	1	571 kB	17.8 s	9.2598	2.1054
SGM	2	28.2 MB	5.4 m	9.2615	2.0962
SGM	3	33.4 MB	37.4 m	9.2614	2.0969
SGM	4	460 MB	12 h	9.2614	2.0969
SCM	1	63.8 kB	17.2 s	9.2587	2.1436
SCM	2	486 kB	3 m	9.2615	2.0970
SCM	3	5 MB	21.8 m	9.2614	2.0970
SCM	4	56 MB	2 h 2 m	9.2614	2.0969
MC 5×10^4	-	-	11 h 10 m	9.2642	2.0954

method which has already been studied in detail in literature. When applying the MoM with N unknowns, the CPU-time required by the SGM is dominated by the $(K+1)N \times (K+1)N$ deterministic matrix problem that has to be solved, where K is the number of multivariate polynomial chaos expansion polynomials. This number rapidly grows with the number of stochastic variables (the so-called curse of dimensionality) and also with the total degree P of the multivariate expansion polynomials. The CPU-time of the SCM is roughly proportional to N_p times solving an $N \times N$ system, with N_p the number of integration points needed to calculate expansion coefficients in the high- dimensional space of the stochastic variables. The two selected examples (with 10 random variables) show that up to total degree $P = 2$ both SCM and SGM remain comparable in CPU-time requirements. From $P = 3$

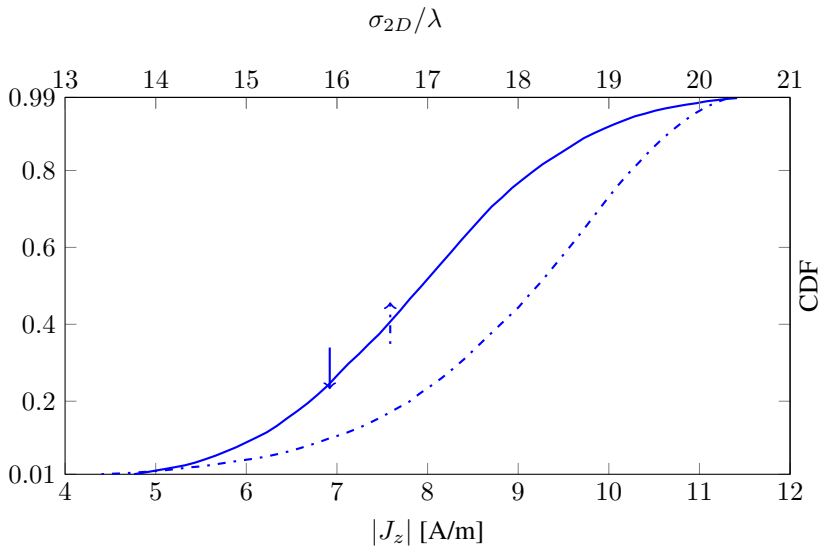

Figure 2.6: CDF for the amplitude of the current for the 90th MoM subdivision (full line) and for the RCS in the direction of specular reflection (dash-dotted line) for the example of Fig.2.4.

on, the SCM clearly becomes more efficient. For problems with a large number of stochastic variables, SCM is the only viable option.
From the numerical results (for the presented examples and several other ones), it also follows that it is very difficult to predict when a predefined accuracy has been reached, especially so for the variance. At present a mathematical criterion predicting the accuracy of the polynomial chaos expansion is lacking. Hence, from an engineering point of view, the best approach seems to be to start calculations with a low total degree P and with the minimum number of integration points needed for that degree. Increasing the total degree and the number of integration points should then reveal how trustworthy the as yet obtained data are.

References

[1] D. B. Xiu and G. E. Karniadakis, "The Wiener-Askey polynomial chaos for stochastic differential equations", *SIAM Journal on Scientific Computing*, vol. 24, no. 2, pp. 619–644, 2002.

[2] D. Xiu, "Efficient collocational approach for parametric uncertainty analysis", *Communications in Computational Physics*, vol. 2, no. 2, pp. 293–309, Apr. 2007.

[3] R. G. Ghanem and P. D. Spanos, *Stochastic Finite Elements. A Spectral Approach*. New York: Springer-Verlag, 1991.

[4] D. Vande Ginste, D. De Zutter, D. Deschrijver, T. Dhaene, P. Manfredi, and F. Canavero, "Stochastic modeling-based variability analysis of on-chip interconnects", *IEEE Transactions on Components, Packaging and Manufacturing Technology*, vol. 2, no. 7, pp. 1182–1192, Jul. 2012.

[5] T. El-Moselhy and L. Daniel, "Variation-aware stochastic extraction with large parameter dimensionality: Review and comparison of state of the art intrusive and non-intrusive technique", in *2011 12th International Symposium on Quality Electronic Design (ISQED 2011), 14-16 March 2011, Santa Clara, CA, USA*, 2011, pp. 508–517.

[6] T. El-Moselhy and L. Daniel, "Stochastic extraction for SoC and SiP interconnect with variability", in *2011 IEEE Electrical Design of Advanced Packaging and Systems Symposium (EDAPS)*, 2011, pp. 1–4.

[7] A. Austin and C. Sarris, "Efficient analysis of geometrical uncertainty in the FDTD method using polynomial chaos with application to microwave circuits", *IEEE Transaction on Microwave Theory and Techniques*, vol. 61, no. 12, pp. 4293–4301, Dec. 2013.

[8] A. Yücel, H. Bağci, and E. Michielssen, "An adaptive multi-element probabilistic collocation method for statistical EMC/EMI chracterization", *IEEE Transaction on Electromagnetic Compatibility*, vol. 55, no. 6, pp. 1154–1168, Dec. 2013.

[9] R. L. Wagner, J. M. Song, and W. Chew, "Monte Carlo simulation of electromagnetic scattering from two-dimensional random rough surfaces", *IEEE Transactions on Antennas and Propagtion*, vol. 45, no. 2, pp. 235–245, Feb. 1997.

[10] C. Chauvière, J. S. Hesthaven, and L. C. Wilcox, "Efficient computation of RCS from scatterers of uncertain shapes", *IEEE Transactions on Antennas and Propagation*, vol. 55, no. 5, pp. 1437–1448, May 2007.

[11] M. Loeve, *Probability Theory II*. Springer, 1994.

[12] S. Smolyak, "Quadrature and interpolation formulas for tensor products of certain classes of functions", *Doklady Akademii Nauk SSSR*, vol. 4, pp. 240–243, 1963.

3

Scattering from two-dimensional objects of varying shape combining the multilevel fast multipole method (MLFMM) with the stochastic Galerkin method (SGM)

Zdravko Zubac, Daniël De Zutter and Dries Vande Ginste

Published in IEEE Antennas and Wireless Propagation Letters, vol. 13, pp. 1275-1278, 2014.

★ ★ ★

In this chapter, the Multilevel Fast Multipole Method (MLFMM) is combined with the Polynomial Chaos Expansion (PCE) approach to model the stochastic variations of a scatterer. In particular, it is demonstrated how the Stochastic Galerkin Method (SGM) can be combined with an MLFMM accelerated Method of Moments (MoM) and how the beneficial effects of the MLFMM for electromagnetically large scatterers are retained in the stochastic case.

3.1 Introduction

Electromagnetic scattering analysis relies on exact data of the considered structures such as material parameters and geometry. In reality, these data exhibit variability and modeling of these uncertainties can be achieved by combining electromagnetic analysis and stochastic analysis methods. The standard approach is to assume that the parameters of interest are random variables with a predefined probability density function (PDF). The goal is to determine the statistics of output parameters of interest, such as the bistatic radar cross-section (RCS) and the current distribution on the scatterer.

A standard way to analyze the effect of variability is by means of straightforward Monte Carlo (MC) simulations which, unfortunately, show quite slow convergence at a rate $1/\sqrt{N_s}$, where N_s is the number of separate runs of the code. As an alternative, spectral methods based on polynomial chaos expansions (PCE) using orthogonal polynomials depending on the particular distribution of the random variables were proposed [1]. Roughly speaking, these methods come in two flavors: the non-intrusive ones, such as the Stochastic Collocation Method (SCM) [2] and the intrusive methods, such as the Stochastic Galerkin method (SGM) [3]. Whereas non-intrusive methods rely on a standard deterministic solver to obtain the statistical information, intrusive methods require the development of a dedicated new solver. PCE-based methods are already used for variability analysis of (on-chip) interconnects [4][5]. Superiority of PCE-based methods over MC simulations for scattering problems is, e.g., demonstrated in [6] and will not be repeated in this chapter.

In this chapter, we will use the SGM approach to model stochastic scattering problem by means of an integral equation. As indicated in [5], applying SGM to integral equations combined with the Method of Moments (MoM), leads to solving a large deterministic problem. In order to decrease the computational complexity, the Multilevel Fast Multipole Method (MLFMM) [7] is invoked. To the best knowledge of the authors, this chapter is the first to discuss the combination of MLFMM with the intrusive SGM for the stochastic analysis of scattering problems. To assess the benefits of the MLFMM approach, we compare it to the standard MoM approach combined with SGM. Section II discusses the theoretical framework, combining the Electric Field Integral Equation (EFIE), its MoM solution, the SGM with its expansion of all variables in the proper stochastic basis functions and the way the MLFMM can be adapted to the stochastic approach. The numerical example in Section III illustrates the acceleration obtained by introducing the MLFMM in the stochastic approach.

3.2 The stochastic scattering problem

We consider two-dimensional frequency domain scattering by perfect electrically conducting (PEC) objects, residing in free space, with a stochastically defined geometry. This geometric variability of the scatterer is described by a set of M independent random variables which are collected in the vector $\boldsymbol{\xi} = [\xi_1\ \xi_2\ ...\ \xi_M]$ with domain Ω. The z-axis is the axis of invariance. The incident wave is a TM-polarized plane wave

with electric field $\boldsymbol{E}^i = E^i \mathbf{u}_z$. To determine the scattered field, we apply an electric field integral equation (EFIE) solved by the MoM. To this end, the scatterer is divided into N segments and pulse basis functions for the current distribution are used. As a result, a stochastic linear system equation is obtained:

$$\overline{\boldsymbol{Z}}(\boldsymbol{\xi})\boldsymbol{I}(\boldsymbol{\xi}) = \boldsymbol{V}(\boldsymbol{\xi}). \tag{3.1}$$

Next, all elements of (3.1) are represented via a PCE, from which we get:

$$\sum_{k=0}^{K} \boldsymbol{V}_k \phi_k(\boldsymbol{\xi}) = \sum_{k=0}^{K}\sum_{l=0}^{K} \overline{\boldsymbol{Z}}_k \boldsymbol{I}_l \phi_k(\boldsymbol{\xi})\phi_l(\boldsymbol{\xi}), \tag{3.2}$$

where $\overline{\boldsymbol{Z}}_k$, $\boldsymbol{V}_k$ and $\boldsymbol{I}_l$ represent the expansion coefficients of system matrix $\overline{\boldsymbol{Z}}$, RHS $\boldsymbol{V}$ and unknown current density $\boldsymbol{I}$, resp. $\phi_k(\boldsymbol{\xi})$ and $\phi_l(\boldsymbol{\xi})$ are multivariate polynomials that are orthonormal with respect to the PDF $W(\boldsymbol{\xi})$ of the random vector $\boldsymbol{\xi}$. The expansion coefficients of any quantity $\boldsymbol{f}(\boldsymbol{\xi})$ are obtained via:

$$\boldsymbol{f}_k =< \boldsymbol{f}(\boldsymbol{\xi}), \phi_k(\boldsymbol{\xi}) >, \tag{3.3}$$

where $< f(\boldsymbol{\xi}), g(\boldsymbol{\xi}) >$ represents an inner product defined as:

$$< f(\boldsymbol{\xi}), g(\boldsymbol{\xi}) >= \int_{\Omega} f(\boldsymbol{\xi}) g(\boldsymbol{\xi}) W(\boldsymbol{\xi}) d\boldsymbol{\xi}, \tag{3.4}$$

with property $< \phi_j(\boldsymbol{\xi}), \phi_k(\boldsymbol{\xi}) >= \delta_{jk}$, where δ_{jk} is the Kronecker δ. Multivariate polynomials $\phi_k(\boldsymbol{\xi})$ are constructed as products of univariate polynomials only depending on a single random variable with sum of the orders of the univariate polynomials (total degree) at most P. The number of polynomials $K+1$ that is used in the PCE is determined as:

$$K + 1 = \frac{(M+P)!}{M!P!}. \tag{3.5}$$

Galerkin projection of both sides of (3.2) on $\phi_m(\boldsymbol{\xi})$ finally leads to the following deterministic set of equations where the dependence on $\boldsymbol{\xi}$ has been eliminated

$$\boldsymbol{V}_m = \sum_{m:\gamma_{klm}\neq 0} \overline{\boldsymbol{Z}}_k \, \boldsymbol{I}_l \, \gamma_{klm} \tag{3.6}$$

with $\gamma_{klm} =< \phi_k(\boldsymbol{\xi})\phi_l(\boldsymbol{\xi}), \phi_m(\boldsymbol{\xi}) >$ and where the summation is taken for all non-zero values of γ_{klm}. Equation (3.6) represents a large deterministic system with $(K+1)N$ unknowns as in [5]. This system has $O(K^2N^2)$ memory complexity and $O(K^3N^3)$ computational complexity when using a direct solver. Memory complexity is reduced to $O(KN^2)$ and computational complexity to $O(nnzN^2)$ when using an iterative solver, where nnz represents the number of non-zero values of γ_{klm}. Numerical calculations show that for $P = 1$, $nnz = O(K)$, while for $P > 1$, $nnz = O(K^{1.5})$ instead of $O(K^3)$ when all coefficients γ_{klm} would be different from zero. This is presented in Fig. 3.1 and more details can be found in [8]. Applying

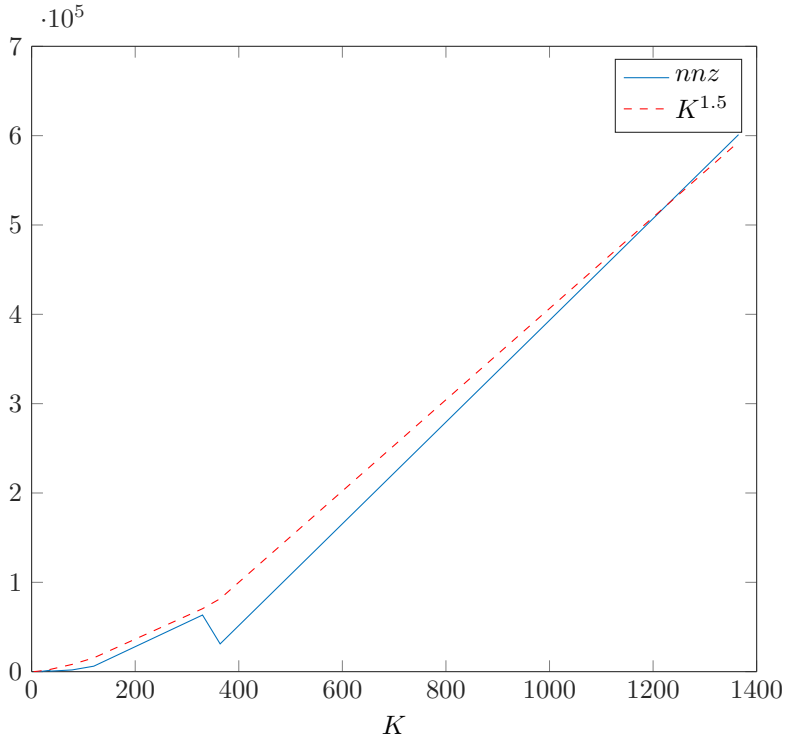

Figure 3.1: The number of non-zero values of nnz (blue) and trending curve with law $O(K^{1.5})$ (red) for different number of polynomials.

MLFMM can further decrease the computational complexity. In the FMM procedure the structure is divided into groups of sources and the matrix-vector product (MVP) is computed by calculation of the electric field radiated by one group of sources with group center $\boldsymbol{\rho}_s$ at the group of observation points with group center $\boldsymbol{\rho}_o$[7]. This is done via the plane wave decomposition of the 2-D Green's function $G(\boldsymbol{\rho}(\boldsymbol{\xi}), \boldsymbol{\rho}'(\boldsymbol{\xi}))$. One element of the matrix $\overline{\boldsymbol{Z}}_k$ of expansion coefficients is calculated as:

$$\overline{\boldsymbol{Z}}_{ij,k} = \int_{\Omega} \int_{s_i} \int_{s_j} G(\boldsymbol{\rho}(\boldsymbol{\xi}), \boldsymbol{\rho}'(\boldsymbol{\xi})) d\boldsymbol{\rho}' d\boldsymbol{\rho}\, \phi_k(\boldsymbol{\xi}) W(\boldsymbol{\xi}) d\boldsymbol{\xi}, \tag{3.7}$$

where $\boldsymbol{\rho}' \in s_j$ and $\boldsymbol{\rho} \in s_i$, as testing and basis function are constant over segments s_i and s_j. If the distance between the source group and observation group is sufficiently large, calculation of the interaction can be decomposed in an aggregation, translation and disaggregation step, i.e.

$$\overline{\boldsymbol{Z}}_k = \int_{\Omega} \overline{\boldsymbol{D}}(\boldsymbol{\rho}(\boldsymbol{\xi}), \boldsymbol{\rho}_o) \overline{\boldsymbol{T}}_q \overline{\boldsymbol{A}}(\boldsymbol{\rho}'(\boldsymbol{\xi}), \boldsymbol{\rho}_s) \phi_k(\boldsymbol{\xi}) W(\boldsymbol{\xi}) d\boldsymbol{\xi}, \tag{3.8}$$

where $\overline{\boldsymbol{T}}_q$ represents the diagonal translation matrix, where $\overline{\boldsymbol{A}}(\boldsymbol{\rho}'(\boldsymbol{\xi}), \boldsymbol{\rho}_s)$ is the aggregation matrix of the source group and where $\overline{\boldsymbol{D}}(\boldsymbol{\rho}(\boldsymbol{\xi}), \boldsymbol{\rho}_o)$ is the disaggregation matrix of the observation group. Since we are dealing with independent random variables which describe the scatterer's geometry and source and observation group are separated, we assume that the aggregation matrix only depends on vector $\boldsymbol{\xi}_s$ which is a subset of vector $\boldsymbol{\xi}$ and is independent of subset $\boldsymbol{\xi}_o$ on which the disaggregation matrix depends. This means that the integral in (3.8) can be represented as a product of two integrals, one over subset $\boldsymbol{\xi}_s$ and one over subset $\boldsymbol{\xi}_o$. This leads to substantial simplifications as the PCE of disaggregation and aggregation matrix can now be determined separately. Furthermore, the translation matrix $\overline{\boldsymbol{T}}_q = \overline{\boldsymbol{T}}_q(\boldsymbol{\rho}_s, \boldsymbol{\rho}_o)$ depends on the group centers and also in case of stochastic variations we can keep these centers fixed. Hence, $\overline{\boldsymbol{T}}_q$ is a deterministic function, independent of $\boldsymbol{\xi}$, as long as the pertinent subsets $\boldsymbol{\xi}_s$ and $\boldsymbol{\xi}_o$ are disjunct.

In the MLFMM approach, groups are hierarchically divided into levels, where higher level groups consist of sets of lower level ones. To perform the MVP, first, in the aggregation step, the radiation pattern of the source group is sampled into outgoing plane waves (OPWs). On the lowest level this is done by multiplying the aggregation matrix of the group with the vector of current strengths of the sources. In the stochastic case, we need the PCE of the OPWs. The PCE coefficients for these OPWs, collected in vectors $\boldsymbol{OPW}_m$, are obtained via:

$$\boldsymbol{OPW}_m = \sum_{m:\gamma_{klm}\neq 0} \overline{\boldsymbol{A}}_k \, \boldsymbol{I}_l \, \gamma_{klm} \tag{3.9}$$

where matrices $\overline{\boldsymbol{A}}_k$ are the expansion coefficients of the aggregation matrix. OPWs of groups on higher levels are calculated via interpolation and shifting operations [7]. Via the translation step, OPWs are converted in incoming plane waves (IPWs) arriving at the observation group. IPWs at lower levels are calculated via anterpolation and shifting operations[7]. Finally, on the lowest level, stochastic IPWs are evaluated at the observations points in the disaggregation step. This leads to the coefficients $\boldsymbol{V}_m$ in (3.6), given by:

$$\boldsymbol{V}_m = \sum_{m:\gamma_{klm}\neq 0} \overline{\boldsymbol{D}}_k \, \boldsymbol{IPW}_l \gamma_{klm} \tag{3.10}$$

where matrices $\overline{\boldsymbol{D}}_k$ are the expansion coefficients of the disaggregation matrix and $\boldsymbol{IPW}_l$ represents the expansion coefficients of the IPWs. In the MLFMM approach advocated here, (3.9) and (3.10) are calculated at the lowest level of the MLFMM tree. The cost of these steps in a deterministic MLFMM scheme is $O(N)$ [7]. From (3.9) and (3.10), it can be seen that the complexity is now increased to $O(nnzN)$. But, since the aggregation and disaggregation matrices only depend on *subsets* of $\boldsymbol{\xi}$, many expansion coefficients $\overline{\boldsymbol{A}}_k$ and $\overline{\boldsymbol{D}}_k$ are zero, and the complexity is substantially decreased, as will be numerically demonstrated in the next section. The complexity of other operations (interpolation, shifting, translation, anterpolation) is $(K+1)$ times higher than in the deterministic case, since OPWs and IPWs are described via PCE. For dense structures, complexity of these operations would be $O(KN)$. In a similar

way, the matrices $\overline{\boldsymbol{Z}}_k$ are however sparse, and the complexity of MVPs in the MoM can be reduced, as will be demonstrated in the next section.

3.3 Numerical example

3.3.1 Scattering by a finite periodic 2D array of PEC strips

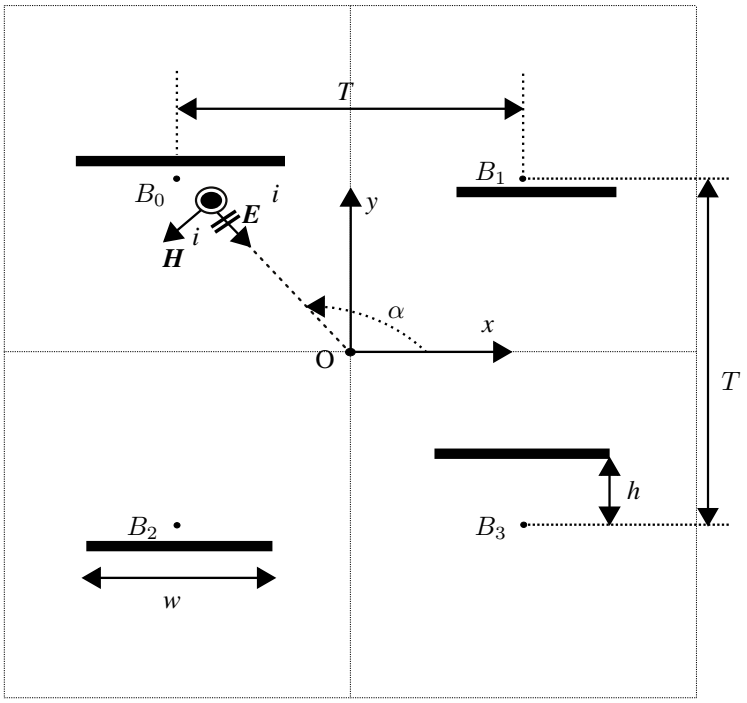

Figure 3.2: Periodic 2D array of PEC strips. Widths w and heights h are random. For clarity, here, the case with only four strips is shown.

We consider TM-scattering by a periodic but finite 2D array of PEC strips with varying widths w as depicted in Fig. 3.2 for the four strips case. The x-coordinates of the position vectors of the centers of the strips remain fixed with constant spacing T. On the other hand, the y-coordinates vary as described by relative heights h w.r.t. the nominal y-values. These nominal values are again equally separated by a spacing T. The variability of the structure is hence described by vectors of widths w and relative heights h which are chosen to be independent uniformly distributed random variables. The widths of the strips vary between $0.5T - \lambda/20$ and $0.5T + \lambda/20$, with $T = \lambda$, and the heights of the strips between $-\lambda/20$ and $\lambda/20$, where λ is the wavelength of the

incident wave, i.e. we introduce 20% variations compared to nominal width $w = 0.5T$. The incident wave is a TM-polarized plane wave impinging under an angle $\alpha = 3\pi/4$ with the positive x-axis and frequency $f = 2.45$ GHz.

In the MLFMM scheme, the structure is divided in square boxes with fixed side T and centers indicated by B_0, B_1, B_2 and B_3 which coincide with the nominal position vectors of the centers of the strips. In order to demonstrate the benefits of using the MLFMM, the number of strips will be increased to 4 by 4, 8 by 8 and 16 by 16, keeping the nominal center positions on a regular T by T grid. At the lowest MLFMM level the box size also remains T by T.

The PCE uses multivariate orthonormal Legendre polynomials which are the proper functions to model uncertainties in the case of uniform distributions. In the MoM approach, matrix elements that describe interactions on the same strip depend on a single random variable, i.e. the width, and matrix elements that describe interactions between two strips depend on four random variables, i.e. two widths and two heights. Hence, in this example, the M dimensional integral in (3.7) is reduced to either a one dimensional or a four dimensional integral. When calculating $\overline{\boldsymbol{A}}_k$ and $\overline{\boldsymbol{D}}_k$, matrix elements only depend on two random variables.
The current on each of the strips is modeled using 20 equal length subdivisions with piecewise constant basis functions. The total number of unknowns in the MoM grows from $N = 80$ in the 2×2 case to $N = 5120$ in the 16×16 case. The total number of random variables also grows with a factor 4 from $M = 8$ to $M = 512$. For this example, the quantities of interest (surface current, RHS, impedance matrix elements) are modeled using expansions with highest polynomial order, i.e. total degree, $P = 2$. Our experience shows that $P = 2$ suffices to describe the wanted statistics with acceptable accuracy. In the last example with 512 random variables, the total number of polynomials in (3.5) is so large, i.e. 131841, that we have restricted ourselves to the $P = 1$ case. Fig. 3.3 represents the mean value and the standard deviation of the induced current for top left strip of the scatterer for the 4×4 case. Results from straightforward application of the SGM-MoM combination and from SGM-MoM with MLFMM acceleration are indistinguishable on the scale of the figure. The most important numerical difference between the two approaches is due to the fact that the MoM-SGM approach uses a PCE for $\overline{\boldsymbol{Z}}(\boldsymbol{\xi})$, $\boldsymbol{I}(\boldsymbol{\xi})$ and $\boldsymbol{V}(\boldsymbol{\xi})$ in (3.1), while the SGM-MoM-MLFMM does the same for $\boldsymbol{V}(\boldsymbol{\xi})$ and $\boldsymbol{I}(\boldsymbol{\xi})$ but on top of that introduces separate PCEs for the disaggregation and aggregation matrices $\overline{\boldsymbol{D}}(\boldsymbol{\xi})$ and $\overline{\boldsymbol{A}}(\boldsymbol{\xi})$ in (3.8), possibly leading to additional truncation errors in (3.9) and (3.10). This truncation error when using SGM is discussed in [9], showing that this error decreases for increasing polynomial order P and for decreasing variations of the random variables. Another numerical difference arises when determining the radiated field due to a group of sources in an MLFMM box. In the SGM-MoM approach this field is directly obtained using the Green's function and the PCE of the currents. In the SGM-MoM-MLFMM approach this field emerges from the group's OPW expansion and depends both on the PCE of these OPWs and on the number of sampling directions. In order to illustrate the numerical differences, results for the mean and the variance of the magnitude of the center current on subdivision 10 of the top left strip for the 4×4 and 8×8 examples

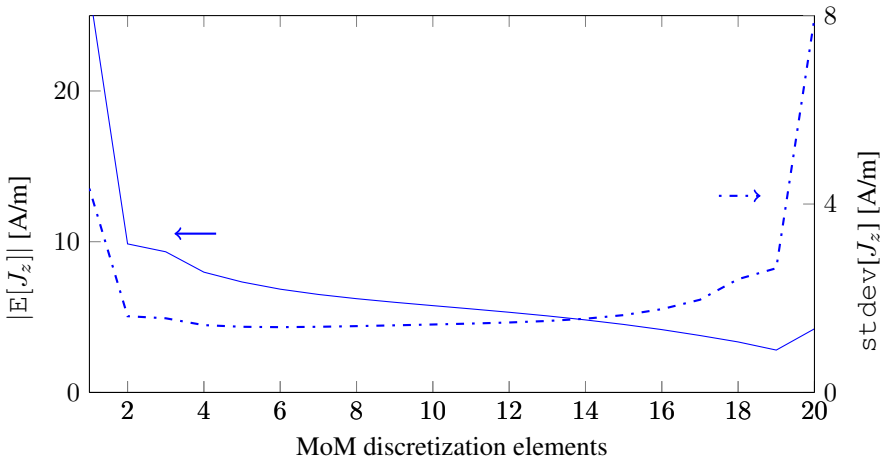

Figure 3.3: Magnitude of the mean value (full line) and standard deviation (dash-dotted line), of the current distribution on the top left strip for the 4×4 example and total degree $P = 2$.

Table 3.1: Mean and variance of the magnitude of the center current of the top left strip for different methods

method	P	mean (4×4)	variance (4×4)
MoM	1	5.7503	2.1910
MoM-MLFMM	1	5.7497	2.1907
MoM	2	5.7598	2.0813
MoM-MLFMM	2	5.7598	2.0817
method	P	mean (8×8)	variance (8×8)
MoM	1	6.0925	2.8665
MoM-MLFMM	1	6.1000	2.8930
MoM	2	6.0991	2.6294
MoM-MLFMM	2	6.0991	2.6298

are shown in Table 3.1, for $P = 1$ and $P = 2$.

The radar cross-section (RCS) per unit length (p.u.l.), also called scattering width, is given by

$$\sigma_{2D} = \lim_{\rho \to \infty} 2\pi\rho \frac{|E_z^s|^2}{|E_z^i|^2}, \tag{3.11}$$

where ρ is the distance to the origin O in Fig. 3.2, E_z^i is the incident electric field and E_z^s is the scattered electric field which can be derived from the induced currents or in the MLFMM approach, by using the OPWs expansion at the highest level. Fig. 3.4 shows the mean value and variations around this mean value with maximum variability

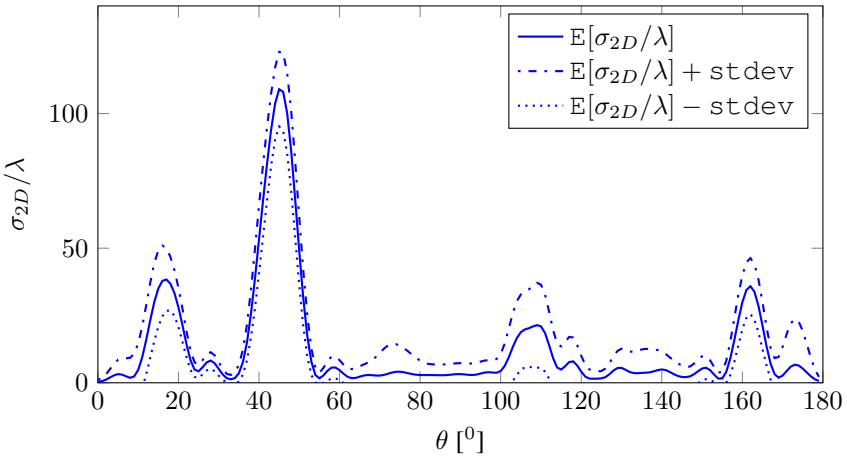

Figure 3.4: Mean RCS p.u.l. with $\pm$ one standard deviation variation for structure with 8×8 strips for polynomial order $P = 2$.

of one standard deviation for the structure with 8×8 strips. It can be seen that the RCS p.u.l. is the highest in the specular reflection direction and that the radiation pattern shows a number of side lobes. The $\pm$ one standard deviation of these lobes is quite substantial. Finally, in Table 3.2, in order to demonstrate the computational

Table 3.2: CPU time for one MVP product

N	P	$K+1$	nnz	MLFMM [s]	MoM [s]
320	0	1	1	0.0017	0.0012
320	1	33	97	0.0658	0.04822
320	2	561	37521	1.8509	1.5181
1280	0	1	1	0.0103	0.0184
1280	1	129	385	1.334	2.3681
1280	2	8385	2171457	118.99	204.33
5120	0	1	1	0.0518	0.2877
5120	1	513	1537	25.34	149.07

efficiency of the proposed MLFMM approach, we present the CPU time for one matrix-vector product (MVP) for different cases and polynomial orders, again comparing the straightforward SGM-MoM approach to the MLFMM accelerated one. In this table, N is the number of unknowns in the MoM (320: 4×4 case; 1280: 8×8 case; 5120: 16×16 case), P is the maximum degree of the multivariate polynomials, $K+1$ is the corresponding total number of polynomials corresponding to a particular P-value and nnz is the number of non-zero values of γ_{klm} in (6). Remark that the case $P = 0$ simply corresponds to using the nominal value of all variables, i.e. the simple

deterministic case. Further remark that nnz has to be weighed against the maximum of K^3 when all γ_{klm} would be different from zero. Table 3.2 shows that the acceleration due to the MLFMM is very substantial for the largest (16×16) scatterer. The crossover point is found at about $N = 1000$, as is also the case for traditional (deterministic) MLFMM.

3.4 Conclusions

In this chapter, two-dimensional TM-scattering at an electrically large, stochastically varying, PEC scatterer was used to demonstrate how the statistics of induced currents and of the radiation pattern can be found by optimally combining the MoM, the SGM and the acceleration due to the MLFMM. The SGM is an intrusive method allowing to replace the original stochastic problem by an equivalent, but much larger, deterministic problem. As the PEC strip array example in the chapter demonstrates, the solution of this larger deterministic problem, greatly benefits from the MLFMM by taking into account the particularities of the matrix-vector product which arises from the application of the SGM.
Further research is needed to include dielectrics objects to extend this approach to the 2D analysis of multiconductor transmission lines, and also to the 3D case in order to find out if all conclusions remain valid.

References

[1] D. B. Xiu and G. E. Karniadakis, "The Wiener-Askey polynomial chaos for stochastic differential equations", *SIAM Journal on Scientific Computing*, vol. 24, no. 2, pp. 619–644, 2002.

[2] D. Xiu, "Efficient collocational approach for parametric uncertainty analysis", *Communications in Computational Physics*, vol. 2, no. 2, pp. 293–309, Apr. 2007.

[3] R. G. Ghanem and P. D. Spanos, *Stochastic Finite Elements. A Spectral Approach*. New York: Springer-Verlag, 1991.

[4] D. Vande Ginste, D. De Zutter, D. Deschrijver, T. Dhaene, P. Manfredi, and F. Canavero, "Stochastic modeling-based variability analysis of on-chip interconnects", *IEEE Transactions on Components, Packaging and Manufacturing Technology*, vol. 2, no. 7, pp. 1182–1192, Jul. 2012.

[5] T. El-Moselhy and L. Daniel, "Variation-aware stochastic extraction with large parameter dimensionality: Review and comparison of state of the art intrusive and non-intrusive technique", in *2011 12th International Symposium on Quality Electronic Design (ISQED 2011), 14-16 March 2011, Santa Clara, CA, USA*, 2011, pp. 508–517.

[6] C. Chauvière, J. S. Hesthaven, and L. C. Wilcox, "Efficient computation of RCS from scatterers of uncertain shapes", *IEEE Transactions on Antennas and Propagation*, vol. 55, no. 5, pp. 1437–1448, May 2007.

[7] W. C. Chew, J. M. Jin, E. Michielssen, and J. Song, *Fast and Efficient Algorithms in Computational Electromagnetics*. Norwood, MA: Artech House, 2001.

[8] T. El-Moselhy, "Field solver technologies for variation-aware interconnect parasitic extraction", PhD thesis, Massachusetts Institute of Technology, 2010.

[9] B. J. Debusschere, H. N. Najm, P. P. Pébay, O. M. Knio, R. G. Ghanem, and O. P. L. Maître, "Numerical challenges in the use of polynomial chaos representations for stochastic processes", *SIAM J. Sci. Comput.*, vol. 26, no. 2, pp. 698–719, Feb. 2005.

4

Preconditioner for a scattering solver based on the intrusive stochastic Galerkin method accelerated with MLFMM

Zdravko Zubac, Jan Fostier, Daniël De Zutter and Dries Vande Ginste

Presented on Computational Electromagnetics (CEM) International Workshop, Izmir, Turkey, 2015.

★ ★ ★

In this chapter, we present a preconditioner for an intrusive Stochastic Galerkin Method (SGM) based scattering solver that also leverages the Multilevel Fast Multipole Method (MLFMM). The proposed preconditioner is essential in developing a general and intrusive SGM method. The simulation results were obtained for a canonical scattering structure with perfect electrically conducting (PEC) strips with statistically varying geometry. Results are reported for the number of iterations, with and without using a preconditioner, and for the time required to setup the preconditioner.

4.1 Introduction

Stochastic modeling of electromagnetic structures that exhibit inherent variability has been studied in recent years. Methods based on polynomial chaos expansion (PCE) have better accuracy and efficiency over traditional Monte Carlo (MC) analysis [1]. These methods can be divided into two classes: non-intrusive ones, which rely on reusing a traditional deterministic solver, and intrusive solvers, which require modification of the computational algorithm. Both types were combined with the Method of Moments (MoM) for solving Boundary Integral Equation (BIE) scattering problems [2]. The basic idea of all PCE based methods is to describe the random variations by a linear combination of polynomials. The number of polynomials K grows rapidly with the number of stochastic parameters and the polynomial order. The intrusive SGM approach results in a large linear system of equations that needs to be solved. To decrease the computational time needed to solve such a large system, the Multilevel Fast Multipole Method (MLFMM) is invoked [3]. It was shown that the calculation of matrix element interactions through a plane wave decomposition of the Green's function remains applicable in the stochastic case if the variations of sources residing in sufficiently separated boxes are mutually independent. The total complexity of one matrix-vector product is shown to be equal to the deterministic MLFMM complexity scaled by a factor that depends on K. To further decrease the solution time, the number of iterations in the iterative solver should be reduced.
We consider the same structure as in [3], which is a standard structure for analyzing novel methods. PEC strips are organized in a periodic two-dimensional, but finite array, as in Fig. 3.2. For each strip, its width w is considered as a random variable, as well as its y-coordinate of the position of its center, which is described by its relative offset h w.r.t. the nominal value. The nominal positions of the centers are equally spaced with a constant spacing T. The variability is described with vectors of widths w and heights h, which are chosen to be independent uniformly distributed random variables. The widths vary between $0.5T - \lambda/20$ and $0.5T + \lambda/20$, while heights vary between $-\lambda/20$ and $\lambda/20$, where $T = 0.5\lambda$, and λ is the wavelength.

In order to show the benefits of the SGM-MLFMM, in [3], the 2×2 structure in Fig. 3.2 was taken as a starting point and expanded into a 4×4 and 8×8 structure, keeping the same rectangular organization of the strips. It was shown that the crossover point, when a SGM-based MoM and MLFMM are compared, is the same as in the deterministic case.
To reduce the number of iterations, we introduce a preconditioner that is based on a block-Jacobi preconditioner. This type of a preconditioner was introduced in [4]. The SGM matrix exhibits a block structure where the diagonal blocks are, in general, equal to the average (mean) matrix $\overline{\boldsymbol{Z}}_0$ of the structure. The random variations are to be found in the other blocks. This means that the resulting matrix is diagonally dominant, and for small relative variations, this block diagonal matrix with $\overline{\boldsymbol{Z}}_0$ on the diagonal is a good representation of the whole matrix and thus it can be used as a preconditioner. However, when using the MLFMM, the entire $\overline{\boldsymbol{Z}}_0$ with size $N \times N$ is never stored. Therefore, the preconditioner is based on the diagonal blocks within the $\overline{\boldsymbol{Z}}_0$ matrix that

correspond to the near interactions, in our case, near interactions between points in one box on the lowest MLFMM level that contain one PEC strip. The organization of this matrix is presented schematically in Fig. 4.1. The black squares within the diagonal block correspond to the near interactions within one box and in the MLFMM approach these blocks are actually stored. The size of the blocks could be increased at the cost of a higher setup time, since the number of sources and random variables inside the block are increased. Moreover, more near interactions in the MLFMM tree would be involved which affects the solution time.

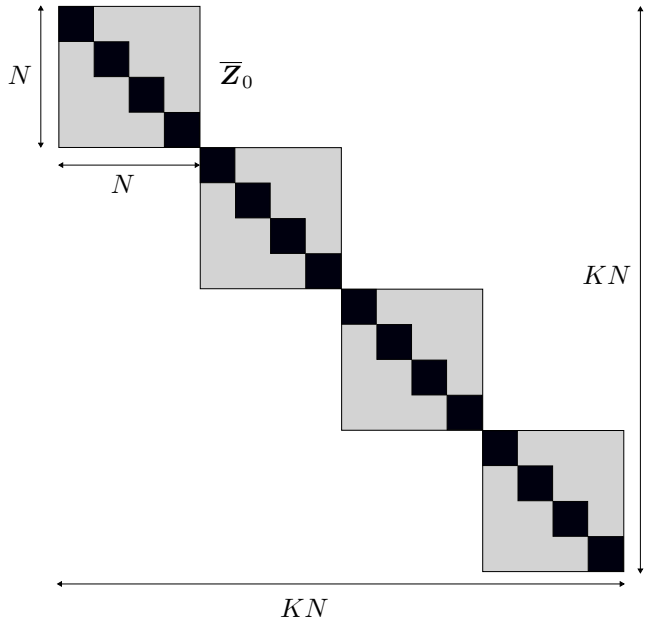

Figure 4.1: Block diagonal organization of the preconditioner matrix. Due to the lack of the space, the simple situation for the 2×2 array with $K = 4$ is presented.

4.2 Simulation results

Here we provide results for two types of the structures, one involving 4×4 and another involving 8×8 strips. The first structure is represented with 32 random variables and discretized with $N = 320$ unknowns. The second one is described with 128 random variables and discretized with 1280 unknowns. Simulations are obtained with total polynomial orders 1 and 2, as presented in Table 4.1. The iterative precision is set to 10^{-8} and a stabilized biconjugate gradient iterative solver is used [5]. To compare results, we will focus on the total setup time t_{se}, solution time t_{so} and the number of iterations N_{iter} needed to obtain the predefined accuracy. The last column in Table 4.1

indicates whether the preconditioner was used or not. The total number of unknowns is $N_{stoc} = KN$.

Table 4.1: Simulation results

N_{stoc}	K	t_{se} [s]	t_{so}[s]	N_{iter}	Preconditioner
10 560	33	16.4	3	49	yes
10 560	33	15.7	12.9	225	no
179 520	561	76	100	56	yes
179 520	561	74.4	450	258	no
165 120	129	90	249	190	yes
165 120	129	88.6	987	778	no
10 732 800	8 385	423	31 114	212	yes
10 732 800	8 385	422	116 816	818	no

It is clear from the table that the number of iterations when using a preconditioner is smaller than without preconditioner. This significantly reduces the solution time, even though the time for a single iteration is increased due to the application of the preconditioner. We can see small differences in setup time, which now involves additional calculation of the inverse of the block matrix. However, this difference is negligible compared to the total time. It is clear that this type of the preconditioner, although simple, remains effective for the SGM-MLFMM solver. Even for small electromagnetic structures, this preconditioner is needed, since complexity grows fast with the number of polynomials K.

4.3 Conclusions

Developing an efficient preconditioner is essential in the construction of general and intrusive MLFMM-based stochastic methods. We have shown that a simple block-Jacobi preconditioner can serve for this purpose. The choice of the preconditioner is based on the particular properties of the SGM matrix and the geometry. One should be careful when determining the size of the blocks on which preconditioning will be applied, especially so for large structures. Further research is needed to combine this preconditioner with large electromagnetic structures and to study its effectiveness.

References

[1] D. B. Xiu and G. E. Karniadakis, "The Wiener-Askey polynomial chaos for stochastic differential equations", *SIAM Journal on Scientific Computing*, vol. 24, no. 2, pp. 619–644, 2002.

[2] Z. Zubac, D. De Zutter, and D. Vande Ginste, "Scattering from two-dimensional objects of varying shape combining the Method of Moments with the Stochastic Galerkin Method", *IEEE Transactions on Antennas and Propagation*, vol. 62, no. 9, pp. 4852–4856, Sep. 2014.

[3] Z. Zubac, D. De Zutter, and D. Vande Ginste, "Scattering from two-dimensional objects of varying shape combining the Multilevel Fast Multipole Method (MLFMM) with the Stochastic Galerkin Method (SGM)", *IEEE Antennas and Wireless Propagation Letters*, vol. 13, pp. 1275–1278, Jul. 2014.

[4] M. F. Pellissetti and R. G. Ghanem, "Iterative solution of systems of linear equations arising in the context of Stochastic Finite Elements", *Advances in Engineering Software*, vol. 31, pp. 607–616, 2000.

[5] R. D. da Cunha and T. Hopkins, *Pim 2.2 the Parallel Iterative Methods Package for Systems of Linear Equations User's Guide (Fortran 77 version)*, UKC, University of Kent, Canterbury, UK, 2000.

5

Efficient uncertainty quantification of large two-dimensional optical systems with a parallelized stochastic Galerkin method

Zdravko Zubac, Jan Fostier, Daniël De Zutter and Dries Vande Ginste

Published in Optics Express, vol. 23, no. 24, pp. 30 833–30 850, Nov. 2015.

★ ★ ★

It is well-known that geometrical variations due to manufacturing tolerances can degrade the performance of optical devices. In recent literature, polynomial chaos expansion (PCE) methods were proposed to model this statistical behavior. Nonetheless, traditional PCE solvers require a lot of memory and their computational complexity leads to prohibitively long simulation times, making these methods intractable for large optical systems. The uncertainty quantification (UQ) of various types of large, two-dimensional lens systems is presented in this chapter, leveraging a novel parallelized Multilevel Fast Multipole Method (MLFMM) based Stochastic Galerkin Method (SGM). It is demonstrated that this technique can handle large optical structures in reasonable time, e.g., a stochastic lens system with more than 10 *million unknowns was solved in less*

than an hour by using 3 compute nodes. The SGM, which is an intrusive PCE method, guarantees the accuracy of the method. By conjunction with MLFMM, usage of a preconditioner and by constructing and implementing a parallelized algorithm, a high efficiency is achieved. This is demonstrated with parallel scalability graphs. The novel approach is illustrated for different types of lens system and numerical results are validated against a collocation method, which relies on reusing a traditional deterministic solver. The last example concerns a Cassegrain system with five random variables, for which a speed-up of more than 12× compared to a collocation method is achieved.

5.1 Introduction

Variability analysis and uncertainty quantification (UQ) have become a major concern during the design step of optical systems and components as manufacturing tolerances and process variations can have a dramatic influence on the performance [1]. In particular, even small variations of geometrical dimensions or material properties affect the electromagnetic behavior of the structures under design. To model these variations, one may simply combine statistical analysis with traditional, deterministic, full-wave solvers. The widely used Monte Carlo (MC) technique is an example of such an approach, repeatedly solving a large number of deterministic problems (samples), leading to an easy to implement and robust analysis. Unfortunately, MC has a slow convergence rate, yielding a high computational cost. For large full-wave problems, as typically encountered during the UQ of optical lens systems, this method rapidly becomes intractable.

To more efficiently assess variability, methods based on Polynomial Chaos Expansions (PCE) have been devised [2]. The basic idea of PCE methods is that any variation of a set of (geometric or material) parameters can be represented as a linear combination of polynomials that depend on these input parameters. Subsequently, the pertinent system equations, e.g. Maxwell's equations, are solved, taking these polynomial variations into account. This leads to a stochastic description of the variability of the desired output parameters, which can for example be electric field strengths. Traditionally, PCE-based methods can be subdivided into two classes. First, the class of non-intrusive PCE methods, such as the Stochastic Collocation Method (SCM), relies, like the MC method, on reusing the deterministic code to solve the system equations. In contrast to MC, SCM chooses the samples in a more clever way, depending on the Probability Density Function (PDF) of the input parameters. Second, the class of intrusive PCE methods, such as the Stochastic Galerkin Method (SGM), requires a thorough modification of the solver that tackles the system equations. In literature, it is argued that the SGM often leads to better accuracy than the SCM. In the domain of electrical engineering, intrusive methods are already successfully applied in the variability analysis of on-chip interconnects [3], [4] and scattering problems [5]–[7]. Recently, in the domain of photonics, the non-intrusive SCM method has been applied for the UQ of a

silicon-on-insulator based directional coupler [8].
In this chapter, the focus is on the UQ of large optical lens systems. Thereto, an intrusive full-wave SGM scheme is proposed. The full-wave character of the problem is described by means of a set of boundary integral equations (BIE) that are solved by means of the Method of Moments (MoM) [9]. To expedite the computations, the Multilevel Fast Multipole Method (MLFMM) has been combined with a SGM-MoM solver. In [7] it was shown that such an approach leads to the traditional $O(N \log N)$ computational complexity, N being the number of unknowns, but scaled with a factor that depends on the number of polynomials. Whereas in [7] relatively small scattering problems were handled, here, we aim to model large optical setups. Therefore, we present the parallelization of the full-wave intrusive SGM-MLFMM solver and we propose an effective preconditioning scheme to further accelerate the computations. Parallelization of SGM applied to elliptic partial differential equations is reported in [10], but as explained further it is still prohibitively slow to deal with the optical systems presented in this chapter. In [11], an asynchronous parallelization of MLFMM for *deterministic* structures consisting of multiple dielectric objects is described. To our best knowledge, however, present chapter is the first that proposes the parallelization of a full-wave SGM-MLFMM solver for Maxwell's equations, capable of handling both dielectric and perfectly electric conducting (PEC) objects.
This chapter is organized as follows. In Section 5.2, we present the theoretical framework of the SGM-MLFMM paradigm for solving BIEs. Section 3 deals with the implementation of the algorithm with a focus on its parallelization and on the design of a preconditioner. In Section 4, we report simulation results for several large optical structures, such as lens systems. We validate our method by comparing the results with a traditional SCM. Finally, in Section 5, we give some concluding remarks.

5.2 Theoretical framework

We start with a very general description of the electromagnetic problem geometry under consideration, which allows deriving a rigorous theoretical framework. Consider two-dimensional (2D) dielectric objects with a refractive index n_i, or equivalently, by means of their permittivity ϵ_i and permeability μ_i, and perfectly electrically conducting (PEC) objects, residing in free space (Fig. 5.1). The geometry of these objects is stochastically described by means of a set of M random variables (RV) that are collected in the random vector $\boldsymbol{\xi} = [\xi_1\ \xi_2\ ...\ \xi_M]$ with domain Ω. One object can depend on zero, one or more RVs. The objects are illuminated by an incoming transverse magnetic (TM) electromagnetic wave E_z^i. In the sequel, an $\exp(j\omega t)$ time dependence, with ω the angular frequency, is assumed and suppressed throughout the text.

Starting from Maxwell's equations, the scattering problem is cast as a boundary integral equation (BIE), which for dielectric objects was written down in [12]. For conciseness, we limit the description to the case of a single object with contour C, for which the

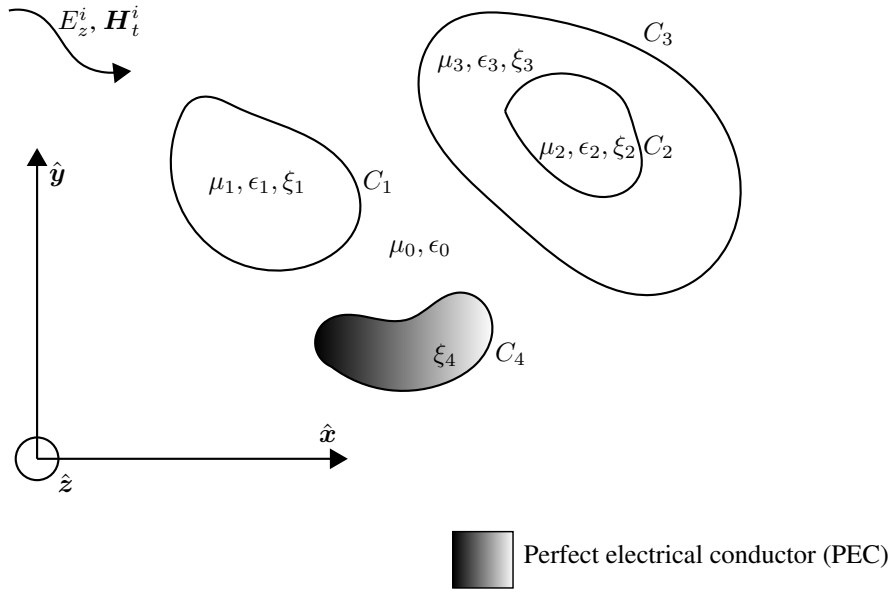

Figure 5.1: Canonical problem geometry. Objects are described by their electrical properties μ_i, ϵ_i and their geometries are defined with contours C_i. Stochastic variations of the geometry are introduced and indicated by means of a set of random variables ξ_i, $i = 1, ..., M$.

pertinent BIEs are given by [13]:

$$\begin{aligned} E_z^i - \lim_{r\to C^+} \oint_C \left[E_z \frac{\partial G_0}{\partial n'} - \frac{jk_0^2}{\omega\epsilon_0} G_0 H_t \right] dc' \\ = \lim_{r\to C^-} \oint_C \left[E_z \frac{\partial G}{\partial n'} - \frac{jk^2}{\omega\epsilon} G H_t \right] dc', \end{aligned} \tag{5.1}$$

$$\begin{aligned} H_t^i - \lim_{r\to C^+} \oint_C \left[-\frac{j\omega\epsilon_o}{k_0^2} E_z \frac{\partial^2 G_0}{\partial n \partial n'} - \frac{\partial G_0}{\partial n} H_t \right] dc' \\ = \lim_{r\to C^-} \oint_C \left[-\frac{j\omega\epsilon}{k^2} E_z \frac{\partial^2 G}{\partial n \partial n'} - \frac{\partial G}{\partial n} H_t \right] dc', \end{aligned} \tag{5.2}$$

where G_o represents the Green's function of the free space background medium with wavenumber k_0 given by:

$$G_0(\boldsymbol{\rho}, \boldsymbol{\rho}') = \frac{j}{4} H_0^{(2)}(k_0 |\boldsymbol{\rho} - \boldsymbol{\rho}'|), \tag{5.3}$$

and G represents a similar Green's function for the i-th medium with wavenumber $k_i = k_0 n_i$, corresponding to the material the object is made of. The unknowns are the

z-oriented electric field E_z and the magnetic field H_t tangential to the contour C. C^+ and C^- represents the path of integration along the contour C when integrating just outside and just inside the object respectively. To solve the BIE, the contour is divided into a number of segments N_{seg}. The unknown magnetic field H_t is expanded into pulse basis functions $b_i(\boldsymbol{\rho}')$ defined over these segments, while the unknown electric field E_z is expanded into triangular basis functions $t_i(\boldsymbol{\rho}')$ as follows:

$$H_t = \sum_{i=1}^{N_{seg}} H_{t,i}\ b_i(\boldsymbol{\rho}'), \tag{5.4}$$

$$E_z = \sum_{i=1}^{N_{seg}} E_{z,i}\ t_i(\boldsymbol{\rho}'). \tag{5.5}$$

This discretization leads to a number of $N = 2N_{seg}$ scalar unknown expansion coefficients $H_{t,i}$ and $E_{z,i}$. To create a traditional MoM linear system of equations, triangular testing functions $t_i(\boldsymbol{\rho})$ for H_t and pulse testing functions $b_i(\boldsymbol{\rho})$ for E_z are used. The resulting linear system of equations is written as:

$$V_i = \sum_{j=1}^{N} Z_{ij}\ I_j, \quad \text{for all } \ i = 1, ..., N, \tag{5.6}$$

with

$$V_i = \int_{l_i} E_z^i\ b_i(\boldsymbol{\rho}) d\boldsymbol{\rho} \tag{5.7}$$

or

$$V_i = \int_{l_i} H_t^i\ t_i(\boldsymbol{\rho}) d\boldsymbol{\rho}, \tag{5.8}$$

and:

$$Z_{ij} = \int_{l_i}\int_{l_j} E_{z,j}\ b_i(\boldsymbol{\rho})\ t_j(\boldsymbol{\rho}')\frac{\partial G_0}{\partial n'} d\boldsymbol{\rho} d\boldsymbol{\rho}' + \int_{l_i}\int_{l_j} E_{z,j}\ b_i(\boldsymbol{\rho})\ t_j(\boldsymbol{\rho}')\frac{\partial G}{\partial n'} d\boldsymbol{\rho} d\boldsymbol{\rho}', \tag{5.9}$$

or

$$Z_{ij} = -\int_{l_i}\int_{l_j} H_{t,j}\ b_i(\boldsymbol{\rho})\ b_j(\boldsymbol{\rho}')\frac{jk_0^2}{\omega\epsilon_0} G_0\, d\boldsymbol{\rho} d\boldsymbol{\rho}' - \int_{l_i}\int_{l_j} H_{t,j}\ b_i(\boldsymbol{\rho})\ b_j(\boldsymbol{\rho}')\frac{jk^2}{\omega\epsilon} G\, d\boldsymbol{\rho} d\boldsymbol{\rho}', \tag{5.10}$$

or

$$Z_{ij} = -\int_{l_i}\int_{l_j} E_{z,j}\ t_i(\boldsymbol{\rho})\ t_j(\boldsymbol{\rho}')\frac{j\omega\epsilon_o}{k_0^2}\frac{\partial^2 G_0}{\partial n \partial n'}\, d\boldsymbol{\rho} d\boldsymbol{\rho}' - \int_{l_i}\int_{l_j} E_{z,j}\ t_i(\boldsymbol{\rho})\ t_j(\boldsymbol{\rho}')\frac{j\omega\epsilon}{k^2}\frac{\partial^2 G}{\partial n \partial n'}\, d\boldsymbol{\rho} d\boldsymbol{\rho}', \tag{5.11}$$

or

$$Z_{ij} = -\int_{l_i}\int_{l_j} H_{t,j}\; t_i(\boldsymbol{\rho})\; b_j(\boldsymbol{\rho}')\frac{\partial G_0}{\partial n}\, d\boldsymbol{\rho} d\boldsymbol{\rho}' - \int_{l_i}\int_{l_j} H_{t,j}\; t_i(\boldsymbol{\rho})\; b_j(\boldsymbol{\rho}')\frac{\partial G}{\partial n}\, d\boldsymbol{\rho} d\boldsymbol{\rho}', \tag{5.12}$$

where the integrations are done over line segments l_i and l_j.
When the geometry of the objects is stochastic, meaning the location of several segments of the contours may depend on one or more of the RVs, the resulting MoM system becomes stochastic and is in general written as:

$$\overline{\boldsymbol{Z}}(\boldsymbol{\xi})\boldsymbol{I}(\boldsymbol{\xi}) = \boldsymbol{V}(\boldsymbol{\xi}), \tag{5.13}$$

where the traditional $N \times N$ interaction matrix $\overline{\boldsymbol{Z}}$, the known right-hand side (RHS) N-vector $\boldsymbol{V}$, and the vector $\boldsymbol{I}$ collecting the N unknown expansion coefficients, all become dependent on the random vector $\boldsymbol{\xi}$. The reader is encouraged to consult [3], [14], [15] and the references therein to gain familiarity with the SGM in the domain of electrical engineering. Here, similarly as in [6], where the SGM was combined with the MoM for small scattering problems, we start from expansions of the stochastic quantities introduced in Eq.(5.13) into polynomial basis functions. These PCEs are given by:

$$\overline{\boldsymbol{Z}}(\boldsymbol{\xi}) \approx \sum_{k=0}^{K} \overline{\boldsymbol{Z}}_k \phi_k(\boldsymbol{\xi}), \tag{5.14}$$

$$\boldsymbol{V}(\boldsymbol{\xi}) \approx \sum_{k=0}^{K} \boldsymbol{V}_k \phi_k(\boldsymbol{\xi}), \tag{5.15}$$

$$\boldsymbol{I}(\boldsymbol{\xi}) \approx \sum_{k=0}^{K} \boldsymbol{I}_k \phi_k(\boldsymbol{\xi}), \tag{5.16}$$

where $\phi_k(\boldsymbol{\xi})$ are multivariate polynomials, i.e. products of M univariate polynomials for the individual RVs ξ_i chosen according to the Wiener-Askey scheme [2] and such that they are orthonormal with respect to the probability density function (PDF) $W(\boldsymbol{\xi})$ with domain Ω of the random vector $\boldsymbol{\xi}$, as follows:

$$< \phi_j(\boldsymbol{\xi}), \phi_k(\boldsymbol{\xi}) >= \delta_{jk} \tag{5.17}$$

where δ_{jk} is the Kronecker δ and with the inner product defined as:

$$< f(\boldsymbol{\xi}), g(\boldsymbol{\xi}) >= \int_{\Omega} f(\boldsymbol{\xi}) g(\boldsymbol{\xi}) W(\boldsymbol{\xi}) d\boldsymbol{\xi}. \tag{5.18}$$

The M univariate polynomials are multiplied following the total degree rule, i.e., so that sum of the orders is at most P. Given this total order P, the number of polynomials $K+1$, as used in the PCEs Eqs. (5.14), (5.15) and (5.16), is determined as:

$$K + 1 = \frac{(M+P)!}{M!P!}. \tag{5.19}$$

The expansion coefficients in Eqs. (5.14) and (5.15) are found via projection:

$$\boldsymbol{X}_k =< \boldsymbol{X}(\boldsymbol{\xi}), \phi_k(\boldsymbol{\xi}) >, \tag{5.20}$$

where $\boldsymbol{X}$ represents $\overline{\boldsymbol{Z}}$ and $\boldsymbol{V}$. Inserting PCE Eqs. (5.14), (5.15) and (5.16) into Eq. (5.13) yields:

$$\sum_{k=0}^{K} \boldsymbol{V}_k \phi_k(\boldsymbol{\xi}) = \sum_{k=0}^{K} \sum_{l=0}^{K} \overline{\boldsymbol{Z}}_k \boldsymbol{I}_l \phi_k(\boldsymbol{\xi}) \phi_l(\boldsymbol{\xi}), \tag{5.21}$$

Galerkin projection of both sides of Eq. (5.21) onto the orthogonal polynomial basis functions leads to:

$$< \sum_{k=0}^{K} \boldsymbol{V}_k \phi_k(\boldsymbol{\xi}), \phi_m(\boldsymbol{\xi}) > = < \sum_{k=0}^{K} \sum_{l=0}^{K} \overline{\boldsymbol{Z}}_k \boldsymbol{I}_l \phi_k(\boldsymbol{\xi}) \phi_l(\boldsymbol{\xi}), \phi_m(\boldsymbol{\xi}) >, \quad \text{for all } m = 0, ..., K, \tag{5.22}$$

which, after using the orthonormal property given by Eq. (5.17), again results in an equivalent system of equations, in which the stochastic dependence is eliminated:

$$\boldsymbol{V}_m = \sum_{m:\gamma_{klm} \neq 0} \overline{\boldsymbol{Z}}_k \, \boldsymbol{I}_l \, \gamma_{klm} \tag{5.23}$$

with $\gamma_{klm} =< \phi_k(\boldsymbol{\xi}) \phi_l(\boldsymbol{\xi}), \phi_m(\boldsymbol{\xi}) >$ and where the summation is taken for all non-zero values of γ_{klm}. The linear system given by Eq. (5.23) shows that the traditional $O(N^2)$ complexity for a standard deterministic MoM is now scaled with factor that corresponds to the number of non-zero values of γ_{klm} and follows an $O(K^{1.5})$ scaling law of [7]. Moreover, the total number of unknowns in (5.23) is actually $N_{stoc} = (K+1)N$. In conclusion, although SGM-MoM is accurate for small scattering problems, the approach rapidly becomes intractable for the variability analysis of a large electromagnetic structures. Therefore, in the next section, MLFMM will be introduced. This then further allows parallelization, which is necessary to expedite the computations.

5.3 Implementation of a parallel SGM-MLFMM solver with a preconditioner

5.3.1 SGM-MLFMM

A vast amount of literature is available describing the traditional, *deterministic* MLFMM scheme [16]. This scheme has, e.g., also been applied to scattering from and radiation by intricate dielectric objects such as printed circuit board antennas [17], [18] and to photonic crystal waveguides [19]. The reader is encouraged to consult these references to gain familiarity with the MLFMM scheme. Here, for conciseness, we only repeat the gist of it and immediately introduce a *stochastic* variant. This algorithm allows improving the computational complexity of the matrix-vector product (MVP) during the

iterative solution of Eq. (5.23) and avoiding the storage of $\overline{\boldsymbol{Z}}(\boldsymbol{\xi})$ or its PCE coefficients $\overline{\boldsymbol{Z}}_k$.

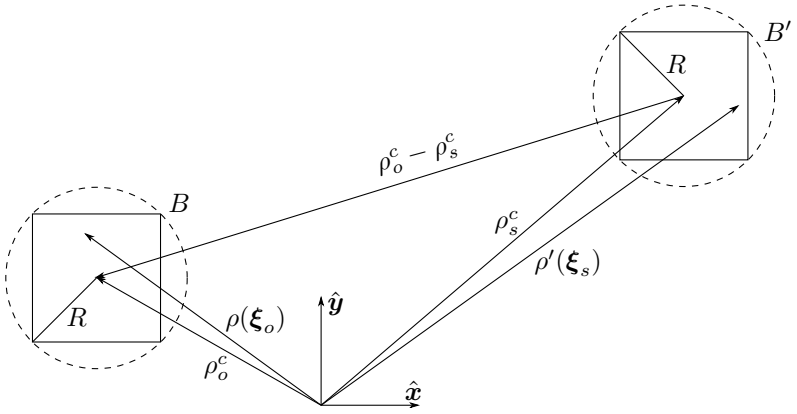

Figure 5.2: Typical MLFMM constellation of a source box B' and an observation box B.

The boundaries of all dielectric objects are discretized into N finite segments, corresponding to the pertinent BIE-MoM approach. Next, all these segments are recursively subdivided in an L-level MLFMM quad-tree. At each level $l = 1, 2, \ldots, L$, the boxes are circumscribed by a hypothetical circle of radius R_l. Any interaction between two segments in the BIE-MoM scheme, corresponding to one element of the matrix $\overline{\boldsymbol{Z}}(\boldsymbol{\xi})$, is readily rewritten as the interaction between many elementary line sources $s_i(\boldsymbol{\xi}_s)$ with strength $J_{s_i}(\boldsymbol{\xi})$. In Fig. 5.2, one such single line source, located at $\boldsymbol{\rho'}(\boldsymbol{\xi}_s)$ and residing in source box B', and a single observer, located at $\boldsymbol{\rho}(\boldsymbol{\xi}_o)$ and residing in source box B, is shown. Note that the locations $\boldsymbol{\rho'}$ and $\boldsymbol{\rho}$ depend on mutually independent subsets $\boldsymbol{\xi}_s$ and $\boldsymbol{\xi}_o$ of the total set of RVs $\boldsymbol{\xi}$, as in MLFMM algorithms the source and observation boxes must be separated sufficiently far from each other. The centers of the source and observation box are located at the deterministic locations $\boldsymbol{\rho}_s^c$ and $\boldsymbol{\rho}_o^c$ respectively.
We invoke the well-known plane-wave decomposition of the pertinent Green's function $G(\boldsymbol{\rho}(\boldsymbol{\xi}_o), \boldsymbol{\rho'}(\boldsymbol{\xi}_s))$ of the background medium to rewrite the MVP as follows [16]. First, during the so-called aggregation step, the radiation pattern of box B' is sampled into $2Q + 1$ outgoing plane waves (OPWs):

$$OPW_{q'}^{B'}(\boldsymbol{\xi}) = \sum_{s_i} e^{j\boldsymbol{k}(\varphi_{q'})\cdot(\boldsymbol{\rho'}(\boldsymbol{\xi}_s)-\boldsymbol{\rho}_s^c)} J_{s_i}(\boldsymbol{\xi}), \tag{5.24}$$

where $\boldsymbol{k}(\varphi_{q'}) = k(\cos\varphi_{q'}\hat{\boldsymbol{x}} + \sin\varphi_{q'}\hat{\boldsymbol{y}})$. The samples are taken at angles $\varphi_{q'} = 2\pi q'/(2Q+1), q' = -Q, \ldots, Q$, and the number of samples is typically chosen such that the radiation pattern is reconstructed with a desired number of digits of accuracy, denoted as d_0. In a well-constructed MLFMM tree, any accuracy up to machine precision can be reached [16], provided Q is chosen to be:

$$Q = 2kR + 1.8d_0^{2/3}(2kR)^{1/3}. \tag{5.25}$$

The stochastic nature of this aggregation step is indicated by the $\boldsymbol{\xi}$ dependence. In the proposed SGM-MLFMM approach, PCE expansion are again invoked:

$$OPW^{B'}(\boldsymbol{\xi}) = \sum_{k=0}^{K} OPW_k^{B'} \phi_k(\boldsymbol{\xi}) \tag{5.26}$$

such that via projection, each PCE-coefficient of the OPWs is computed as:

$$OPW_m^{B'} = \sum_{m:\gamma_{klm}\neq 0} \overline{\boldsymbol{A}}_k \, \boldsymbol{I}_l \, \gamma_{klm} \tag{5.27}$$

where $\overline{\boldsymbol{A}}_k$ are PCE coefficients of the aggregation matrix, defined as:

$$\overline{\boldsymbol{A}}(\boldsymbol{\xi}_s)_{q',s_i} = e^{j\boldsymbol{k}(\varphi_{q'})\cdot(\boldsymbol{\rho'}(\boldsymbol{\xi}_s)-\boldsymbol{\rho}_s^c)}, \quad q' = -Q, \ldots, Q, \tag{5.28}$$

and $\boldsymbol{I}_l$ are PCE coefficients of the current density which contain PCE coefficients of the elementary current strengths $J_{s_i}(\boldsymbol{\xi})$.
Second, during the translation step, a deterministic and diagonal translation matrix $\overline{\boldsymbol{T}}$ converts the PCE-coefficients of the OPWs about the center of box B' to incoming plane waves (IPWs) about the center of box B, as follows:

$$IPW_{k,q'}^{B} = T_{qq}(k, |\rho_{so}^{cc}|, \varphi_{so}^{cc}) OPW_{k,q'}^{B'}, \quad q' = -Q, \ldots, Q, \quad k = 0, \ldots, K, \tag{5.29}$$

where the numbers $T_{qq}(k, |\rho_{so}^{cc}|, \varphi_{so}^{cc})$ represent the $2Q+1$ (non-zero) diagonal elements of the translation matrix, given by:

$$T_{qq}(k, \rho, \varphi) = \frac{1}{2Q+1} \sum_{q''=-Q}^{Q} H_{q''}^{(2)}(k\rho) e^{jq''(\varphi-\varphi_q-\frac{\pi}{2})} \tag{5.30}$$

with $\rho_{so}^{cc} = |\boldsymbol{\rho}_o^c - \boldsymbol{\rho}_s^c|$ the distance between the centers of the boxes and φ_{so}^{cc} the angle between vector $\boldsymbol{\rho}_o^c - \boldsymbol{\rho}_s^c$ and the x-axis.
Third, during the disaggregation step, the IPWs are evaluated at the observation points. In case of a single, elementary line source at $\boldsymbol{\rho'}(\boldsymbol{\xi}_s)$, the field at a single observer at $\boldsymbol{\rho}(\boldsymbol{\xi}_o)$ in box B is nothing else than the pertinent Green's function, now expanded using the plane-wave formalism, as follows:

$$G(\boldsymbol{\rho}(\boldsymbol{\xi}_o); \boldsymbol{\rho'}(\boldsymbol{\xi}_s)) = \frac{j}{4} \sum_{q=-Q}^{Q} e^{-j\boldsymbol{k}(\varphi_q)\cdot(\boldsymbol{\rho}(\boldsymbol{\xi}_o)-\boldsymbol{\rho}_o)} IPW_q^B(\boldsymbol{\xi}) \tag{5.31}$$

To obtain an efficient multilevel scheme, the interaction between boxes occurs at well-chosen levels in the MLFMM tree. Up- and downsampling of OPWs and IPWs happens via Fast Fourier Transforms (FFTs).

In the deterministic MLFMM simulation, the total cost of all steps is $O(N \log N)$. The aggregation step and disaggregation steps are calculated with cost $O(N)$. In the SGM-MLFMM approach, as the aggregation and disaggregation steps now also depend on subsets of $\boldsymbol{\xi}$, the computational cost increases up to $O(KN)$ [7]. Similar observations are valid for the memory complexity.

5.3.2 Parallelization

An efficient implementation of the deterministic MLFMM has allowed handling problems with up to one million of unknowns on a single workstation. Parallel implementations on several nodes has led to tackling deterministic problems with billions of unknowns [20]. In our stochastic case, however, the total number of unknowns is not only determined by the spatial discretization into N segments, but also by the number of polynomials, i.e. $K + 1$. Therefore, the UQ of medium- and large-scale problems, such as the variability analysis of the optical lens systems presented in this chapter, should be performed via a parallel algorithm, leveraging the computational and memory resources of every available computing node.
Parallel solvers require a parallel iterative method (e.g. TFQMR [21]) and a parallel algorithm to compute the MVP. For the former, libraries like PIM [22] can be readily applied. From SGM Eq. (12), a straightforward way to parallelize the MVP may be revealed, namely the distribution of the matrix-vector products $\overline{\boldsymbol{Z}}_k \boldsymbol{I}_l$ among several processes. Each process then computes only a subset of all required matrix-vector products $\overline{\boldsymbol{Z}}_k \boldsymbol{I}_l$. This idea is applied in [10]. Despite its simplicity, this approach suffers from the fact that a given product $\overline{\boldsymbol{Z}}_k \boldsymbol{I}_l$ in itself is not parallelized. Each such product can be handled by a single process, but as the dimensions of each matrix $\overline{\boldsymbol{Z}}_k$ correspond to the number of spatial discretization elements N, the simulation of large structures with high N is still prohibitively expensive.
As opposed to this approach, we proprose a parallelization scheme where each product $\overline{\boldsymbol{Z}}_k \boldsymbol{I}_l$ in itself is parallelized among all of the processes. This scheme has the advantage that the geometrical discretization elements are distributed among the processes. We provide an overview of the underlying concepts and refer to the extensive literature that exists for parallel *deterministic* MLFMM algorithms where appropriate.
The MLFMM tree is created for the complete electromagnetic structure under consideration. The boxes at a prespecified level-of-partitioning (LoP) in this tree are partitioned and assigned to different processes. If a certain box is a assigned to a certain process, the entire subtree of that box and all corresponding geometrical segments and unknown stochastic expansion coefficients ($K + 1$ coefficients per segment) are also assigned to that process. The partitioning is done in such way that approximately the same number of expansion coefficients is assigned to each process. To ensure a good spatial locality between boxes assigned to a given process, boxes are ordered according to a Hilbert space filling curve (SFC) prior to partitioning. Smaller dielectric regions will be partitioned among fewer processes whereas large dielectric regions (e.g. the background medium) will be partitioned among many processes.
For a given LoP and all levels below, it holds that a box is assigned to only one single process. All $K + 1$ radiation patterns (both outgoing and incoming) in such a box are

also assigned to that process and the process is responsible for their computation. For levels higher than the LoP, it becomes increasingly difficult to achieve a good load balance because the number of boxes decreases for higher levels. Nevertheless, the amount of required computations on those levels does not decrease because of the size of the radiation patterns increases with higher levels. To deal with this, we propose to extend the hierarchical partitioning strategy [23], [24] developed for deterministic MLFMM to the stochastic case. As illustrated in Fig. 5.3, rather than assigning a box

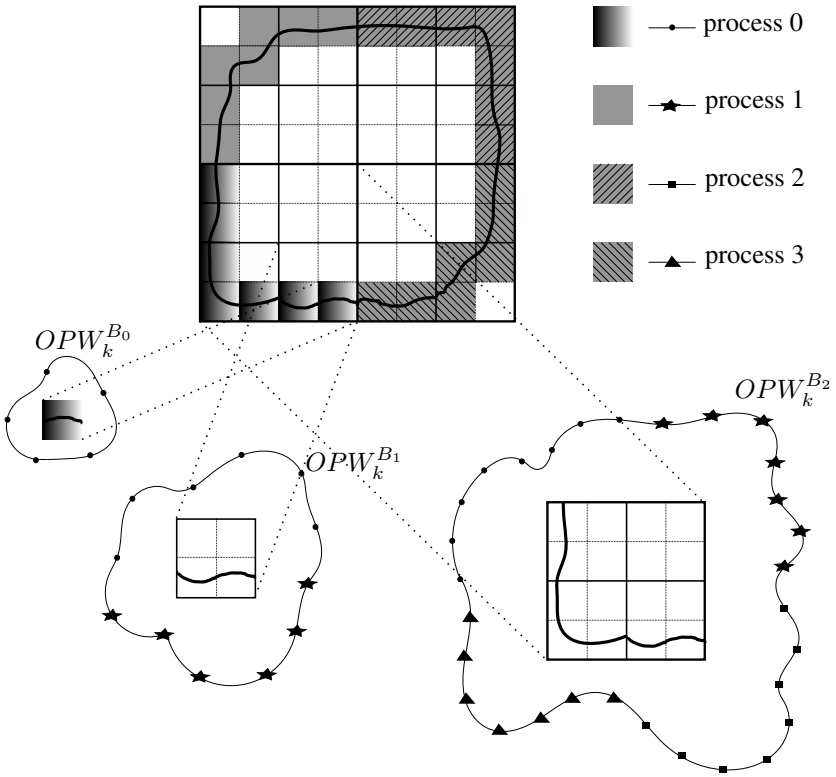

Figure 5.3: Organization of MLFMM boxes and partitioning scheme for an arbitrary structure. On the lowest level each box is handled by one process; on higher levels, K radiation samples are shared among all processes. $OPW_k^{B_i}$ is k-th PCE coefficient of the box on the level i.

and its radiation patterns as a whole to a single process, boxes are shared between an increasing number of processes as the number of radiation pattern samples increases. Specifically, from the LoP onwards, for every next level, each of the $K + 1$ radiation pattern samples in a box are partitioned in an increasing number of 2, 4, 8, 16, ... etc. partitions. A process then holds only a single partition of the radiation pattern samples in its memory. It has been shown that, in the deterministic case, such a hierarchical partitioning scheme is able to effectively balance the load among processes [24]. Processes

are responsible for the computation of all radiation pattern samples and expansion coefficients that are locally held in memory using the execution of the MLFMM algorithm. Some of these computations rely on data that is not locally stored and thus needs to be communicated through the interconnection network. As we are dealing with multiple dielectric objects, we opted for the asynchronous approach described in [11]. At a given point in time, different processes can perform different kind of tasks: certain processes might be communicating while others are performing (different kinds of) calculations. All computations that need to be performed by a process are partitioned into work packages. These work packages are sorted in a priority queue. Some work packages depend on data to be received from other processes and can only be scheduled once these data have actually been received. Similarly, certain work packages result in (intermediate) data that needs to be sent to other processes. The priority queue ensures that work packages are handled in such order that the overall idle time of processes is minimized. Organization of these working packages and priorities of the operations are well described in [11].

5.3.3 Preconditioner

For any iterative process, the number of iterations needed to obtain a result with a predefined accuracy is an important factor. This number depends on the condition number of the system matrix [25] . By rewriting Eq. (5.23) in matrix form, it can be seen that the equivalent system matrix of the SGM possesses a block-structure [4]. The zeroth-order PCE coefficient which corresponds to the mean of the $\overline{\boldsymbol{Z}}(\boldsymbol{\xi})$ matrix, i.e. $\overline{\boldsymbol{Z}}_0$, is located on diagonal blocks. Higher PCE coefficients of the matrix only marginally contribute to these diagonal blocks. For small variations, which is the case in most practical applications, the equivalent SGM system matrix is thus block-diagonal dominant and a block-Jacobi preconditioner could be used [26].
However, given our MLFMM-approach, the submatrix $\overline{\boldsymbol{Z}}_0$ is never stored. Moreover, calculation of its inverse for large structures would rapidly become prohibitively expensive. Therefore, a different type of preconditioner is proposed here. Within $\overline{\boldsymbol{Z}}_0$, there are so-called *near interactions* that are calculated with a classical MoM approach. These interactions are found on and around the main diagonal of the $\overline{\boldsymbol{Z}}_0$ matrix. Our preconditioner is based on these "near" blocks. The size of these blocks, i.e. the number of interactions which are calculated in this classical MoM fashion, determines the efficiency of the preconditioner. On the one hand, if the blocks are large, then preconditioning becomes stronger, but the memory, setup time and time required for one MVP also increases. On the other hand, if these blocks are chosen small, then the preconditioner may become rather useless, especially for large electromagnetic structures.

5.4 Numerical results

All simulations were performed on a system supporting the Message Passing Interface (MPI), which was used to implement the parallel SGM-MLFMM solver. As indicated

further, some simulations were performed on one node with multiple cores, while others were performed on several nodes connected by an InfiniBand network. The linear system of equations is solved with Parallel Iterative Methods (PIM) using TFQMR.

5.4.1 Validation example: lens system with translational variation

As a validation example, we consider a lens system of two circular lenses with a permittivity $\epsilon_r = 4$ and a PEC aperture, as shown in Fig. 5.4. The size of the lenses is 2000λ and 5000λ, respectively, and they are separated by a distance of 30000λ. The size of the gap in the PEC shield is 2500λ and the shield is placed at a distance of 20000λ from the leftmost lens. The structure is illuminated with a Gaussian beam of width 500λ impinging upon the center of the leftmost lens along the optical axis. A deterministic simulation of this system was presented in [27], where good accuracy between Gaussian-beam, 1.5D and 2D full-wave methods was reported. Moreover, the 2D full-wave method has been validated up to 100 million of unknowns for both dielectric and PEC cylinders for which analytical solutions exist [28].

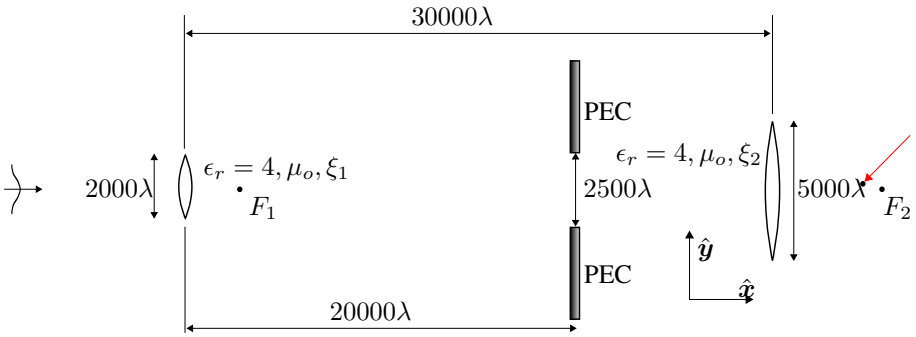

Figure 5.4: The lens system setup.

The structure and the total field calculated in a region with a width of 40000λ and a height of 8000λ is presented in Fig. 5.5. One pixel corresponds to a cell of size $10\lambda \times 10\lambda$. A block-Jacobi preconditioner was used on blocks with dimension $16\lambda \times 16\lambda$. The iterative precision was set to 10^{-3}. For this deterministic simulation, the number of unknowns is 705008 and the iterative precision is reached after $N_{iter} = 369$ iterations. To induce variations, the y-coordinates of the positions of the lenses are now uniformly varied between $-\lambda/20$ and $\lambda/20$ of their nominal values. The uniform distribution is chosen as all realizations are equally probable and it also leads to the largest variation in the field values. Stochastic simulations are performed by two methods: (i) a robust and easy to implement SCM and (ii) the novel SGM-MLFMM, in order to validate the accuracy of the latter. As our results are validated with a non-intrusive SCM that merely reuses results from the deterministic 2D algorithm [27], the output variability

of our novel stochastic SGM-MLFMM is expected to match well with Gaussian beam based methods.

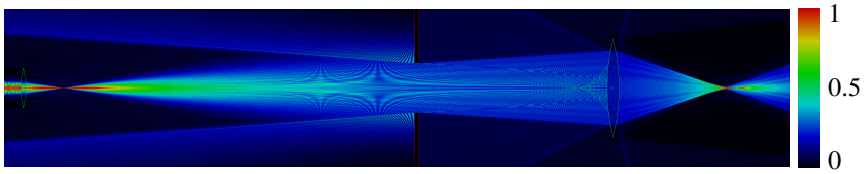

Figure 5.5: Field density $|E_z|$(V/m) for the deterministic simulation for the configuration of Fig. 5.4.

To present the influence of the variations, the average field density and its standard deviations (`stdev`) around the two focal points (indicated with F_1 and F_2 in Fig. 5.4), i.e. in an area with a width of 2000λ and a height of 1000λ, are presented in Fig. 5.6. The influence of the geometrical variations are clearly appreciated from this figure. It is also observed that left from the PEC slit the variations are concentrated mainly around the focal point, i.e. where the field value reaches its maximum. At the right side of the PEC slit, the variations are more evenly distributed in the neighbourhood of the focal point. To give an indication of the variation, we mention that at the point where the standard deviation is maximal and equal 0.0828 V/m, the average field density is 1.5287 V/m, i.e. the output variation of the field is about $0.0828/1.5287 \approx 5.4\%$. This location is near the right focal point, indicated with the red arrow in Fig. 5.4.

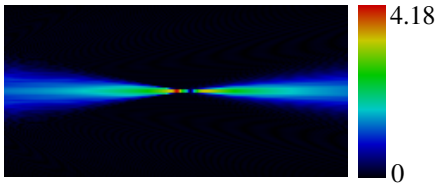

(a) mean - first focal point

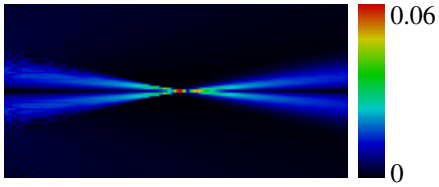

(b) standard deviation - first focal point

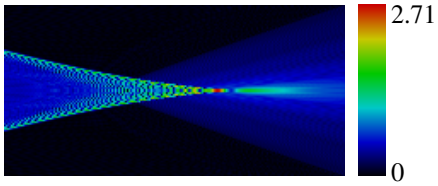

(c) mean - second focal point

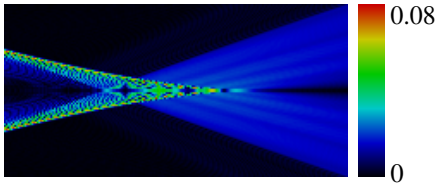

(d) standard deviation - second focal point

Figure 5.6: Mean and standard deviation of the field density $|E_z|$(V/m) around the focal points.

To validate our method, its accuracy is compared to SCM, as presented in Table 5.1. The accuracy of both solvers is set to 10^{-3}. Both methods converge to the same result

for different polynomial orders and even for $P = 1$ we get accurate results. For all polynomial orders, the number of iterations is about the same as in the deterministic case. This is important, since one MVP is computationally expensive. For example, for $P = 3$, the total number of unknowns is $N_{stoc} = 7\,050\,080$ and the number of iterations is 372. This means that our preconditioner is efficient for this stochastically varying structure. Note that for the SCM method, the number of iterations is equal to the average number of iterations for all considered realizations of the RVs.

Table 5.1: Mean and standard deviation for the point indicated on Fig. 5.4, i.e. the point close to the second focal point with maximum variance.

Method	P	N_{stoc}	N_{iter}	Mean (V/m)	`stdev` (V/m)	CPU time
SGM	1	2 115 024	365	1.5287	0.0828	2 h
SGM	2	4 230 048	355	1.5287	0.0828	5.1 h
SGM	3	7 050 080	372	1.5287	0.0828	9 h
SCM	1	2 115 024	385	1.5329	0.0829	3.8 h
SCM	2	4 230 048	363	1.5329	0.0829	8 h
SCM	3	7 050 080	370	1.5329	0.0829	15.5 h

Regarding the computational cost, SGM shows a clear advantage over SCM. To make a fair comparison, both SGM and SCM simulations were performed on the same machine. In the case of SCM, a wrapper function sequentially executes the parallelized deterministic code for different realizations of a random vector. Using a single node containing two quad-core CPUs (8 cores in total) running at 2 GHz, where simulations are performed with 8 parallel processes, and for $P = 2$, the SGM-MLFMM computation takes about 5h, while the SCM simulation for all realizations takes about 8 h.

For larger P, we need more nodes to get results in a reasonable time. To give an indication, running the SGM-MLFMM for this lens setup with $P = 4$ and $N_{stoc} = 10\,575\,120$, takes about 1h, when using 3 nodes and 16 parallel processes per node. This simulation was performed on the Flemish Supercomputer Center (VSC) infrastructure where one node has a dual-socket octo-core CPU (16 CPU cores in total) running at 2.6 GHz. On the same machine we also performed a benchmark test for the MVPs for a varying number of processes and we calculated the speedup and parallel efficiency. The speedup is defined as the ratio of the runtime on a single process T_1 and the runtime T_n using p processes:

$$S_p = \frac{T_1}{T_p}. \tag{5.32}$$

In the ideal case the speedup factor is equal to the number of processes that is used. The parallel efficiency η is the ratio of the speedup and the theoretical maximum speedup:

$$\eta_p = \frac{S_p}{p} = \frac{T_1}{pT_p}. \tag{5.33}$$

The graphs for the scalability and speedup are presented in Fig. 5.7. All simulations were performed for the $P = 2$ case. It is visible that our algorithm scales very well

with an increasing number of processes. The efficiency decreases due to the increasing amount of data that needs to be communicated.

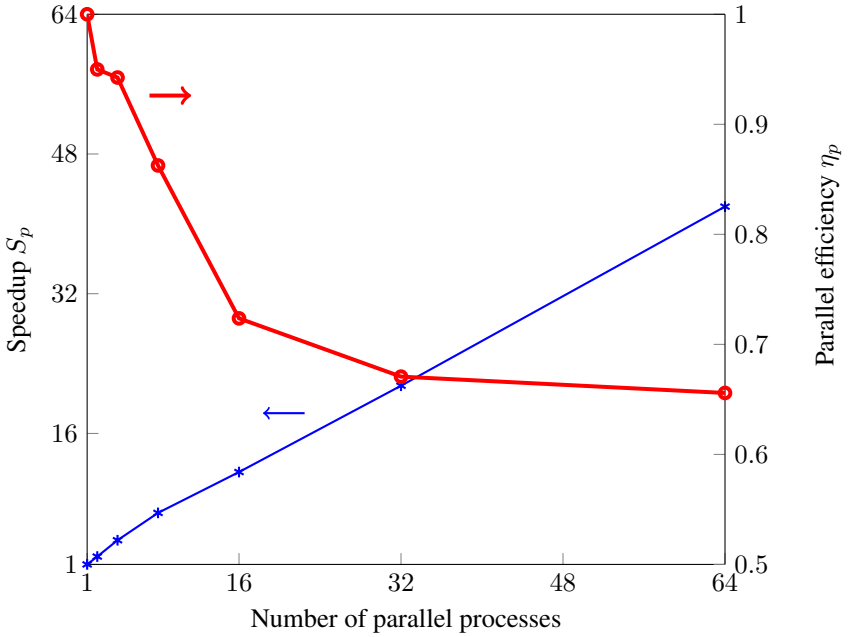

Figure 5.7: Speedup and parallel efficiency for a varying number of parallel processes.

5.4.2 Application example 1: Lens system with rotational variation

As a second example, we consider the same lens system as in Section 5.4.1, but now, the variations of the lenses' positions are induced by rotation in the (x, y)-plane of the lenses around their centers. The lenses' rotations are described by a uniform stochastic process with a maximum deviation of $1/60$ of a degree. The average field pattern looks like in Fig. 5.6, but the field pattern for standard deviation is different and is shown in Fig. 5.8. We can observe that the standard deviation is now slightly smaller. However, the relative variation is higher as the maximal variations occurs at points where the field strength is low.

The number of iterations required to obtain an iterative precision of 10^{-3} is higher in this case, e.g. for $P = 2$, 1018 iterations are required. This is a consequence of the larger variations on the phase of the field and the loss of symmetry with respect to the optical axis of the setup. Additionally, in Table 5.2, we provide results for the point close to second focal point at which the standard deviation is the highest.

In this case, we can see that $P = 3$ is sufficient to obtain convergence and with $P = 2$ we get acceptable results. Due to the phase effect, $P = 1$ provides a slightly

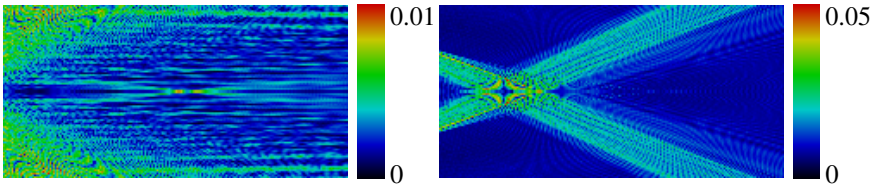

(a) standard deviation - first focal point (b) standard deviation - second focal point

Figure 5.8: Standard deviation of the field density $|E_z|$(V/m) around the focal points.

Table 5.2: Mean and standard deviation for the point close to the second focal point with maximum variance.

Method	P	Mean (V/m)	`stdev` (V/m)
SGM	1	0.4482	0.0407
SGM	2	0.4603	0.0541
SGM	3	0.4601	0.0526

different result than for that obtained for the higher orders. Simulation with $P = 3$ and $N_{stoc} = 7\,050\,080$ unknowns takes about 1h on 3 nodes with 16 parallel processes.

A typical quantity of interest describing such lens system is the local intensity, defined as:

$$I = \frac{cn\epsilon_0}{2}|E_z|^2, \tag{5.34}$$

where c is speed of light in vacuum and n is the refractive index. To get a better insight in the variation of the local intensity when lenses are prone to variability, the PDFs of the local intensity for the second focal point and the point with maximum variance are presented in Fig. 5.9. It is clearly visible that the local intensity in both observation points is considerably affected by the variation of the lenses.

5.4.3 Application example 2: Cassegrain antenna system with induced variations

As a final example, we consider a Cassegrain antenna system, with a 35-meter parabolic main reflector and a 6-meter hyperbolic sub-reflector. Additionally, this system consists of one flat mirror and one elliptical mirror. The structure is based on a similar problem described in [28]. The operating frequency is chosen to be 32 GHz, so we perform one harmonic simulation at that frequency. The structure is excited with a Gaussian beam with a waist of 2 m impinging upon a coated lens with a 4 meter diameter. This is a lens with a relative permittivity of $\epsilon_r = 4$ and a $\lambda/4$ coating with a relative permittivity $\epsilon_r = 2$, such that reflections are largely eliminated. The uncertainty is induced by varying the relative positions of every part (lens, mirrors, one reflector, one sub-reflector) of the system. In particular, the y-coordinate of every part is again a

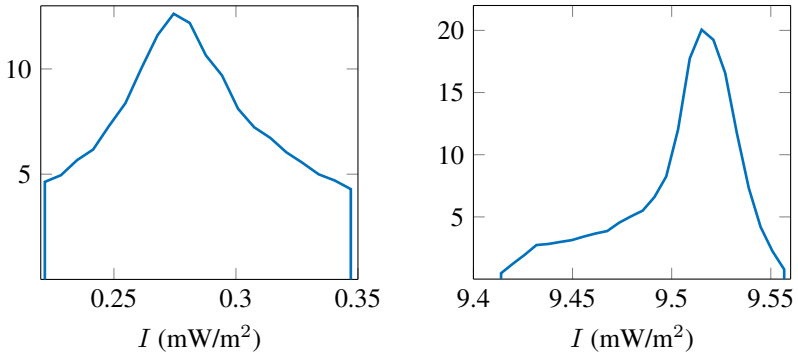

(a) PDF - point with maximum variance

(b) PDF - second focal point F_2

Figure 5.9: PDF of the local intensity I (mW/m^2) for two points behind the rightmost lens.

random variable such that the relative variation w.r.t. its nominal center is uniformly distributed within the interval $[-\lambda/20, \lambda/20[$. In this way, we introduce 5 RVs that describe the stochastic nature of the geometry. In Fig. 5.10, the average field density

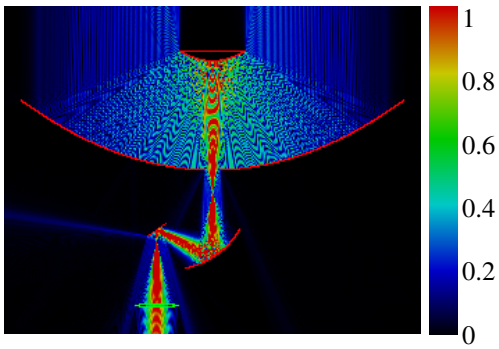

Figure 5.10: The average total field density $|E_z|$(V/m) of the Cassegrain antenna system illuminated with a Gaussian beam incident from the bottom onto the coated lens. The results are obtained with a polynomial order $P = 3$.

of the Cassegrain antenna system is shown. The standard deviation of the total field for this structure is presented in Fig. 5.11. We can see that the highest variation of the field is induced around the focal points, but due to the phase effect variation, a standing wave pattern is also visible.
The simulation is performed by using 4 nodes with 16 CPU cores per node (64 parallel processes in total). The block size of the preconditioner is chosen to be $16\lambda \times 16\lambda$. For $P = 2$, $K + 1 = 21$ and $N_{stoc} = 5\,073\,579$, the system was solved after 2630 iterations and 2h 44 min. For $P = 3$, $K + 1 = 56$ and $N_{stoc} = 13\,529\,544$, the system

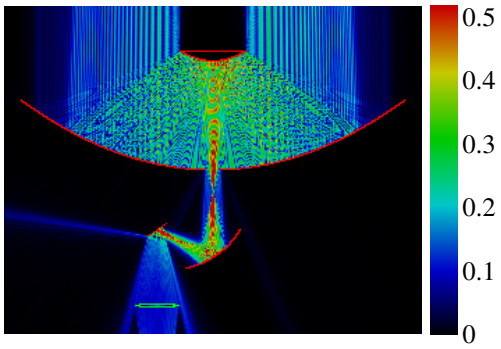

Figure 5.11: The standard deviation of the total field density $|E_z|$(V/m) of the Cassegrain antenna system illuminated with a Gaussian beam incident from the bottom onto the coated lens. The results are obtained with polynomial order $P = 3$.

was solved after 2767 iterations and 7h 47 min. The setup time and post-processing time are negligible compared to the solution time. However, for a different block-Jacobi size of $32\lambda \times 32\lambda$, we get a better run time. For example, then, for $P = 3$, the system is solved in 3h and 50 min after 783 iteration with a negligible increase of the setup time. This shows that one should carefully select the preconditioner size. We also remark that the time needed to solve this problem using the same computational resources with the SCM and with $P = 2$ is about 30h, which again demonstrates the necessity of the advocated parallel SGM-MLFMM solver.

Finally, we also provide a graph for the average total field density $|E_z|$ radiated upward. The field is calculated on the line segment connecting the left and the right top corner of Fig. 5.10, i.e. $1\,400\lambda$ above the center of the main parabolic reflector. The line segment has a length $3\,800\lambda$ and the field is calculated in 380 points. The results are again compared with the SCM, showing the accuracy of the proposed method.

5.5 Conclusions

In this chapter, we have described the parallelization of the MLFMM-based SGM solver. The chapter provides a theoretical background together with the complexity issues of the algorithm. Since this complexity grows fast with the number of spatial and stochastic unknowns, the solver leverages parallelization which allows simulation of large optical structures. Moreover, to decrease the number of iterations in the iterative solver, a block-Jacobi preconditioner is proposed. It was shown that a carefully chosen size of the preconditioner can reduce the computational time by a factor of two. Compared to a more traditional SCM, the selected examples clearly demonstrate the effectiveness of our novel algorithm, with speed-up factors of more than $12\times$, still maintaining excellent accuracy. Moreover, they show the need for the advocated intrusive stochastic modeling algorithm when dealing with large-scale optical problems.

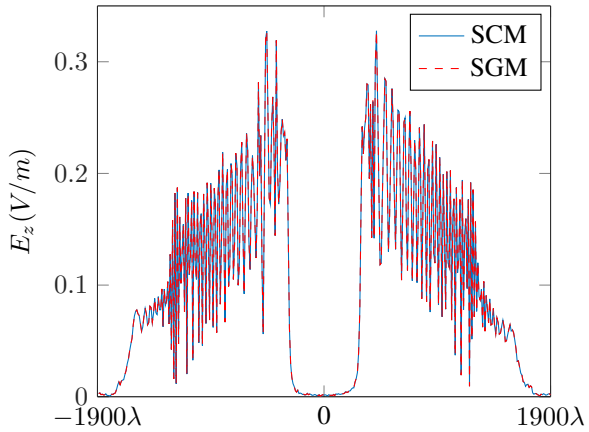

Figure 5.12: The average total field density $|E_z|$(V/m) radiated away from the Cassegrain antenna system along an $3\,800\lambda$ long line segment, $1\,400\lambda$ above the center of the main parabolic reflector.

Acknowledgment

The computational resources (Stevin Supercomputer Infrastructure) and services used in this work were provided by the VSC (Flemish Supercomputer Center), funded by Ghent University, the Hercules Foundation and the Flemish Government, department EWI.

References

[1] X. Chen, M. Mohamed, Z. Li, L. Shang, and A. R. Mickelson, "Process variation in silicon photonic devices", *Appl. Opt.*, vol. 52, no. 31, pp. 7638–7647, 2013.

[2] D. B. Xiu and G. E. Karniadakis, "The Wiener-Askey polynomial chaos for stochastic differential equations", *SIAM Journal on Scientific Computing*, vol. 24, no. 2, pp. 619–644, 2002.

[3] D. Vande Ginste, D. De Zutter, D. Deschrijver, T. Dhaene, P. Manfredi, and F. Canavero, "Stochastic modeling-based variability analysis of on-chip interconnects", *IEEE Transactions on Components, Packaging and Manufacturing Technology*, vol. 2, no. 7, pp. 1182–1192, Jul. 2012.

[4] T. El-Moselhy and L. Daniel, "Variation-aware stochastic extraction with large parameter dimensionality: Review and comparison of state of the art intrusive and non-intrusive technique", in *2011 12th International Symposium on Quality Electronic Design (ISQED 2011), 14-16 March 2011, Santa Clara, CA, USA*, 2011, pp. 508–517.

[5] C. Chauvière, J. S. Hesthaven, and L. C. Wilcox, "Efficient computation of RCS from scatterers of uncertain shapes", *IEEE Transactions on Antennas and Propagation*, vol. 55, no. 5, pp. 1437–1448, May 2007.

[6] Z. Zubac, D. De Zutter, and D. Vande Ginste, "Scattering from two-dimensional objects of varying shape combining the Method of Moments with the Stochastic Galerkin Method", *IEEE Transactions on Antennas and Propagation*, vol. 62, no. 9, pp. 4852–4856, Sep. 2014.

[7] Z. Zubac, D. De Zutter, and D. Vande Ginste, "Scattering from two-dimensional objects of varying shape combining the Multilevel Fast Multipole Method (MLFMM) with the Stochastic Galerkin Method (SGM)", *IEEE Antennas and Wireless Propagation Letters*, vol. 13, pp. 1275–1278, Jul. 2014.

[8] T.-W. Weng, Z. Zhang, Z. Su, Y. Marzouk, A. Melloni, and L. Daniel, "Uncertainty quantification of silicon photonic devices with correlated and non-gaussian random parameters", *Opt. Express*, vol. 23, no. 4, pp. 4242–4254, 2015.

[9] R. F. Harrington, *Field Computation by Moment Methods*. New York: IEEE Press, 1993.

[10] A. Keese and H. G. Matthies, "Hierarchical parallelisation for the solution of stochastic finite element equations", *Computers & Structures*, vol. 83, no. 14, pp. 1033 –1047, 2005, Uncertainties in Structural Mechanics and Analysis–Computational Methods.

[11] J. Fostier and F. Olyslager, "An asynchronous parallel mlfma for scattering at multiple dielectric objects", *IEEE Transactions on Antennas and Propagation,*, vol. 56, no. 8, pp. 2346–2355, 2008.

[12] A. J. Poggio and E. K. Miller, "Integral equation solutions for three dimensional scattering problems", in *Computer techniques for electromagnetics*, R. Mittra, Ed., Pergamon Press, 1973, pp. 159–264.

[13] F. Olyslager, D. De Zutter, and K. Blomme, "Rigorous analysis of the propagation characteristics of general lossless and lossy multiconductor transmission lines in multilayered media", *IEEE Transactions on Microwave Theory and Techniques,*, vol. 41, no. 1, pp. 79–88, 1993.

[14] A. Biondi, D. Vande Ginste, D. De Zutter, P. Manfredi, and F. Canavero, "Variability analysis of interconnects terminated by general nonlinear loads", *IEEE Transactions on Components, Packaging and Manufacturing Technology,*, vol. 3, no. 7, pp. 1244–1251, Jul. 2013.

[15] P. Manfredi, D. Vande Ginste, D. De Zutter, and F. Canavero, "Uncertainty assessment of lossy and dispersive lines in spice-type environments", *IEEE Transactions on Components, Packaging and Manufacturing Technology,*, vol. 3, no. 7, pp. 1252–1258, Jul. 2013.

[16] W. C. Chew, J. M. Jin, E. Michielssen, and J. Song, *Fast and Efficient Algorithms in Computational Electromagnetics*. Norwood, MA: Artech House, 2001.

[17] D. Vande Ginste, H. Rogier, F. Olyslager, and D. De Zutter, "A fast multipole method for layered media based on the application of perfectly matched layers - the 2-d case", *IEEE Transactions on Antennas and Propagation,*, vol. 52, no. 10, pp. 2631–2640, 2004.

[18] D. Vande Ginste, E. Michielssen, F. Olyslager, and D. De Zutter, "An efficient perfectly matched layer based multilevel fast multipole algorithm for large planar microwave structures", *IEEE Transactions on Antennas and Propagation,*, vol. 54, no. 5, pp. 1538–1548, 2006.

[19] D. Pissoort, E. Michielssen, D. Vande Ginste, and F. Olyslager, "Fast-multipole analysis of electromagnetic scattering by photonic crystal slabs", *Lightwave Technology, Journal of*, vol. 25, no. 9, pp. 2847–2863, 2007.

[20] B. Michiels, J. Fostier, I. Bogaert, and D. De Zutter, "Full-wave simulations of electromagnetic scattering problems with billions of unknowns", *IEEE Transactions on Antennas and Propagation*, vol. 63, pp. 796–799, Feb. 2015.

[21] R. W. Freund, "A transpose-free quasi-minimal residual algorithm for non-hermitian linear systems", *SIAM Journal on Scientific Computing*, vol. 14, no. 2, pp. 470–482, 1993.

[22] R. D. da Cunha and T. Hopkins, *Pim 2.2 the Parallel Iterative Methods Package for Systems of Linear Equations User's Guide (Fortran 77 version)*, UKC, University of Kent, Canterbury, UK, 2000.

[23] O. Ergul and L. Gurel, "Efficient parallelization of the multilevel fast multipole algorithm for the solution of large-scale scattering problems", *IEEE Transactions on Antennas and Propagation,*, vol. 56, no. 8, pp. 2335–2345, 2008.

[24] J. Fostier and F. Olyslager, "A provably scalable parallel multilevel fast multipole algorithm", *Electronics Letters*, vol. 44, no. 19, pp. 1111–1113, 2008.

[25] D. Pissoort, E. Michielssen, D. Vande Ginste, and F. Olyslager, "Fast-multipole analysis of electromagnetic scattering by photonic crystal slabs", *Journal of lightwave technology*, vol. 25, no. 9, pp. 2847–2863, 2007.

[26] M. F. Pellissetti and R. G. Ghanem, "Iterative solution of systems of linear equations arising in the context of Stochastic Finite Elements", *Advances in Engineering Software*, vol. 31, pp. 607–616, 2000.

[27] I Ocket, B Nauwelaers, J. Fostier, L. Meert, F. Olyslager, G Koers, J Stiens, R Vounckx, and I Jager, "Characterization of speckle/despeckling in active millimeter wave imaging systems using a first order 1.5d model - art. no. 619409.", *Millimeter-wave and Terahertz photonics*, vol. 6194, pp. 19 409–19 409, 2006.

[28] J. Fostier and F. Olyslager, "An open-source implementation for full-wave 2d scattering by million-wavelength-size objects", *IEEE Antennas & Propagation Magazine*, vol. 52, no. 5, pp. 23–34, 2010.

6

A Cholesky-Based SGM-MLFMM for Stochastic Full-Wave Problems Described by Correlated Random Variables

Zdravko Zubac, Luca Daniel, Daniël De Zutter and Dries Vande Ginste

Based on a paper submitted to Antennas and Wireless Propagation Letters, April 2016

★ ★ ★

In this chapter, the Multilevel Fast Multipole Method (MLFMM) is combined with the Polynomial Chaos Expansion (PCE) based Stochastic Galerkin Method (SGM) to stochastically model scatterers with geometrical variations that need to be described by a set of correlated *random variables (RVs). It is demonstrated how Cholesky decomposition is the appropriate choice for the RVs transformation, leading to an efficient SGM-MLFMM algorithm. The novel method is applied to the uncertainty quantification (UQ) of the currents induced on a rough surface, being a classic example of a scatterer described by means of correlated RVs, and the results clearly demonstrate its superiority compared to non-intrusive PCE methods and to the standard Monte Carlo (MC) method.*

6.1 Introduction

Electromagnetic simulation of objects prone to variability has become an important issue. Often, Uncertainty Quantification (UQ) relies on Monte Carlo (MC) analysis, which requires many calls to a standard deterministic (full-wave) solver, making it not tractable. Recently, the Polynomial Chaos Expansion (PCE) approach was introduced and combined with known computational electromagnetics (CEM) methods, both in an intrusive and a non-intrusive way [1][2]. For the scattering analysis of large structures, the Multilevel Fast Multipole Method (MLFMM) was combined with the PCE-based Stochastic Galerkin Method (SGM) [3]. Parallelization of the SGM-MLFMM even led to the efficient UQ of large optical systems [4]. Yet, only variability described by *independent* random variables (RVs) could be treated with this method. However, problems affected by variability, e.g. introduced by the manufacturing process, can most often only be described by a set of *correlated* RVs, rather than independent ones. Then, traditionally, this set of correlated RVs is transformed into a set of independent RVs via the well-known Karhunen-Loève (KL) transformation [5]. Unfortunately, when in the space of the correlated RVs, the so-called correlation length is small, then the total number of independent RVs after KL transform stays as large as the number of correlated RVs, leading to a high-dimensional problem. In [6], where a finite element method (FEM) was adopted, this was dealt with by dividing the space of variables into subspaces with a correlation length comparable to their size. Nevertheless, when using an integral equation (IE) formulation, where the electromagnetic behavior is described globally, such an approach as described in [6] is not possible. Therefore, in this chapter, we introduce another transformation to tackle the correlation, i.e. the Cholesky transformation. This alleviates the curse of dimensionality within the IE-based SGM-MLFMM framework.
This chapter is organized as follows. Section 5.1 describes the theoretical framework of the stochastic MLFMM with correlated RVs. An illustrative numerical example of the scattering at a two-dimensional (2D) rough surface is given in Section 5.2. Section 5.3 concludes the chapter.

6.2 Cholesky-based SGM-MLFMM

As a generic example for full-wave stochastic problems with correlated RVs, in this chapter, we consider two-dimensional frequency domain scattering from a perfect electrically conducting (PEC) plate of width w, residing in free space. As depicted in Fig. 6.1, the plate's roughness is stochastically defined by letting the height of M nodes, equidistantly spaced along the x-axis, vary randomly. These heights are described by a set of M correlated Gaussian variables, collected in vector $\boldsymbol{h} = [h_1, h_2, ..., h_M]$, and with correlation matrix $\overline{\boldsymbol{\Sigma}}$. The elements of the correlation matrix are given by:

$$\Sigma_{ij} = \sigma^2 \exp\left(-\frac{|x_i - x_j|^2}{L_c^2}\right),\ i, j = 1, ..., M, \tag{6.1}$$

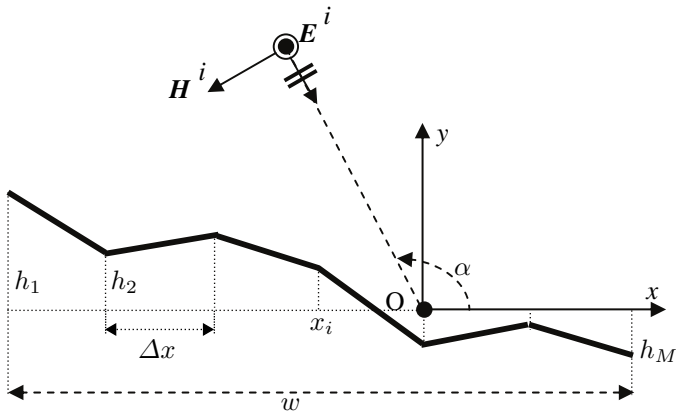

Figure 6.1: Rough surface described by a set of correlated random variables (RVs) h_i.

where σ is the standard deviation and L_c the correlation length. Traditionally, in order to apply PCE, the correlated RVs are converted into independent RVs, collected in vector $\boldsymbol{\xi} = [\xi_1, \xi_2, ..., \xi_R]$ via the KL transform as follows:

$$\boldsymbol{h} = \boldsymbol{\mu} + \overline{\boldsymbol{U}}\,\overline{\boldsymbol{\Lambda}}^{1/2}\boldsymbol{\xi}, \tag{6.2}$$

where $\boldsymbol{\mu}$ is the mean value of $\boldsymbol{h}$, and $\overline{\boldsymbol{U}}$ and $\overline{\boldsymbol{\Lambda}}$ are matrices defined by the eigenvalue decomposition of the correlation matrix $\overline{\boldsymbol{\Sigma}}$, i.e.

$$\overline{\boldsymbol{\Sigma}} = \overline{\boldsymbol{U}}\,\overline{\boldsymbol{\Lambda}}\,\overline{\boldsymbol{U}}^{T}. \tag{6.3}$$

Note that the number of independent parameters R may be smaller than the number of correlated parameters M ($R \leqslant M$). The standard electric field IE description of the scattering problem of Fig. 6.1 in conjunction with the Method of Moments (MoM) yields a linear system that is dependent on $\boldsymbol{\xi}$:

$$\overline{\boldsymbol{Z}}(\boldsymbol{\xi})\boldsymbol{I}(\boldsymbol{\xi}) = \boldsymbol{V}(\boldsymbol{\xi}), \tag{6.4}$$

with $\overline{\boldsymbol{Z}}(\boldsymbol{\xi})$ the MoM system matrix, $\boldsymbol{I}(\boldsymbol{\xi})$ the vector collecting the unknown current densities and $\boldsymbol{V}(\boldsymbol{\xi})$ the known RHS. All quantities in (6.4) are expressed in PCE form, e.g. for $\overline{\boldsymbol{Z}}(\boldsymbol{\xi})$:

$$\overline{\boldsymbol{Z}}(\boldsymbol{\xi}) = \sum_{k=0}^{K} \overline{\boldsymbol{Z}}_k\, \phi_k(\boldsymbol{\xi}), \tag{6.5}$$

where $\{\phi_k(\boldsymbol{\xi})\}_{k=0,...,K}$ represents a set of $K+1$ mutually orthonormal multivariate polynomials according to the Wiener-Askey scheme. In the case of Gaussian variables $\boldsymbol{h}$ (and thus $\boldsymbol{\xi}$), these are products of univariate Hermite polynomials, dependent on a single RV ξ_i. The total number of polynomials grows rapidly with R as

$$K + 1 = \frac{(R+P)!}{R!P!}, \tag{6.6}$$

where P is the total order of the polynomials $\phi_k(\boldsymbol{\xi})$, calculated as the sum of the orders of the univariate polynomials they are composed of. Calculation of the PCE coefficients $\overline{\boldsymbol{Z}}_k$ is done via projection, necessitating a multidimensional integration in the R-dimensional space of $\boldsymbol{\xi}$:

$$\overline{\boldsymbol{Z}}_k =< \overline{\boldsymbol{Z}}(\boldsymbol{\xi}), \phi_k(\boldsymbol{\xi}) >= \int_{\xi_1} ... \int_{\xi_R} \overline{\boldsymbol{Z}}(\boldsymbol{\xi})\, \phi_k(\boldsymbol{\xi})\, W(\boldsymbol{\xi}) d\xi_1 ... d\xi_R, \quad (6.7)$$

where $W(\boldsymbol{\xi})$ represents the multivariate Gaussian probability density function (PDF) of $\boldsymbol{\xi}$. In particular, when the correlation length L_c is low, the KL transform may lead to a dense, square matrix $\overline{\boldsymbol{U}}\,\overline{\boldsymbol{\Lambda}}^{1/2}$, i.e. $R = M$ and each correlated RV h_i is dependent on all RVs $\boldsymbol{\xi}$. Moreover, each matrix element of $\overline{\boldsymbol{Z}}(\boldsymbol{\xi})$ will also depend on all RVs $\boldsymbol{\xi}$, and the multidimensional integrals of type (6.7) become cumbersome to compute.
After calculating the coefficients $\boldsymbol{V}_k$ in a similar way, solution of the system (6.4), for the unknown coefficients $\boldsymbol{I}_k$, is obtained via Galerkin projection:

$$\boldsymbol{V}_m = \sum_{\substack{k,l=0 \\ \gamma_{klm} \neq 0}}^{K} \overline{\boldsymbol{Z}}_k\, \boldsymbol{I}_l\, \gamma_{klm},\ m = 0, .., K, \quad (6.8)$$

where γ_{klm} represents a three-term inner product of Hermite polynomials:

$$\gamma_{klm} =< \phi_k(\boldsymbol{\xi})\, \phi_l(\boldsymbol{\xi}), \phi_m(\boldsymbol{\xi}) > . \quad (6.9)$$

Note that (6.8) constitutes a deterministic linear system with a complexity that scales with the number of non-zero numbers γ_{klm}, which follows an $O(K^{1.5})$ law.
To expedite the solution of the linear system, MLFMM [7] is invoked, by dividing the structure into groups of sources. If the distance between a source and an observation group is large enough, then the system (6.4) can be approximated as:

$$\overline{\boldsymbol{D}}(\boldsymbol{\xi})\,\overline{\boldsymbol{T}}\,\overline{\boldsymbol{A}}(\boldsymbol{\xi})\,\boldsymbol{I}(\boldsymbol{\xi}) \approx \overline{\boldsymbol{Z}}(\boldsymbol{\xi})\,\boldsymbol{I}(\boldsymbol{\xi}), \quad (6.10)$$

where $\overline{\boldsymbol{D}}(\boldsymbol{\xi})$, $\overline{\boldsymbol{T}}$ and $\overline{\boldsymbol{A}}(\boldsymbol{\xi})$ represent the well-known dissagregation, translation and aggregation matrix respectively. However, in contrast to the problems described in [3], whereas the aggregation and disaggregation matrices were dependent only on a group of sources, and thus only on few h_i, here, they are still dependent on all independent RVs $\boldsymbol{\xi}$. Besides the aforementioned curse of dimensionality in calculating PCE projections (6.7), this also entails an unacceptably long solution time of (6.8). Indeed, since the aggregation and the disaggregation matrices are dependent on all independent RVs, their PCE coefficients are all nonzero and the complexity does not scale linearly with the number of polynomials K as in [3], but with the total number of γ_{klm}.
To tackle this issue, instead of using the traditional KL transform, we propose to adopt a Cholesky transformation. Then, the correlated RVs are expressed via another vector of independent RVs $\boldsymbol{\eta}$:

$$\boldsymbol{h} = \boldsymbol{\mu} + \overline{\boldsymbol{L}}\,\boldsymbol{\eta}, \quad (6.11)$$

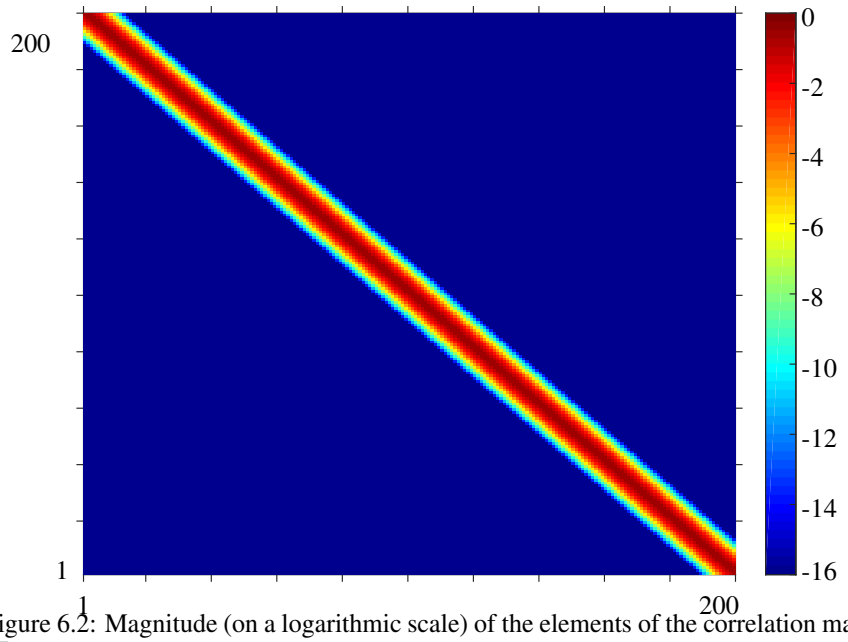

Figure 6.2: Magnitude (on a logarithmic scale) of the elements of the correlation matrix $\overline{\boldsymbol{\Sigma}}$ for a canonical problem.

where $\overline{\boldsymbol{L}}$ is a lower triangular matrix related to the correlation matrix as follows:

$$\overline{\boldsymbol{\Sigma}} = \overline{\boldsymbol{L}}\,\overline{\boldsymbol{L}}^{T}. \tag{6.12}$$

To show the benefits of this Cholesky decomposition, for a canonical structure as shown in Fig. 6.1, with $M = 200$, $L_c = \lambda/5$, $\sigma = \lambda/20$ and $w = 20\lambda$ (with λ the free-space wavelength), we present the structure of the correlation matrix in Fig. 6.2 and its corresponding KL and Cholesky matrices in Fig. 6.3. Whereas the KL matrix $\overline{\boldsymbol{U}}\,\overline{\boldsymbol{\Lambda}}^{1/2}$ is a densely filled matrix, the off-diagonal elements of the Cholesky matrix $\overline{\boldsymbol{L}}$ rapidly vanish. Consequently, when dimensionality reduction with KL transform is not possible, the benefits of the advocated Cholesky approach are:

- The M correlated RVs $\boldsymbol{h}$ depend only on a few independent RVs $\boldsymbol{\eta}$. Thus, the M-dimensional integrals of type (6.7) depending on these correlated RVs, are reduced in dimension, and their computation is expedited
- Many PCE coefficients are zero, as their corresponding stochastic quantities, in particluar the elements of $\overline{\boldsymbol{Z}}(\boldsymbol{\eta})$, only depend on a few independent RVs. This substantially improves the computational and memory complexity.

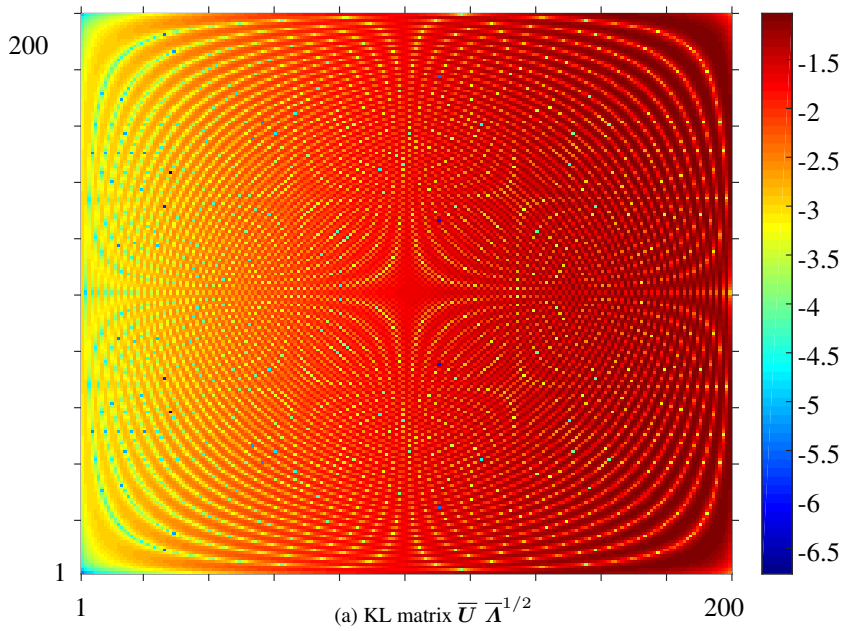

(a) KL matrix $\overline{\boldsymbol{U}}\ \overline{\boldsymbol{\Lambda}}^{1/2}$

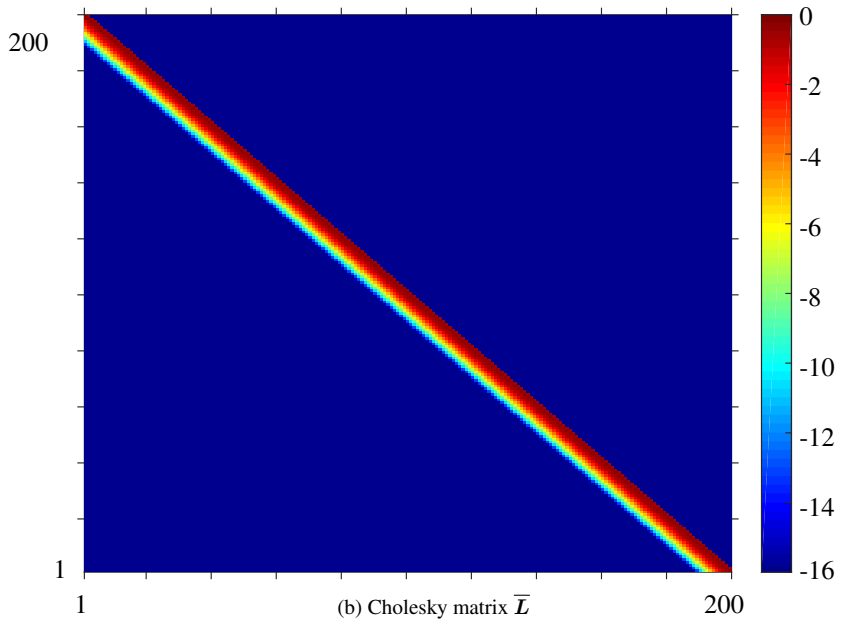

(b) Cholesky matrix $\overline{\boldsymbol{L}}$

Figure 6.3: Magnitude (on a logarithmic scale) of the elements the matrices pertaining to the decomposition of $\overline{\boldsymbol{\Sigma}}$, shown in Fig. 6.2.

6.3 Numerical example

We consider scattering from a rough PEC strip of width $w = 100\lambda$, whose roughness is described by 81 RVs that determine the y-coordinates of the equally distributed points on the structure, as presented in Fig. 6.1. The correlation length is $L_c = \lambda$ and the standard deviation is $\sigma = \lambda/20$. The incident field is a TM-polarized plane wave impinging under an angle of $\alpha = 3\pi/4$. The structure is discretized with $N = 2\,000$ segments and the unknown current density is defined adopting piecewise constant basis functions. All computations are carried out on a Dell PC with a quad-core Intel(R) Core(TM) i7-2600 processor operating at 3.40 GHz and with 8 GB RAM memory.
To validate the accuracy and demonstrate the efficiency of our novel method, a standard MC analysis with $10\,000$ samples is used as a reference solution. This MC analysis takes about 7h. Moreover, the stochastic scattering problem is also solved by means of the *non*-intrusive PCE-based Stochastic Collocation Method (SCM) leveraging sparse Smolyak integration [8]. To achieve an accuracy of 0.15% compared to MC for the average current density, the SGM-MLFMM scheme uses polynomial order $P = 2$. Also, SCM uses $P = 2$ and $13\,285$ Smolyak integration points. The timing analysis is as follows: the novel SGM-MLFMM scheme takes about 1h and SCM takes around 10h. The gain is achieved in both the setup and the solution phase, as visible from Table 6.1. If the KL transform would be used in combination with SGM, then the setup time for calculation of the PCE coefficients of $\overline{\boldsymbol{D}}$ and $\overline{\boldsymbol{A}}$ coefficients would be determined by (6.7), and would be of the same order of magnitude as the setup time of SCM.

Table 6.1: Setup and solution time

method	setup	solution
SGM	99 s	3 948 s
SCM	26 570 s	7 971 s

The average current density on the strip is given in Fig. 6.4 and its standard deviation is presented in Fig. 6.5. A good agreement between SGM and MC is visible. These results are presented for polynomial order $P = 2$ and the corresponding total number of stochastic unknowns $N_{stoc} = (K + 1)N = 6\,806\,000$.
To reduce possible truncation errors, as described in [9], the polynomial order should be chosen large enough such that the PCE of $\overline{\boldsymbol{Z}}$ can be found accurately through multiplication and Galerkin projection of the PCE coefficients of $\overline{\boldsymbol{D}}$ and $\overline{\boldsymbol{A}}$. To demonstrate the influence of the truncation error on the average current density, in Fig. 6.6 we present $\mathrm{E}[J_s]$ in the middle of the strip for several polynomial orders. From this figure, the convergence of the advocated SGM-MLFMM scheme is clearly visible, which also again validates our method. Moreover, at this point, it is important to point out that, in particular when dealing with full-wave problems, variations of the output parameters, such as current density, can be substantial and the Smolyak integration rule used in SCM may fail to produce good results. This is visible from Fig. 6.7, where the standard deviation of the current density J_s in the middle of the rough strip is shown.

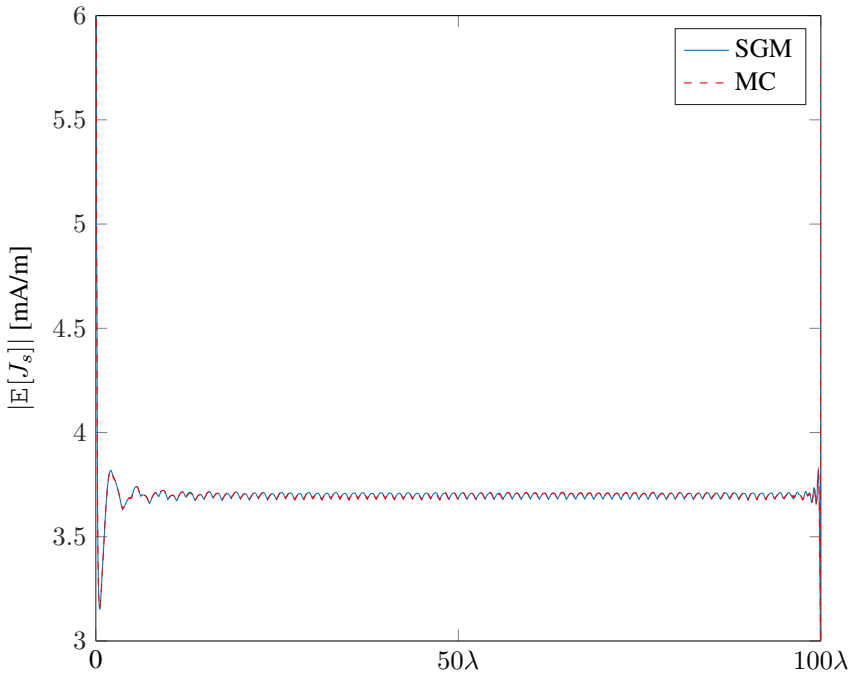

Figure 6.4: Average current density $\mathrm{E}[J_s]$ on the rough strip, with $\mathrm{E}[\cdot]$ the expectation operator.

This behavior is well known for integration of functions that are not smooth enough [10]. The proposed SGM-MLFMM does not suffer from this issue, however, since the integration was done in a lower dimensional space thanks to the advocated Cholesky transformation. To achieve the same level of accuracy for the standard deviation, with the SGM, the number of Smolyak integration points should be increased to $722\,089$, which becomes prohibitively expensive. This clearly demonstrates the huge advantage the novel SGM-MLFMM scheme over SCM.

6.4 Conclusions

In this chapter, the UQ of full-wave stochastic problems, described by *correlated* RVs, was investigated. Classically, the KL transformation is applied to decorrelate the RVs. However, for the envisaged applications, the SGM-MLFMM scheme, presented in literature before by the authors, cannot be straightforwardly extended by incorporating a KL transformation, and this because of two reasons: (i) the computation of the PCE coefficients entails integration in a highly-dimensional space; (ii) all these PCE are nonzero, as the stochastic quantities are dependent on all independent RVs after KL transformation. We proposed to tackle these issues by invoking Cholesky

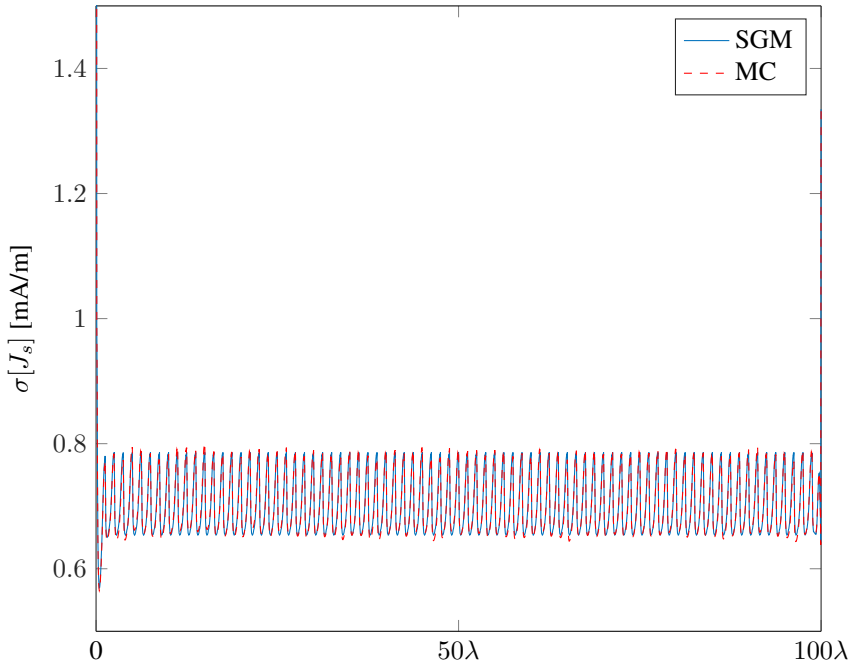

Figure 6.5: Standard deviation of the current density $\sigma[J_s]$ on the rough strip, with $\sigma[J_s] = \sqrt{E[(J_s - E[J_s])(J_s - E[J_s])^H]}$.

decomposition of the correlation matrix instead, leading to a very accurate and efficient SGM-MLFMM algorithm. The novel method was validated and compared against a MC analysis and a SCM for the case of scattering at rough PEC plate.

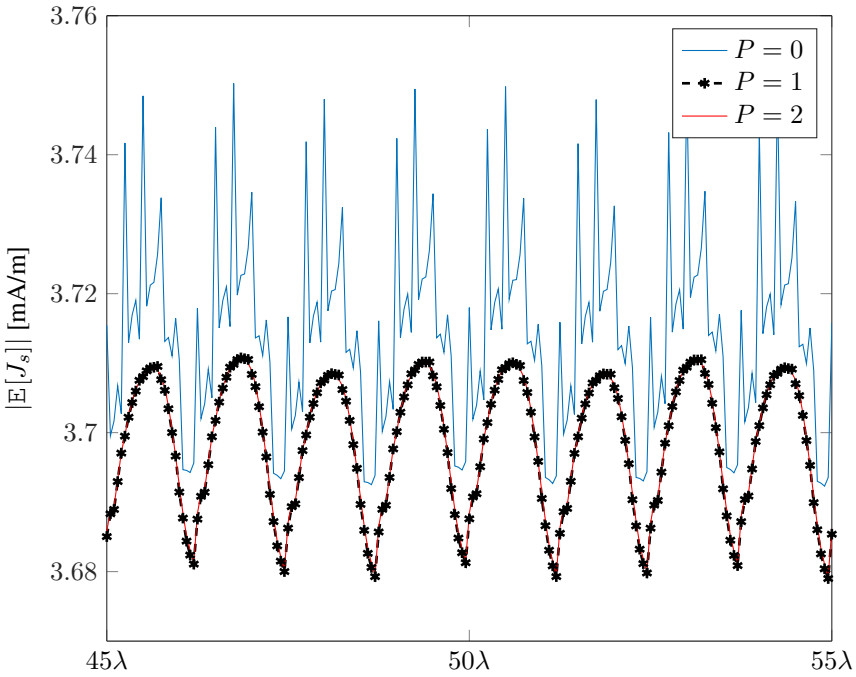

Figure 6.6: Average current density in the middle of the rough strip for several polynomial orders.

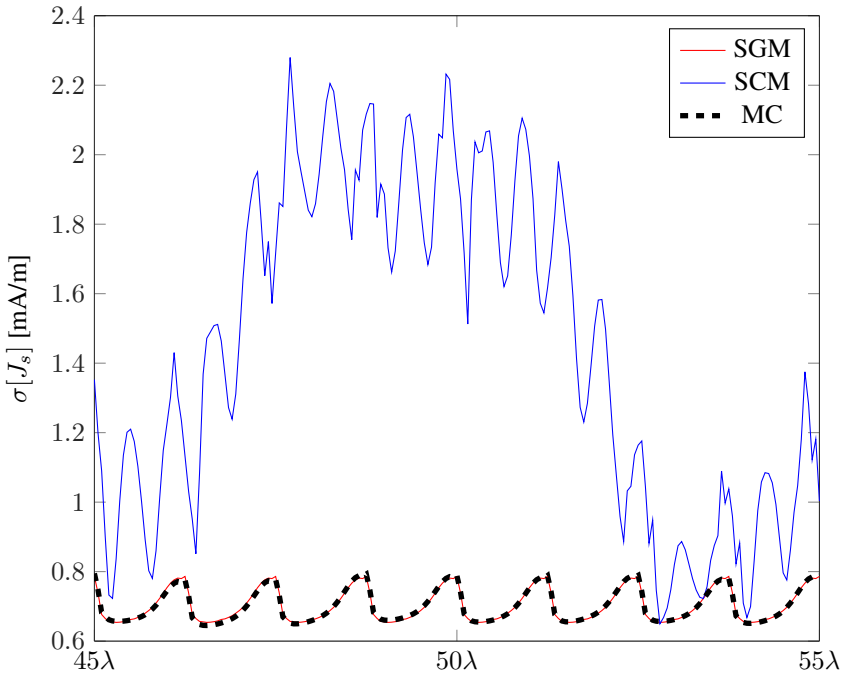

Figure 6.7: Standard deviation of the current density J_s in the middle of the rough strip.

References

[1] T. El-Moselhy and L. Daniel, "Variation-aware stochastic extraction with large parameter dimensionality: Review and comparison of state of the art intrusive and non-intrusive technique", in *2011 12th International Symposium on Quality Electronic Design (ISQED 2011), 14-16 March 2011, Santa Clara, CA, USA*, 2011, pp. 508–517.

[2] C. Chauvière, J. S. Hesthaven, and L. C. Wilcox, "Efficient computation of RCS from scatterers of uncertain shapes", *IEEE Transactions on Antennas and Propagation*, vol. 55, no. 5, pp. 1437–1448, May 2007.

[3] Z. Zubac, D. De Zutter, and D. Vande Ginste, "Scattering from two-dimensional objects of varying shape combining the Multilevel Fast Multipole Method (MLFMM) with the Stochastic Galerkin Method (SGM)", *IEEE Antennas and Wireless Propagation Letters*, vol. 13, pp. 1275–1278, Jul. 2014.

[4] Z. Zubac, J. Fostier, D. De Zutter, and D. Vande Ginste, "Efficient uncertainty quantification of large two-dimensional optical systems with a parallelized Stochastic Galerkin Method", *Opt. Express*, vol. 23, no. 24, pp. 30 833–30 850, Nov. 2015.

[5] M. Loeve, *Probability Theory II*. Springer, 1994.

[6] Y. Chen, J. Jakeman, C. Gittelson, and D. Xiu, "Local polynomial chaos expansion for linear differential equations with high dimensional random inputs", *SIAM Journal on Scientific Computing*, vol. 37, no. 1, A79–A102, 2015.

[7] W. C. Chew, J. M. Jin, E. Michielssen, and J. Song, *Fast and Efficient Algorithms in Computational Electromagnetics*. Norwood, MA: Artech House, 2001.

[8] Z. Zubac, D. De Zutter, and D. Vande Ginste, "Scattering from two-dimensional objects of varying shape combining the Method of Moments with the Stochastic Galerkin Method", *IEEE Transactions on Antennas and Propagation*, vol. 62, no. 9, pp. 4852–4856, Sep. 2014.

[9] B. J. Debusschere, H. N. Najm, P. P. Pébay, O. M. Knio, R. G. Ghanem, and O. P. L. Maître, "Numerical challenges in the use of polynomial chaos representations for stochastic processes", *SIAM J. Sci. Comput.*, vol. 26, no. 2, pp. 698–719, Feb. 2005.

[10] P. Tsuji, D. Xiu, and L. Ying, "Fast method for high-frequency acoustic scattering from random scatterers", *International Journal for Uncertainty Quantification*, vol. 1, no. 2, pp. 99–117, 2011.

7

Combination of Tensor-Train (TT) Decomposition with Statistical Moments preserving Model Order Reduction (SMOR) for the efficient variation aware analysis of scattering problems

Zdravko Zubac, Luca Daniel, Daniël De Zutter and Dries Vande Ginste

★ ★ ★

In this chapter, two methods, Tensor-Train (TT) decomposition and Statistical Moments preserving Model Order Reduction (SMOR), are described as a starting point for the usage of these two methods in conjuction with the Multilevel Fast Multipole Mrthod (MLFMM). Computational complexity of such a novel approach is discussed and illustrated by means of some numerical examples. This chapter can be seem as a starting point of the development of novel (semi-) intrusive methods for full-wave stochastic EM problems.

7.1 Introduction

Accurate simulation of electromagnetic structures must include process variation effects as they may lead to performance degradation. These variations render the geometry of the structure stochastic and, hence, standard deterministic solvers cannot be used. The set of random variables (RVs), describing the stochastic nature of the geometry, can be large. Traditionally, the Monte Carlo (MC) method, despite the fact that it entails slow convergence, is the only acceptable choice for stochastic analysis in case of a large number of RVs [1], as methods based on polynomial chaos expansion (PCE) suffer from the curse of dimensionality. To mitigate this problem, i.e. to maintain good convergence of the PCE-based methods even for a huge number of RVs, alternatives have been proposed, in particular for the non-intrusive class of methods, such as, e.g., the Stochastic Collocation Method (SCM). Two such alternatives, the analysis of variance (ANOVA) technique [2] and compressed sampling (CS) [3], exploit the sparsity of high-dimensional PCE.

The curse of dimensionality stems from the multidimensional integrations of the type (6.7), necessitating many deterministic costly simulations for the corresponding integration points. One way to reduce the number of points is by using sparse-grid Smolyak integration, but this method can produce non-physical results for non-smooth functions [4]. Also, the cost of one EM evaluation for one integration point may be reduced by using Model Order Reduction (MoR). The reduced model is rapidly evaluated for a large number of points, while only a few costly deterministic simulations are needed to construct it [5]. As this method preserves statistical moments, it is called Statistical Moments preserving Model Order Reduction (SMOR).

Recently, tensor-based methods were introduced to the PCE community as a promising solution for high-dimensional problems [6]. The idea is to extend the usage of tensor-product integration to high-dimensional problems by using a low-rank approximation of the tensors. One class of such methods leverages tensor-train (TT) decomposition [7] and another class is based on the optimization of a non-convex problem that seeks to represent a tensor as an outer product of a few vectors [8].

In this chapter, we propose the combination of TT decomposition and SMOR for the non-intrusive stochastic analysis of high-dimensional problems. On the one hand, we show how the low-rank nature of the tensor is exploited to reduce the number of integration points. On the other hand, we explain how, by using deterministic simulations, a reduced model can be built, starting from deterministic simulations. This chapter lays the foundations for the hybridization of these two methods. By means of some numerical examples, the usability of this novel TT + SMOR method is demonstrated.

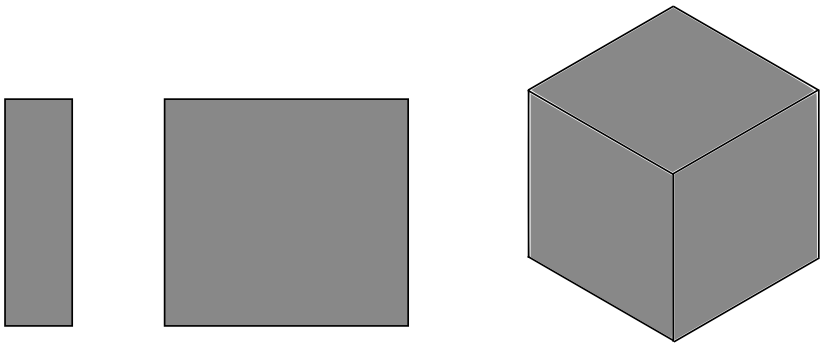

Figure 7.1: Visualization of vectors (left), matrices (middle) and 3-mode tensors (right).

7.2 Description of the core techniques

7.2.1 Tensor-Train (TT) Decomposition

A tensor is a multidimensional array of data. It is a natural extension of vectors (1D array of data) and matrices (2D array of data). The number of dimensions in a tensor d is called the mode of the tensor. Thus, a scalar is a 0-mode tensor, a vector is a 1-mode tensor and a matrix is a 2-mode tensor. A visualization of a vector, a matrix and a 3-mode tensor is given in Fig 7.1. Mathematically, a tensor of real elements is denoted $\boldsymbol{\mathcal{A}} \in \mathbb{R}^{M_1 \times M_2 \times ... \times M_d}$, where M_k represents the size of the k-th dimension. An element of the tensor is written as $\boldsymbol{\mathcal{A}}(i_1, i_2, ..., i_d)$ where the positive integer i_k is the index of the k-th dimension and $1 \leq i_k \leq M_k$. More details about operations on tensors are found in [6], [9]. One property of a tensor, in which we are interested in in this work, is its tensor rank. It is defined as the smallest positive integer r, such that

$$\boldsymbol{\mathcal{A}} = \sum_{j=1}^{r} \boldsymbol{v}_j^{(1)} \circ \boldsymbol{v}_j^{(2)} \circ ... \circ \boldsymbol{v}_j^{(d)}, \tag{7.1}$$

where the operator $\circ$ denotes the tensor product and with vectors $\boldsymbol{v}_j^{(k)} \in \mathbb{R}^{M_k}$. A rank one tensor can be written as

$$\boldsymbol{\mathcal{A}} = \boldsymbol{v}^{(1)} \circ \boldsymbol{v}^{(2)} \circ ... \circ \boldsymbol{v}^{(d)}, \tag{7.2}$$

with $\boldsymbol{v}^{(k)} \in \mathbb{R}^{M_k}$ or thus,

$$\boldsymbol{\mathcal{A}}(i_1, i_2, ..., i_d) = \prod_{k=1}^{d} \boldsymbol{v}^{(k)}(i_k). \tag{7.3}$$

A multidimensional integration procedure may be written in terms of tensors. Consider, e.g., the integral that represents the expectation of a stochastic process $h(\boldsymbol{\xi}) =$

$h(\xi_1, \xi_2, ..., \xi_d)$:

$$\mathbb{E}[h(\xi_1, \xi_2, ..., \xi_d)] = \int_{\xi_1} \int_{\xi_2} \cdots \int_{\xi_d} h(\xi_1, \xi_2, ..., \xi_d) W(\xi_1, \xi_2, ..., \xi_d) d\xi_1 d\xi_2 ... d\xi_d, \tag{7.4}$$

where $W(\xi_1, \xi_2, ..., \xi_d)$ denotes the process's probability density function (PDF). This d-dimensional integral may be computed by using an appropriate Gauss quadrature rule, chosen according to the PDF. If M_k points are used in the k-th dimension, then the integral is numerically calculated as:

$$\mathbb{E}[h(\xi_1, \xi_2, ..., \xi_d)] \approx \sum_{i_1=1}^{M_1} \sum_{i_2}^{M_2} ... \sum_{i_d=1}^{M_d} h(\xi_1^{i_1}, \xi_2^{i_2}, ..., \xi_d^{i_d}) \prod_{k=1}^{d} w_k^{i_k}, \tag{7.5}$$

where, for the k-th dimension, $\xi_k^{i_k}$ and $w_k^{i_k}$ denote the i_k-th Gauss quadrature point and weight respectively. This integral can also be seen as an inner product of two d-mode tensors. Denote

$$\boldsymbol{\mathcal{H}}(i_1, i_2, ..., i_d) = h(\xi_1^{i_1}, \xi_2^{i_2}, ..., \xi_d^{i_d}), \tag{7.6}$$

$$\boldsymbol{\mathcal{W}}(i_1, i_2, ..., i_d) = \prod_{k=1}^{d} w_k^{i_k}, \tag{7.7}$$

then, (7.5) is rewritten as:

$$\mathbb{E}[h(\xi_1, \xi_2, ..., \xi_d)] \approx < \boldsymbol{\mathcal{H}}, \boldsymbol{\mathcal{W}} >, \tag{7.8}$$

where $< \cdot, \cdot >$ represents the tensor inner product, defined as follows:

$$< \boldsymbol{\mathcal{H}}, \boldsymbol{\mathcal{W}} > = \sum_{i_1=1}^{M_1} \sum_{i_2}^{M_2} ... \sum_{i_d=1}^{M_d} \boldsymbol{\mathcal{H}}(i_1, i_2, \cdots, i_d) \boldsymbol{\mathcal{W}}(i_1, i_2, \cdots, i_d) \tag{7.9}$$

Suppose the number of points in each dimension is equal, i.e. $M_1 = M_2 = ... = M_k = M$, then the cost of computing the tensor and the tensor inner product is $O(M^d)$. This becomes rapidly intractable for large d.
To tackle the huge computational cost, a low-rank representation of the tensors is invoked. Clearly, $\boldsymbol{\mathcal{W}}$ is a rank-1 tensor:

$$\boldsymbol{\mathcal{W}} = \boldsymbol{w}^{(1)} \circ \boldsymbol{w}^{(2)} \circ \cdots \circ \boldsymbol{w}^{(d)}, \tag{7.10}$$

where $\boldsymbol{w}^{(k)} = [w_k^1 \dots w_k^d]^T \in \mathbb{R}^{M \times 1}$, with T the transpose operator,contains all Gauss quadrature weights for parameter ξ_k. The cost of storing this tensor $\boldsymbol{\mathcal{W}}$ is $O(Md)$.
Tensor $\boldsymbol{\mathcal{H}}$ can be approximated via tensor-train (TT) decomposition [7] using a low rank tensors. Each element of $\boldsymbol{\mathcal{H}}$ is then given by:

$$\boldsymbol{\mathcal{H}}(i_1, i_2, ..., i_d) \approx \boldsymbol{\mathcal{G}}_1(:, i_1, :) \boldsymbol{\mathcal{G}}_2(:, i_2, :) \cdots \boldsymbol{\mathcal{G}}_d(:, i_d, :), \tag{7.11}$$

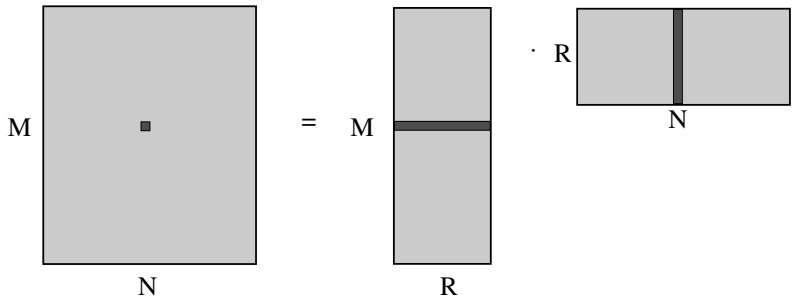

Figure 7.2: Representation of matrix as a product of two low-rank matrices.

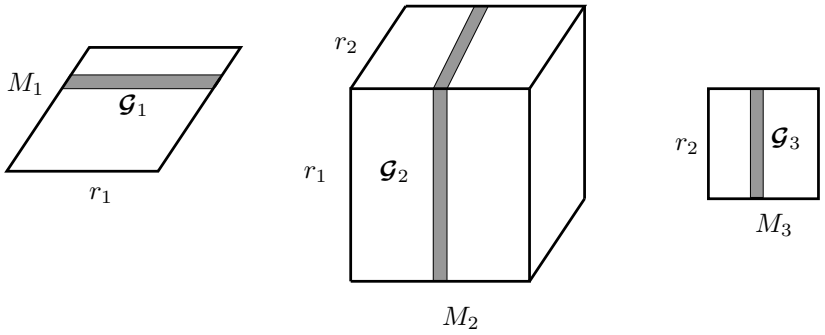

Figure 7.3: Tensor-train decomposition of a 3-mode tensor $\boldsymbol{\mathcal{A}} \in \mathbb{R}^{M_1 \times M_2 \times M_3}$.

where $\boldsymbol{\mathcal{G}}_k \in \mathbb{R}^{r_{k-1} \times M \times r_k}$ are the cores of the tensor $\boldsymbol{\mathcal{H}}$ and the arguments $(:, i_k, :)$ denote that the pertinent subpart of k-th core $\boldsymbol{\mathcal{G}}_k$ is used to end up with the desired $(i_1, i_2, ..., i_d)$-th element of $\boldsymbol{\mathcal{H}}$. When $h(\xi_1, ..., \xi_d)$ is a scalar-valued function the numbers $r_1 = r_d = 1$. The vector $\boldsymbol{r} = [r_1 r_2 \dots r_k]$ is called the TT-rank. Assuming that $r_1 = r_2 = ... = r_d = r$, memory complexity scales as $O(Mr^2 d)$. This decomposition is similar to the singular value decomposition (SVD) or QR decomposition of matrices, i.e. when matrix $\overline{\boldsymbol{A}} \in \mathbb{R}^{M \times N}$ is represented as a product of two low-rank matrices $\overline{\boldsymbol{A}}_1 \in \mathbb{R}^{M \times R}$ and $\overline{\boldsymbol{A}}_2 \in \mathbb{R}^{R \times N}$, as indicated in Fig. 7.2. One element of the matrix $\overline{\boldsymbol{A}}(i_1, i_2)$ is then calculated as:

$$\overline{\boldsymbol{A}}(i_1, i_2) = \overline{\boldsymbol{A}}_1(i_1, :)\overline{\boldsymbol{A}}_2(:, i_2), \tag{7.12}$$

where $\overline{\boldsymbol{A}}_1(i_1, :)$ represents a row vector and $\overline{\boldsymbol{A}}_2(:, i_2)$ a column vector. When tensor-train decomposition is considered, the decomposition cores are 3-mode tensors instead of matrices, as represented in Fig. 7.3, except for the first and last one if $h(\xi_1, ..., \xi_d)$ is a scalar value function. Therefore, one element of the tensor $\boldsymbol{\mathcal{A}}$ can be written as:

$$\boldsymbol{\mathcal{A}}(i_1, i_2, i_3) \approx \boldsymbol{\mathcal{G}}_1(i_1, :)\boldsymbol{\mathcal{G}}_2(:, i_2, :)\boldsymbol{\mathcal{G}}_3(:, i_3), \tag{7.13}$$

where $\boldsymbol{\mathcal{G}}_1(i_1, :)$ represents a $1 \times r_1$ vector, $\boldsymbol{\mathcal{G}}_2(:, i_2, :)$ represents a $r_1 \times r_2$ matrix and $\boldsymbol{\mathcal{G}}_3(:, i_3)$ represents a $r_2 \times 1$ vector. In general decompositions of the type (7.11), by

fixing the second index i_k, the TT cores become matrices. More about calculation of tensor cores is found in [7]. Note that the TT decomposition differs from (7.1), called canonical decomposition, and Tucker decomposition that is described in [9].
When the TT decomposition of $\boldsymbol{\mathcal{H}}$ is found, the inner product (7.8) can be calculated as follows:

$$< \boldsymbol{\mathcal{H}}, \boldsymbol{\mathcal{W}} > \approx \boldsymbol{H}_1 \boldsymbol{H}_2 \cdots \boldsymbol{H}_d, \tag{7.14}$$

with

$$\boldsymbol{H}_k = \sum_{i_k=1}^{M} w_k^{i_k} \boldsymbol{\mathcal{G}}_k(:, i_k, :). \tag{7.15}$$

In a similar fashion, the $\boldsymbol{\mathcal{H}}$ tensor is projected onto an orthonormal polynomial basis $\phi_k(\boldsymbol{\xi}_k)$ can also be done in a similar fashion. More details can be found in [6], [10].

7.2.1.1 Numerical example: integration of a multivariate function

We consider a function $h(\boldsymbol{\xi}) = \sum_{i=1}^{25} \xi_i^4$, where $\boldsymbol{\xi}$ is a vector of 25 independent RVs with a standard normal distribution $\mathcal{N}(0, 1)$.
It is readily analytically calculated that $\mathrm{E}[h(\boldsymbol{\xi})] = 75$. This result is used as a reference to test our numerical integration routines. When a full tensor integration with 3 nodes in each dimension would be applied (integration is exact up to polynomial order 5), the total number of integration points would be $3^{25} \approx 8 \cdot 10^{11}$, which is prohibitively expensive. By using the capabilities of TT toolbox [11], in particular by computing the cross approximation as described in [12], the integral is calculated via only $11\,124$ function evaluations with machine precision accuracy.
Another alternative is to use Smolyak integration rule with an exactness up to polynomial order 5. For this particular example, the total number of Smolyak points is then $1\,301$, which is smaller than the number of function evaluations in the TT approximation. However, for larger polynomial orders, e.g. when $h_2(\boldsymbol{\xi}) = \sum_{i=1}^{25} \xi_i^6$ is integrated, TT becomes more efficient than the Smolyak rule. Indeed, for a numerical integration that is exact up to polynomial order 7, the number of points with TT decomposition is $20\,192$ and with Smolyak integration rule it is already $22\,201$. For a larger number of RVs, the difference, will only increase, making TT even more beneficial. The advantage of TT approximation is that it can integrate polynomials up to a maximum order in each dimension separately, whereas Smolyak rule only allows to integrate polynomial exactly up to a total order.

7.2.2 Statistical Moment Preserving Model order Reduction

In a non-intrusive algorithm, the number of consecutive calls to the deterministic solver can be large. For the scattering problems considered in this dissertation, which are tackled via a BIE-MoM approach, each step involves solving a linear systems $\overline{\boldsymbol{Z}}(\boldsymbol{\xi}_k)\, \boldsymbol{I}(\boldsymbol{\xi}_k) = \boldsymbol{V}(\boldsymbol{\xi}_k)$ for a different realization $\boldsymbol{\xi}_k$ of the random vector $\boldsymbol{\xi}$, where $\overline{\boldsymbol{Z}}(\boldsymbol{\xi}_k) \in \mathbb{R}^{N \times N}$ is the system matrix, $\boldsymbol{V}(\boldsymbol{\xi}_k) \in \mathbb{R}^{N \times 1}$ is the known RHS and $\boldsymbol{I}(\boldsymbol{\xi}_k) \in \mathbb{R}^{N \times 1}$ represents the vector collecting the unknown current density coefficients. As these linear systems originate from the same nominal structure, one way to expedite

their solution is to exploit their similarity.
The SMOR method assumes that the solution can be spanned by a smaller number of basis vectors. Consider the solution for the k-th realization, expressed in terms of r basis vectors, as follows:

$$\boldsymbol{I}(\boldsymbol{\xi}_k) = \overline{\boldsymbol{U}}_r\, \boldsymbol{z}, \tag{7.16}$$

where $\overline{\boldsymbol{U}}_r \in \mathbb{R}^{N\times r}$ is a matrix whose columns are these basis vectors. The determination of this basis will be discussed below and $\boldsymbol{z} \in \mathbb{C}^{r\times 1}$ is a new sought-for vector of unknowns. The linear system is now rewritten as:

$$\overline{\boldsymbol{Z}}(\boldsymbol{\xi}_k)\, \overline{\boldsymbol{U}}_r\, \boldsymbol{z} = \boldsymbol{V}(\boldsymbol{\xi}_k). \tag{7.17}$$

To obtain an $r \times r$ solvable linear system, the left projection matrix $\overline{\boldsymbol{U}}_r^H$, where H indicates the Hermitian operator, is used for Galerkin projection of the system:

$$\overline{\boldsymbol{U}}_r^H\, \overline{\boldsymbol{Z}}(\boldsymbol{\xi}_k)\, \overline{\boldsymbol{U}}_r\, \boldsymbol{z} = \overline{\boldsymbol{U}}_r^H\, \boldsymbol{V}(\boldsymbol{\xi}_k). \tag{7.18}$$

The original unknown vector $\boldsymbol{I}(\boldsymbol{\xi}_k)$ is then found via:

$$\boldsymbol{I}(\boldsymbol{\xi}_k) = \overline{\boldsymbol{U}}_r\, (\overline{\boldsymbol{U}}_r^H\, \overline{\boldsymbol{Z}}(\boldsymbol{\xi}_k)\, \overline{\boldsymbol{U}}_r)^{-1}\, \overline{\boldsymbol{U}}_r^H\, \boldsymbol{V}(\boldsymbol{\xi}_k). \tag{7.19}$$

The key issue in this method is constructing the matrix $\overline{\boldsymbol{U}}_r$. In [5], this matrix is constructed by a Gram-Schmidt orthogonalization of the vectors that are obtained by solving the system for several realizations. The idea is to dynamically expand the basis and check whether the solution for a new realization can be expressed in terms of the previously calculated basis. This is checked by computing the residual

$$\boldsymbol{r}(\boldsymbol{\xi}_k) = \boldsymbol{V}(\boldsymbol{\xi}_k) - \overline{\boldsymbol{Z}}\, \overline{\boldsymbol{U}}_r\, (\overline{\boldsymbol{U}}_r^H\, \overline{\boldsymbol{Z}}(\boldsymbol{\xi}_k)\, \overline{\boldsymbol{U}}_r)^{-1}\, \overline{\boldsymbol{U}}_r^H\, \boldsymbol{V}(\boldsymbol{\xi}_k). \tag{7.20}$$

If the residual is smaller than some predefined threshold, then the current subspace $\overline{\boldsymbol{U}}_r$ encompasses the solution which is found via (7.19). If this residual is large, the original linear system has to be solved via a traditional approach. Afterwards, the basis is extended with a vector $\boldsymbol{u}$, given by

$$\boldsymbol{u} = \boldsymbol{I}(\boldsymbol{\xi}_k) - \overline{\boldsymbol{U}}_r\, \overline{\boldsymbol{U}}_r^H\, \boldsymbol{I}(\boldsymbol{\xi}_k). \tag{7.21}$$

The new matrix $\overline{\boldsymbol{U}}_{r+1}$ is formed by extending the previous basis as follows $\overline{\boldsymbol{U}}_{r+1} = [\overline{\boldsymbol{U}}_r\, \boldsymbol{u}]$. The final number of basis vectors needed to accurately span the entire solution space is denoted R and it depends on the structure, its variability and predefined threshold value. More implementation details are found in [5].

7.2.2.1 Numerical example: Rough strip with Gaussian statistics

We consider a rough two-dimensional (2D) PEC strip with width $w = 100\lambda$, similar as the one shown in Fig. 6.1, but whose roughness is described by a set of 81 independent RVs with a normal distribution. We investigate to what extent the reduced space depends on the standard deviation σ of these normal distributions. For a predefined

threshold 10^{-3}, when $\sigma = \lambda/10\,000$, only $R = 2$ basis vectors are needed to span the entire space. For $\sigma = \lambda/100$, and the same threshold, this number is $R = 83$, and for $\sigma = \lambda/20$ the size of the reduced basis is $R = 242$. In all cases 500 realizations were considered. These results are logical, since for a larger input variability we expect that the solutions for different realization points are "less similar".
The results also clearly show the benefits of using a reduced model. Any non-intrusive algorithm (standard SCM, MC, TT) can be used in conjunction with SMOR. For the stochastic analysis of the rough strip with $\sigma = \lambda/100$, e.g., and assuming that a non-intrusive method requires the evaluation of $10\,000$ realizations of $\boldsymbol{\xi}$, only about 1% of linear systems needs to be solved in a traditional way, whereas all others are solved by making use of the basis $\overline{\boldsymbol{U}}_r$ and by checking the residual $\boldsymbol{r}(\boldsymbol{\xi}_q)$, as described above. Still, for every realization $\boldsymbol{\xi}_k$ the linear system (7.18) needs to be constructed. When the Multilevel Fast Multipole Method (MLFMM) is used, this includes performing fast matrix vector multiplications (MVP) of the matrix $\overline{\boldsymbol{Z}}(\boldsymbol{\xi}_k)$ with the R basis vectors of the matrix $\overline{\boldsymbol{U}}_R$. The complexity of this step is $RP(N)$, where $P(N)$ denotes the complexity of the standard deterministic MLFMM, i.e. $P(N) = O(N \log N)$ for 2D scatterers. The total complexity of constructing the system $\overline{\boldsymbol{U}}_r^H\, \overline{\boldsymbol{Z}}(\boldsymbol{\xi}_k)\, \overline{\boldsymbol{U}}_r$ during the setup phase of the algorithm is then $RO(N \log(N)) + R^2 O(N)$. The solution time scales as $N_{ir} O(R^2)$, when iterative solvers are used and where N_{ir} represents total number of iterations. Still, for $R \ll N$, it is clear that the $RO(N \log(N)$ time of the setup phase dominates.
When we compare the SMOR with a standard non-intrusive method leveraging MLFMM, the computational complexity for the latter one scales as $N_i O(N \log N)$, where N_i in number of matrix-vector products (MVPs) needed to solve the system. So, the SMOR method becomes efficient only if $R < N_i$. For the present example, the average value of N_i is about 90 for a 10^{-4} accuracy. Hence, this implementation of SMOR becomes inefficient when $\sigma > \lambda/100$.

7.3 Combination of TT and SMOR

On the one hand, It is clear that TT can offer a huge advantage when Smolyak's sparse rule fails to produce good results. On the other hand, SMOR can exploit the similarity between the several linear systems, that need to be solved. The main bottleneck of constructing the linear system (7.18) can be removed by using the multivariate polynomial PCE of the system matrix [5]:

$$\overline{\boldsymbol{Z}}(\boldsymbol{\xi}) = \sum_{k=0}^{K} \overline{\boldsymbol{Z}}_k \phi_k(\boldsymbol{\xi}), \tag{7.22}$$

where $\phi_k(\boldsymbol{\xi})$ are multivariate orthonormal polynomial basis functions, as also described in the previous chapters. By using PCE, the new system matrix, projected onto basis

$\overline{\boldsymbol{U}}_{r+1}$, is written as: follows:

$$\overline{\boldsymbol{U}}_{r+1}^{H}\,\overline{\boldsymbol{Z}}(\boldsymbol{\xi})\,\overline{\boldsymbol{U}}_{r+1}=\sum_{k=0}^{K}\overline{\boldsymbol{U}}_{r+1}^{H}\,\overline{\boldsymbol{Z}}_{k}\,\overline{\boldsymbol{U}}_{r+1}\,\phi_{k}(\boldsymbol{\xi}). \tag{7.23}$$

So, it can be found from the previous basis $\overline{\boldsymbol{U}}_r$ and the new basis vector $\boldsymbol{u}$ by computing the product in the right hand side of (7.23) in the following manner:

$$\begin{bmatrix}\overline{\boldsymbol{U}}_{r}^{H}\\ \boldsymbol{u}^{H}\end{bmatrix}\overline{\boldsymbol{Z}}_{k}\begin{bmatrix}\overline{\boldsymbol{U}}_{r} & \boldsymbol{u}\end{bmatrix}=\begin{bmatrix}\overline{\boldsymbol{U}}_{r}^{H}\,\overline{\boldsymbol{Z}}_{k}\,\overline{\boldsymbol{U}}_{r} & \overline{\boldsymbol{U}}_{r}^{H}\,\overline{\boldsymbol{Z}}_{k}\,\boldsymbol{u}\\ \boldsymbol{u}^{H}\,\overline{\boldsymbol{Z}}_{k}\,\overline{\boldsymbol{U}}_{r} & \boldsymbol{u}^{H}\,\overline{\boldsymbol{Z}}_{k}\,\boldsymbol{u}\end{bmatrix} \tag{7.24}$$

The products $\overline{\boldsymbol{U}}_{r}^{H}\,\overline{\boldsymbol{Z}}_{k}\,\overline{\boldsymbol{U}}_{r}$, $\overline{\boldsymbol{U}}_{r}^{H}\,\overline{\boldsymbol{Z}}_{k}$ and $\overline{\boldsymbol{Z}}_{k}\,\overline{\boldsymbol{U}}_{r}$ are already available at step $r+1$, so the only additional cost is to find $\boldsymbol{u}^{H}\,\overline{\boldsymbol{Z}}_{k}\,\boldsymbol{u}$. After the reduced model is built, the system matrix of type (7.18) is calculated using the multivariate polynomial evaluation (7.23).
This approach, when used in conjuction with MLFMM, as described in the previous chapter, leads to a very efficient evaluation of the $\overline{\boldsymbol{Z}}_k$. However, to build reduced models of type (7.24), the evaluation of $\overline{\boldsymbol{Z}}_k\,\boldsymbol{u}$ has a complexity that scales with the number of polynomials K. In contrast to [5] where coefficients are calculated via simple matrix-vector multiplications, here this requires one Galerkin projection at the disaggregation side [13]. So, some parts of the algorithm need to be rewritten, making this approach both intrusive and non-intrusive in nature.
It is clearly visible that this novel approach could be more efficient than a standard non-intrusive method. However, further optimization of the algorithm and its application and many numerical tests are needed to gain more insight.

7.4 Conclusions

In this chapter, we have introduced methods based on tensor decomposition, which are nowadays often used in the domain of UQ. These methods are combined with non-intrusive methods, so we have suggested their combination with SMOR in order to derive a new and efficient algorithm. However, by means of very simple numerical examples, we have indicated that many parameters, type of structure, variability, number of RVs, etc affect the total solution time. Still, conjuction of MLFMM with TT decomposition and SMOR seems to be a promising way to conceive novel, efficient tools for stochastic EM modeling.

References

[1] T. El-Moselhy, "Field solver technologies for variation-aware interconnect parasitic extraction", PhD thesis, Massachusetts Institute of Technology, 2010.

[2] Z. Zhang, X. Yang, G. Marucci, P. Maffezzoni, I. M. Elfadel, G. E. Karniadakis, and L. Daniel, "Stochastic testing simulator for integrated circuits and MEMS: hierarchical and sparse techniques", *CoRR*, vol. abs/1409.4822, 2014.

[3] J. Hampton and A. Doostan, "Compressive sampling of polynomial chaos expansions: Convergence analysis and sampling strategies", *Journal of Computational Physics*, vol. 280, pp. 363–386, Jan. 2015.

[4] P. Tsuji, D. Xiu, and L. Ying, "Fast method for high-frequency acoustic scattering from random scatterers", *International Journal for Uncertainty Quantification*, vol. 1, no. 2, pp. 99–117, 2011.

[5] T. El-Moselhy and L. Daniel, "Variation-aware interconnect extraction using statistical moment preserving model order reduction", in *Design, Automation Test in Europe Conference Exhibition (DATE), 2010*, 2010, pp. 453–458.

[6] Z. Zhang, X. Yang, I. V. Oseledets, G. E. Karniadakis, and L. Daniel, "Enabling high-dimensional hierarchical uncertainty quantification by ANOVA and tensor-train decomposition", *CoRR*, vol. abs/1407.3023, 2014.

[7] I. V. Oseledets, "Tensor-train decomposition", *SIAM Journal on Scientific Computing*, vol. 33, no. 5, pp. 2295–2317, 2011.

[8] Z. Zhang, H. D. Nguyen, K. Turitsyn, and L. Daniel, "Probabilistic power flow computation via low-rank and sparse tensor recovery", *CoRR*, vol. abs/1508.02489, 2015.

[9] T. G. Kolda and B. W. Bader, "Tensor decompositions and applications", *SIAM REVIEW*, vol. 51, no. 3, pp. 455–500, 2009.

[10] D. Bigoni, A. P. Engsig-Karup, and Y. M. Marzouk, "Spectral tensor-train decomposition", *ArXiv e-prints*, May 2014.

[11] I. V. Oseledets, *TT-toolbox 2.2*, `http://spring.inm.ras.ru/osel/?page_id=24`.

[12] I. Oseledets and E. Tyrtyshnikov, "TT-cross approximation for multidimensional arrays", *Linear Algebra and its Applications*, vol. 432, no. 1, pp. 70 –88, 2010.

[13] Z. Zubac, D. De Zutter, and D. Vande Ginste, "Scattering from two-dimensional objects of varying shape combining the Multilevel Fast Multipole Method (MLFMM) with the Stochastic Galerkin Method (SGM)", *IEEE Antennas and Wireless Propagation Letters*, vol. 13, pp. 1275–1278, Jul. 2014.

8 Conclusions

8.1 General conclusions

In this thesis, novel uncertainty quantification (UQ) methods for full-wave scattering problems were investigated. The main focus was on developing intrusive polynomial chaos expansion (PCE) based techniques. Starting from a stochastic boundary integral equation (BIE) description of the scattering problems, solutions were found via a standard Method of Moments (MoM) in combination with the PCE-based stochastic Galerkin Method (SGM). The Multilevel Fast Multipole Method (MLFMM) was introduced to speed up the computations, and as such, an efficient SGM-MLFMM algorithm was constructed. The efficiency and accuracy with which typical statistical quantities such as mean, variance, PDF, etc, can be calculated, were thoroughly validated, tested, and compared with the non-intrusive Stochastic Collocation Method (SCM) and the standard Monte Carlo (MC) approach. The hybridization of the (MLFMM-accelerated) BIE-MoM with the SGM to efficiently solve Maxwell's equations or the Helmholtz equation were never attempted before in literature, and, hence, this is considered as the main novel contribution of this work. The several flavors of the newly developed algorithms are detailed next.

After a general introduction in Chapter 1, the second chapter covers the standard MoM scheme and its combination with both the SGM and the SCM method. It is important to mention here again that, for the scattering problems under consideration, even a small variation of the input parameters (i.e. the properties of the scatterer) can already lead to a significant variability of the output parameters, such as the current density on the scatterer's surface. This is due to the stochastically varying phase of the electromagnetic fields. This is unavoidable for full-wave (scattering) problems, and justifies the need of dedicated solvers, as presented in this work. The third chapter describes the SGM-MoM of Chapter 2 accelerated by means of the MLFMM. Special

attention was devoted to the computational complexity and truncation error of the novel SGM-MLFMM scheme. To further expedite the computations, in particular to reduce the number of iterations during the solution of the linear system evolving from the MoM, a preconditioner was constructed, as presented in Chapter 4. The parallelization of the SGM-MLFMM is proposed in the fifth chapter. In this chapter, scattering at both perfectly electrically conducting and dielectric objects were considered. Moreover, two-dimensional equivalents of real optical systems were simulated and the results show a great advantage over SCM and MC methods. Chapter 6 introduced the new Cholesky-based strategy to deal with *correlated* random variables as opposed to the traditionally used Karhunen-Loève transformation (KLT). It was shown that this approach deals well with low correlation lengths and it mitigates the curse of dimensionality issues evolving from the multidimensional integrations. The Cholesky approach outperforms the KLT during both the setup and the solution phase of the algorithm. Finally, in Chapter 7, the groundwork is laid for a promising sampling-based hybrid method, leveraging tensor-train (TT) decomposition and Statistical Moment Preserving Model Order Reduction (SMOR).

All novel methods show an excellent accuracy and efficiency. For many situations, the standard deterministic complexity is simply scaled with the number of polynomials used in the PCE, which makes these methods usable for any situation where SGM-MoM can be used. However, as discussed in this work, the choice between adopting a non-intrusive versus an intrusive method may depend on the specific application and is not always straightforward.

8.2 Future research

The research in the domain of uncertainty quantification of electromagnetic problems is not a finished story. Despite the fact that several important issues were successfully addressed in this works, also many new questions arise from it. Thus, future research can be split into several directions.

From an electromagnetic point of view, it would be interesting to combine the SGM with MLFMM for three-dimensional scattering problems and real-life applications. Studying the impact of the typical, low-frequency breakdown on the SGM-MLFMM scheme and dealing with it, is another challenging path. In particular, one might wonder whether the scalability with the number of polynomials remains intact and it has to be checked whether the method is still competitive compared to the standard SCM.

Parallelization of the SGM-MLFMM for large electromagnetic structures whose variability is described by a set of few random variables was tackled in this thesis. However, for a large number of variables, the approach described in this thesis might not be sufficient. Further research on the parallelization of the proposed schemes, in particular from a stochastic viewpoint, i.e. to deal with many RVs, is required.

As stated before, the choice between intrusive and non-intrusive methods remains difficult for full-wave electromagnetic problems. For a large number of polynomials, the PCE problem becomes a big data problem. To the best of the author's knowledge, novel UQ methods are mostly based on non-intrusive formalisms and the usage of tensors. From this perspective, intrusive methods become obsolete. However, methods that allow the fast computation of the stochastic matrix vector product (MVP) of type $\overline{\boldsymbol{Z}}(\boldsymbol{\xi})\boldsymbol{I}(\boldsymbol{\xi})$ are still decent alternatives. Novel algorithms based on SGM should be, at least, scalable for a large number of polynomials K and phase effects should be properly dealth with. In particular, truncating PCE series in the MLFMM scheme, might lead to phase errors, and consequently, more research on the development of fast MVPs is needed.

In many areas of electrical engineering, there are lot of uncertainties that influence the behavior of circuits and devices. Therefore, studying and analyzing the stochastic nature is of the utmost importance. Based on novel stochastic models, such as the ones developed in this thesis, optimization of the initial design might make the circuit less sensitive to process variations. PCE-based UQ methods can be used, in the forward loop, of novel robust optimizers and pave the way to variability-aware design.